DATA REPORT FOR COMPLETED SPUR-DIKE CONFIGURATIONS WITHIN THE NATIVE TOPOGRAPHY MODEL

Prepared for the

U. S. Department of the Interior
Bureau of Reclamation
Albuquerque Area Office
555 Broadway N.E., Suite 100
Albuquerque, New Mexico 87102-2352

This research was supported in part by funds provided by the
Rocky Mountain Research Station, Forest Service, U. S. Department of Agriculture.

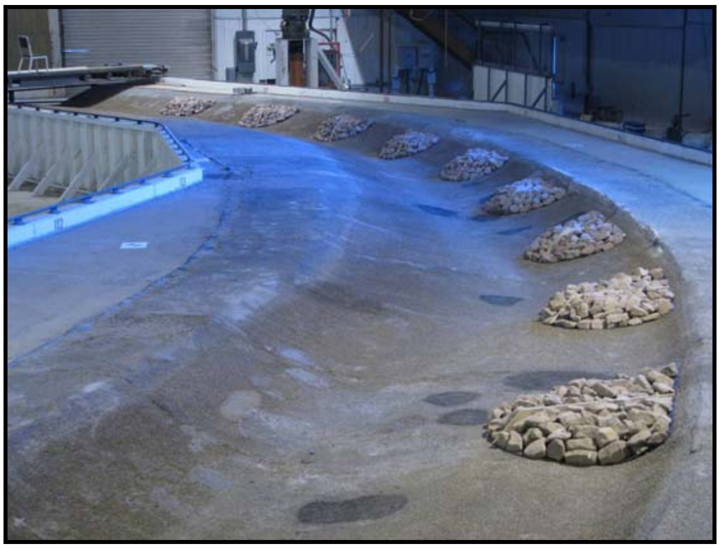

Prepared by

Natalie A. Youngblood, Michael E. Ursic, Amanda L. Cox, Christopher I. Thornton, and Steven R. Abt

June 2012

Colorado State University
Daryl B. Simons Building *at the*
Engineering Research Center
Fort Collins, Colorado 80523

DATA REPORT FOR COMPLETED SPUR-DIKE CONFIGURATIONS WITHIN THE NATIVE TOPOGRAPHY MODEL

Prepared for the

U. S. Department of the Interior
Bureau of Reclamation
Albuquerque Area Office
555 Broadway N.E., Suite 100
Albuquerque, New Mexico 87102-2352

This research was supported in part by funds provided by the
Rocky Mountain Research Station, Forest Service, U. S. Department of Agriculture.

Prepared by

Natalie A. Youngblood, Michael E. Ursic, Amanda L. Cox, Christopher I. Thornton, and Steven R. Abt

June 2012

Colorado State University
Daryl B. Simons Building *at the*
Engineering Research Center
Fort Collins, Colorado 80523

EXECUTIVE SUMMARY

At the request of the U. S. Bureau of Reclamation, laboratory testing was performed on a physical model at the Colorado State University Hydraulics Laboratory to obtain data for use in developing design procedures for spur dikes. An existing undistorted physical model was used to collect data on varying spur-dike designs. The physical model was previously constructed to simulate geometric characteristics of bends found along the Middle Rio Grande study reach at a 1:12 Froude scale and included an upstream bend and a downstream bend. Four different spur-dike designs were generated and laboratory tested for the native-topography model: 1) a minimum flow-velocity reduction design for the upstream bend, 2) a maximum flow-velocity reduction design for the upstream bend, 3) a minimum flow-velocity reduction design for the downstream bend, and 4) a maximum flow-velocity reduction design for the downstream bend. The spur-dike designs corresponded to minimum and maximum outer-bank flow-velocity reductions observed during previous laboratory testing of spur dikes in the physical model with a trapezoidal cross-section geometry. Six test configurations were evaluated using the four spur-dike designs. Water-surface elevations, flow velocities, and boundary shear stresses were measured at specified locations for each configuration. Descriptions of the physical model construction, spur-dike design and construction, test program, and test matrix are presented in this report. Further, graphical representations of the resulting data are provided for reference and all the collected data are provided in the Electronic Appendix.

TABLE OF CONTENTS

LIST OF FIGURES

LIST OF TABLES

LIST OF SYMBOLS, UNITS OF MEASURE, AND ABBREVIATIONS

Symbols

b	channel width [L]
dH	differential head in inches [L]
dV	differential voltage recorded $[L^2MT^{-2}Q^{-1}]$
$d\theta$	offset angle
θ	angle between spur dikes
θ_w	planform angle
L_{arc}	length of arc between spur dikes [L]
L_B	length of bend [L]
L_{cw}	length of spur-dike crest [L]
$L_{cw,proj}$	length of spur-dike crest projected onto the cross section perpendicular to flow
L_r	structure length ratio
L_{rem}	length of bend remainder [L]
L_w	length of spur dike [L]
$L_{w,proj}$	length of spur dike projected onto the cross section perpendicular to flow [L]
$\overline{L}_{xsweiravg}$	average spur-dike length taken as a cross-sectional spur-dike average [L]
n	Manning's coefficient of hydraulic resistance
Q	flow rate $[L^3T^{-1}]$
r	radius of curvature [L]
R	arc radius [L]
R_c	relative curvature
S	arc length [L]
SR	spacing ratio
TW	channel top width [L]
τ_o	boundary shear stress $[ML^{-1}T^{-2}]$
V_x, V_y, V_z	component of flow velocity in x-, y-, or z-direction, respectively $[LT^{-1}]$
W_{bw}	width of spur-dike base [L]
W_{cw}	width of spur-dike crest [L]
Φ_w	crest slope

Units of Measure

cfs	cubic feet per second
cm	centimeter(s)
°	degree(s)
ft	foot or feet
ft/ft	foot per foot
ft/s	feet per second
ft^2	square feet
Hz	Hertz
in.	inch(es)
L	length dimension

m	meter(s)
M	mass dimension
mA	milliampere(s)
mi	mile(s)
mi^2	square mile(s)
%	percent
psf	pound(s) per square foot
Q	electrical charge dimension
sec	second(s)
T	time dimension
V	Volt(s)

Abbreviations

±	plus or minus
®	registered
a – g	cross-section data-collection locations
ADV	acoustic Doppler velocimeter
DCL	data-collection location
DS	downstream
ERC	Engineering Research Center
FY	Fiscal Year
GIS	geographic information system
H:V	Horizontal:Vertical
HEC-RAS	Hydrologic Engineering Centers - River Analysis System
M1 – M10	cross sections
MSL	Mean Sea Level
NW	Native Topography Spur-Dike Design
NW01	Native Topography Spur-Dike Design 1
NW02	Native Topography Spur-Dike Design 2
NW03	Native Topography Spur-Dike Design 3
NW04	Native Topography Spur-Dike Design 4
Piezo Loc	piezometer location
PVC	polyvinyl chloride
TH	thalweg
Trap	trapezoidal
TSW04	prismatic model spur-dike test configuration 04
TSW10	prismatic model spur-dike test configuration 10
US	upstream
USBR	U. S. Bureau of Reclamation
WSE	water surface elevation
x, y, z	probe direction
XS	cross section

1 INTRODUCTION

1.1 Project Background

The Middle Rio Grande is a 29-mi reach of the Rio Grande in central New Mexico extending from the downstream side of Cochiti Dam to Bernalillo, New Mexico. A map of the Middle Rio Grande reach is presented in Figure 1.1. In recent years, the Middle Rio Grande has been the focus of a variety of channel restoration techniques, including the use of native material and rock spur-dike structures in attempts to control bank erosion rates, channel migration rates, and habitat degradation (Darrow 2004).

The Middle Rio Grande has historically been classified as a perennial braided stream. In 1973, the Cochiti Dam was built to provide flood control and sediment detention for the Albuquerque area. As a result, the dam traps nearly all the sediment supplied by a 14,600-mi^2 watershed (Richard 2001). Due to substantial reservoir sedimentation and the consequential sediment deficit of the Middle Rio Grande, an alteration in planform has occurred. Richard (2001) stated that, in general, the channel has been transformed from a braided channel to a meandering stream containing a pool-riffle sequence with coarse gravel substrate. Previous to 1970, two large tributaries to the Middle Rio Grande (Galisteo Creek and the Jemez River) were dammed, which further contributed to the sediment deficiency (Schmidt 2005).

Lateral migration caused by the change in morphology has marginalized riverside infrastructure and reduced riparian vegetation and aquatic habitat (Heintz 2002). In an effort to protect riverside infrastructure, the U. S. Bureau of Reclamation (USBR) has implemented a channel maintenance program to stabilize the channel with an additional goal of improving aquatic habitat. Traditional methods of bank stabilization such as riprap revetment and concrete structures are not aesthetically pleasing and do not promote aquatic habitat or riparian vegetation. Alternative methods such as spur dikes have been proven to stabilize banks and increase aquatic habitat (Davinroy *et al.* 1998, Derrick 1998, Shields *et al.* 1998). Although spur dikes have proven to be a suitable alternative to traditional methods, no standard design guidelines have been created. Previously implemented designs have largely been based on engineering judgment.

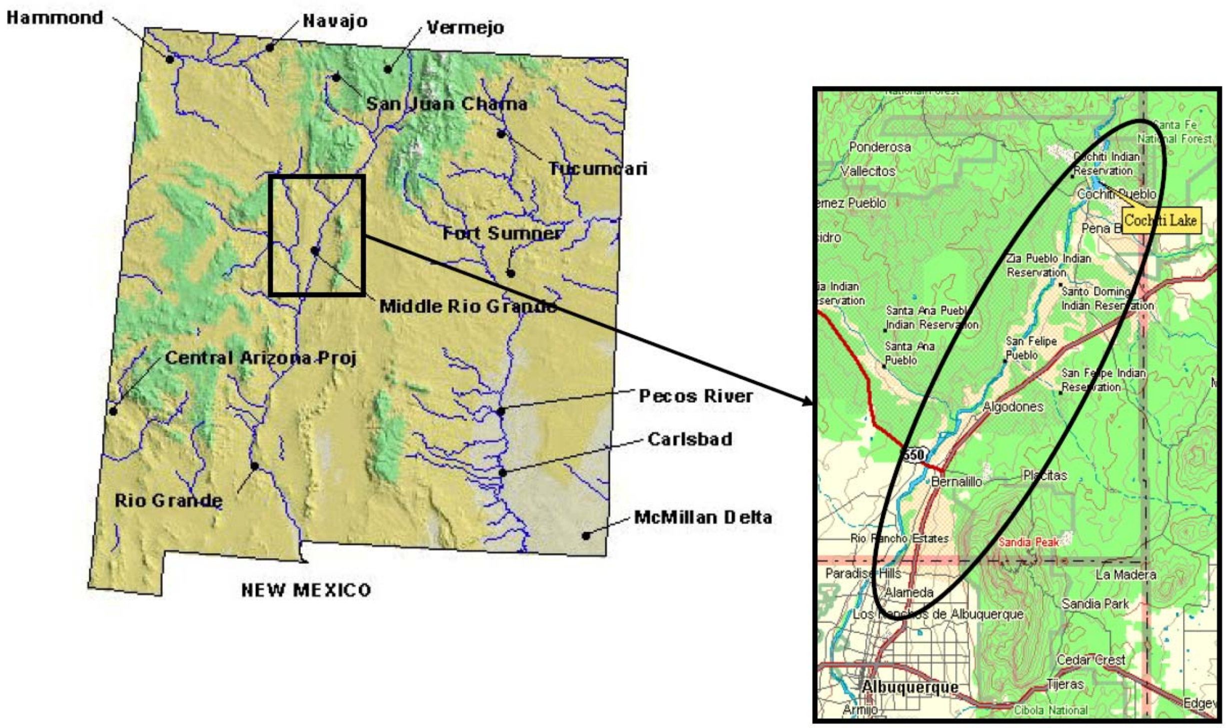

Figure 1.1: Project Area (Walker 2009)

1.2 Model Background

In an effort to create design guidelines for spur dikes, the USBR contracted Colorado State University to create a physical model depicting geometric characteristics similar to those of bends found within the Middle Rio Grande study reach. An undistorted physical model with a 1:12 Froude scale was created in the Hydromachinery Laboratory located at the Engineering Research Center (ERC). Three different types of bends were identified within the study reach, two of which were modeled (Heintz 2002). The original model was trapezoidal with reference to geometric properties of the representative reaches. Multiple spur-dike designs were tested in the model at various stages, resulting design guidelines for spur dikes in a prismatic channel and a wealth of other design considerations (Heintz 2002, Darrow 2004, Cox 2005, Kasper 2005, Kinzli 2005, Schmidt 2005, Walker 2009). Currently, the model is proportionally similar to two native topographic bends, the Cochiti and San Felipe Bends, which are found along the study reach and shown Figure 1.2. The current model is discussed further in Chapter 2.

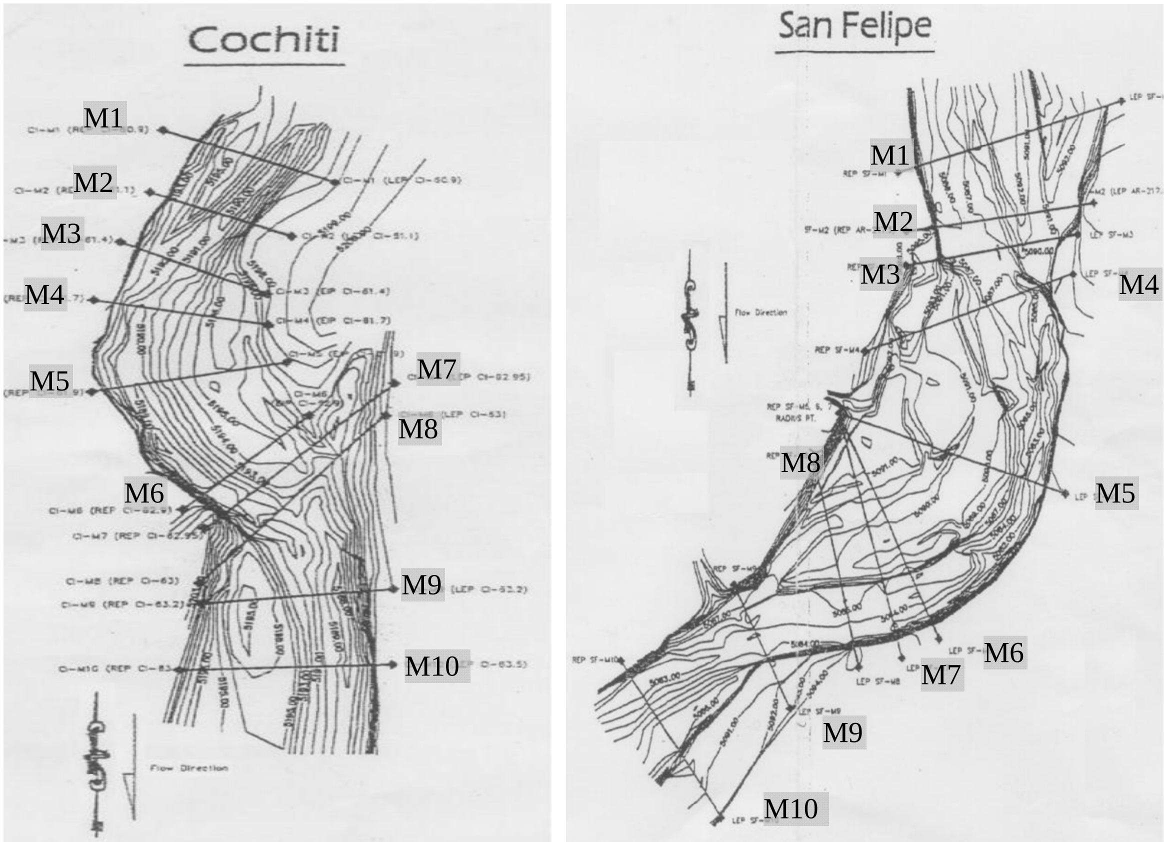

Figure 1.2: Plan View of Cochiti and San Felipe Cross-section Surveys (Walker 2009)

1.3 Scope of Work

The testing program for native topography spur dikes was broken down into two components:

1. Fiscal Year 2007 and
2. Fiscal Year 2008.

For each Fiscal Year (FY), three configurations were to be tested. Each configuration included one or more specific spur-dike designs, which are denoted with NW for Native Topography Spur-Dike Design and a number corresponding to the test order. The native topography spur-dike design parameters and the relationship to prismatic spur-dike designs are given in Chapter 3. Figures depicting the spur-dike designs and testing locations for each configuration are presented in Chapter 5.

For FY 2007, testing was conducted on the following configurations with the design discharge of 12 cubic feet per second (cfs):

1. **Configuration 1**
    a. Design and install NW01 spur dikes in the downstream bend with no spur dikes in the upstream bend
    b. Data to be collected in the downstream bend at nine cross-section and seven lateral positions with an average of nineteen vertical samples
    c. Data to be collected around the spur dikes at seven locations with nineteen vertical samples
    d. Data to be collected at the thalweg for the nine upstream bend cross sections with ten vertical samples (10% increments)
2. **Configuration 2**
    a. Design and install NW02 spur dikes in the upstream bend and retain NW01 spur dikes in the downstream bend
    b. Data to be collected at the thalweg for the nine downstream bend cross sections with ten vertical samples (10% increments)
3. **Configuration 3**
    a. Remove NW01 spur dikes from the downstream bend and retain NW02 spur dikes in the upstream bend
    b. Data to be collected in the upstream bend at nine cross-section and seven lateral positions with an average of nineteen vertical samples
    c. Data to be collected around the spur dikes at seven locations with nineteen vertical samples
    d. Data to be collected at the thalweg for the nine downstream bend cross sections with ten vertical samples

Again, native topography spur-dike design parameters and the relationship to the prismatic spur-dike designs are given in Chapter 3. For FY 2008, testing was conducted on the following configurations with the design discharge of 12 cfs:

1. **Configuration 4**
   a. Design and install NW03 spur dikes in the downstream bend with no spur dikes in the upstream bend
   b. Data to be collected in the downstream bend at nine cross-section and seven lateral positions with an average of nineteen vertical samples
   c. Data to be collected around the spur dikes at seven locations with nineteen vertical samples
   d. Data to be collected at the thalweg for the nine upstream bend cross sections with ten vertical samples (10% increments)
2. **Configuration 5**
   a. Design and install NW04 spur dikes in the upstream bend and retain NW03 spur dikes in the downstream bend
   b. Data to be collected at the thalweg for the nine downstream bend cross sections with ten vertical samples (10% increments)
3. **Configuration 6**
   a. Remove NW03 spur dikes from the downstream bend and retain NW04 spur dikes in the upstream bend
   b. Data to be collected in the upstream bend at nine cross-section and seven lateral positions with an average of nineteen vertical samples
   c. Data to be collected around the spur dikes at seven locations with nineteen vertical samples
   d. Data to be collected at the thalweg for the nine downstream bend cross sections with ten vertical samples

To facilitate an overview of the testing configurations presented in the *Scope of Work*, a matrix is provided in Table 1.1.

Table 1.1: Scope of Work Matrix

		Spur Dikes Present in Model				Data to be Collected						
						Spur Dikes			US Bend Cross Sections		DS Bend Cross Sections	
Fiscal Year	Config-uration	NW01	NW02	NW03	NW04	Bend Location	Sample Positions	Vertical Samples	Lateral Positions	Vertical Samples	Lateral Positions	Vertical Samples
2007	1	√				DS	7	19	TH	10	7	19
	2	√	√								TH	10
	3		√			US	7	19	7	19	TH	10
2008	4			√		DS	7	19	TH	10	7	19
	5			√	√						TH	10
	6				√	US	7	19	7	19	TH	10

DS = downstream bend (Cochiti Bend), US = upstream bend (San Felipe Bend), TH = thalweg

2 PHYSICAL MODEL

2.1 Trapezoidal Model

Due to the magnitude of the study reach, modeling of the entire system was not feasible. Therefore, bend types were classified by planform geometry for all bends throughout the 29-mi study reach. The planform geometry was determined using geographic information system (GIS) software and a 1992 Orthophoto aerial photograph. Three types of bends were identified by plotting relative curvature (R_c) against the channel width (b), as presented in Figure 2.1. The representative geometry of bend Types I and III were modeled with a 1:12 Froude scale and are presented in Table 2.1 and Table 2.2 (Heintz 2002).

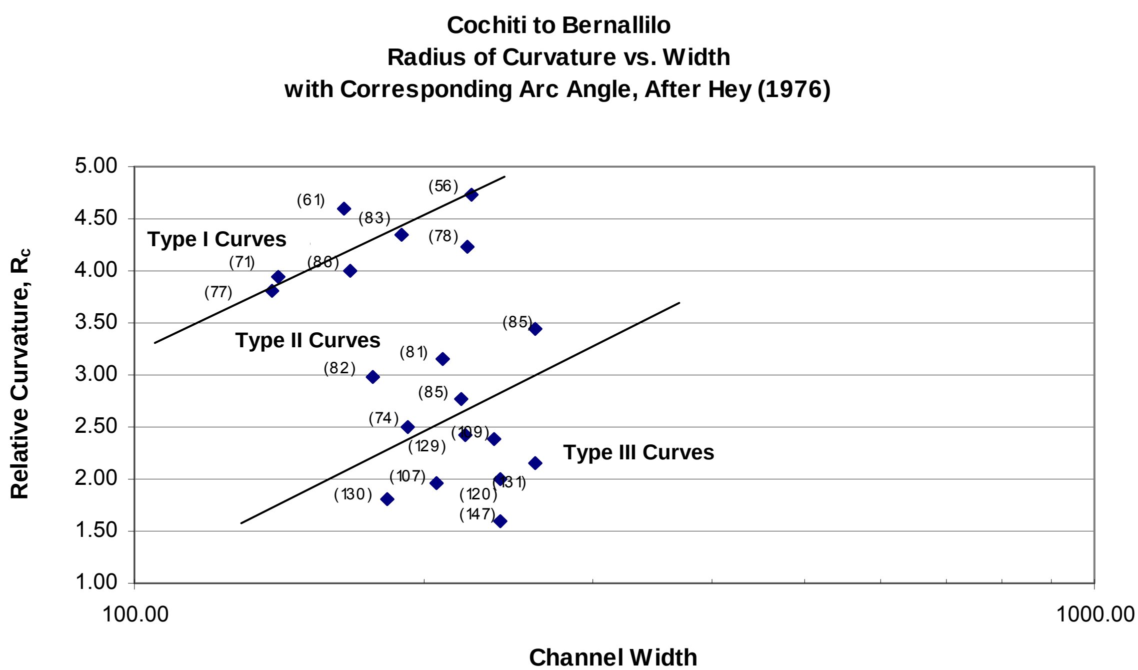

Figure 2.1: Bend Planform Geometry Curve Types (Heintz 2002)

Table 2.1: Prototype Planform Geometry Characteristics (Heintz 2002)

Bend Type	Top Width		Radius of Curvature		Bend Angle	Relative Curvature	Channel Length	
	(ft)	(m)	(ft)	(m)	(°)		(ft)	(m)
I	230.40	70.20	465.00	141.73	125	2.02	1014	309
III	180.00	54.86	789.96	240.77	73	4.39	1002	305

Table 2.2: Model Planform Geometry Characteristics (Heintz 2002)

Bend Type	Top Width		Radius of Curvature		Bend Angle	Relative Curvature	Channel Length	
	(ft)	(m)	(ft)	(m)	(°)		(ft)	(m)
I	19.20	5.90	38.75	11.81	125	2.02	84.5	25.8
III	15.00	4.60	65.83	20.06	73	4.39	83.5	25.5

The cross-sectional geometry in both bends remained constant with 3H:1V (Horizontal:Vertical) side slopes. The bed slope determined for the prototype was 0.000863 ft/ft, which was implemented as closely as possible throughout the model. The total flow depth of 1.5 ft was chosen to accommodate the required flow rates for testing. A 10:1 transition between bends ensured the entry of uniform flow to the second bend (Heintz 2002). A plan view of the prismatic physical model schematic is presented in Figure 2.2.

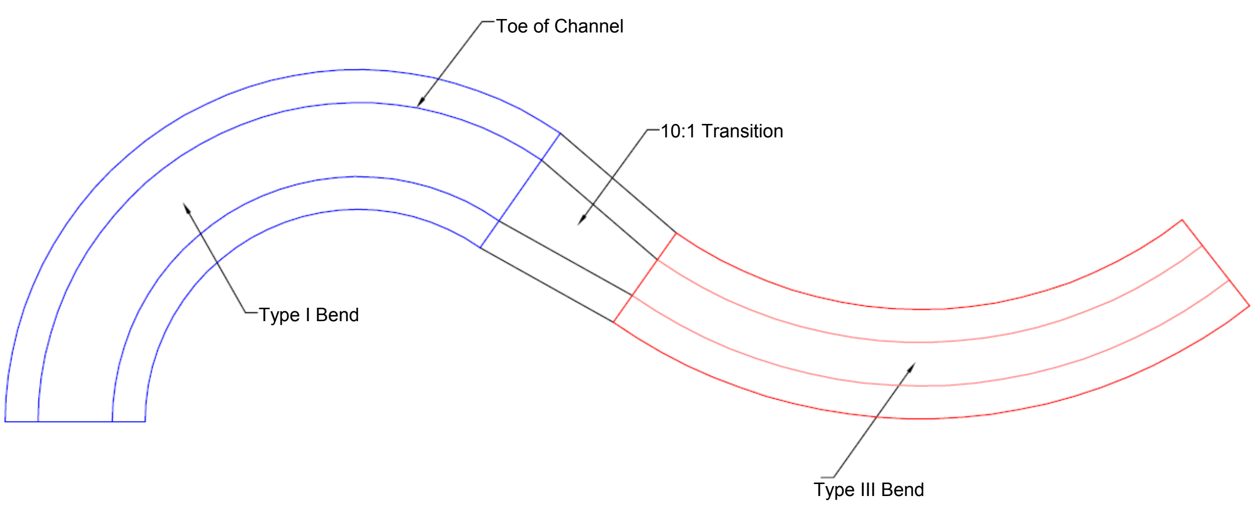

Figure 2.2: Plan View of Prismatic Physical Model (Heintz 2002)

As described by Heintz (2002), tests were conducted at four different discharges, 8, 12, 16, and 20 cfs corresponding to prototype discharges of 4,000, 6,000, 8,000, and 10,000 cfs, respectively. The design discharge for spur-dike design was 12 cfs, or 6,000-cfs prototype (Heintz 2002). The roughness characteristics of the prototype varied with Manning's roughness coefficients (n) between 0.026 and 0.035. Due to the scope of work of the project, a rigid boundary model was considered suitable. The model bed and banks were constructed of roughened concrete that was found to have a Manning's roughness coefficient of 0.018. The model value relates to a prototype Manning's roughness coefficient of 0.027, which is within the bounds of prototype conditions (Heintz 2002).

2.2 Native Topography Design

The design of the native topography model was based on cross-sectional data taken by the USBR of two bends found in the Middle Rio Grande reach: 1) the Cochiti (Type III) bend and 2) the San Felipe (Type I) bend (USBR 2000). The USBR provided plan views of bed topography and cross-section locations as presented in Figure 2.3. The inflection points for both bends are located at M2 and M8 (USBR 2000). Therefore, Cross Sections M2 through M8 were used in model cross-sectional development. An average bankfull flow rate of 1,420 cfs was used to determine cross-sectional flow area so the main channel could be isolated. Initially, a 1:12 Froude scaling of the cross sections was attempted. The 1:12 Froude scaling appeared problematic due to the size of the resulting cross sections, exemplified in Figure 2.4. In order to reduce construction costs, it was decided to build the native topography model within the trapezoidal channel. To facilitate this, a proportionality method was used to develop model cross sections. Proportions were determined for each station and elevation based on maximum channel depth and top width as shown in Table 2.3 and Table 2.4. Additionally, vertical and lateral offsets were applied to ensure the correct migration of the thalweg (Walker 2009).

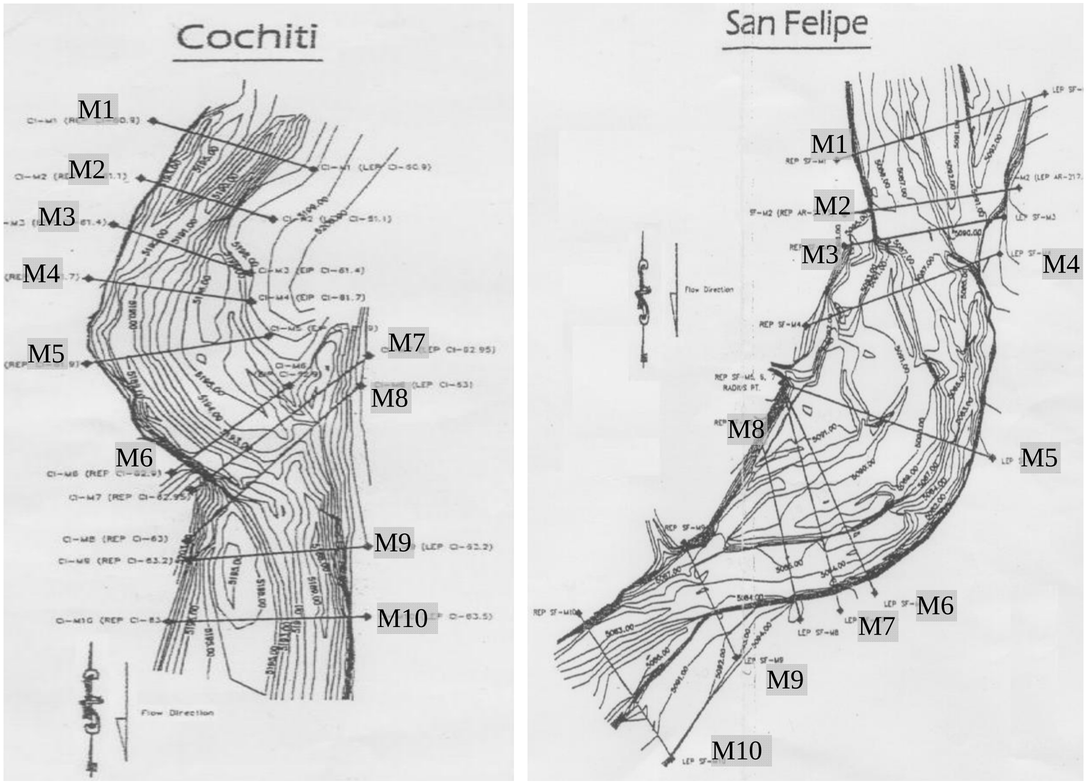

Figure 2.3: Plan View of Cross Sections Provided by the USBR for the Cochiti and San Felipe Bends (Walker 2009)

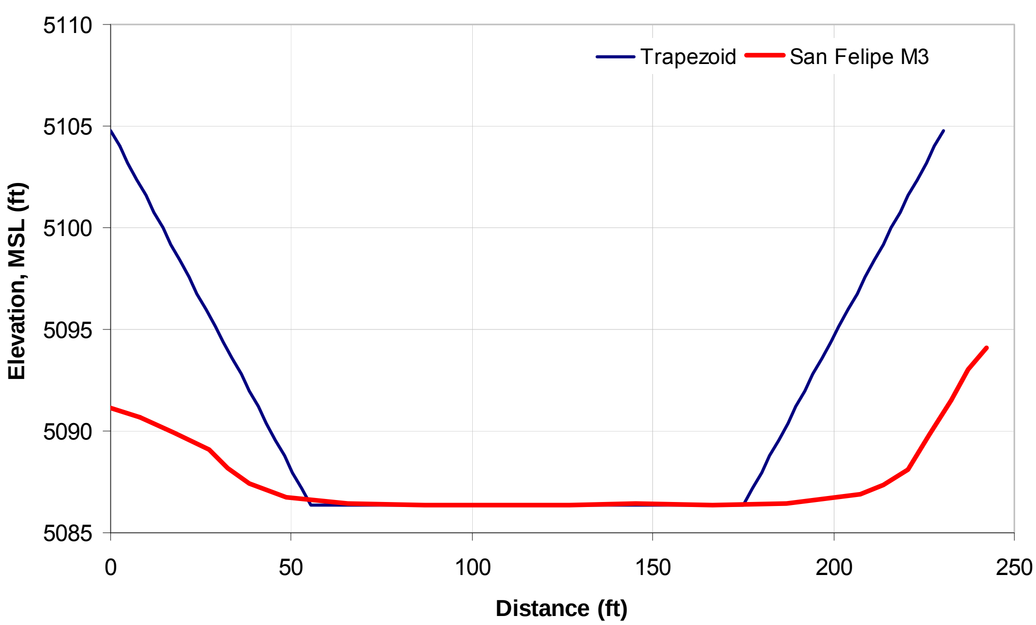

Figure 2.4: 1:12 Froude Scale Representation of Cross Section M3 of the San Felipe Reach and Trapezoidal Configuration (modified from Walker (2009))

Table 2.3: Native Topography Model Characteristics Derived by the Proportional Method for the San Felipe Reach

River Station (ft)	USBR Cross-section Name	Top Width (ft)	Depth (ft)	Proportional % of Maximum Prototype Depth	Proportional Depth Allowed by Trapezoidal Model (ft)	Proportional % of Maximum Prototype Width	Proportional Width Allowed by Trapezoidal Model (ft)
990	M2	187.30	3.52	44.28%	0.66	86.44%	16.57
980	M3	195.20	3.00	37.79%	0.57	90.09%	17.27
970	M4	216.68	4.26	53.67%	0.80	100.00%	19.17
960	M5	107.17	7.94	100.00%	1.50	49.46%	9.48
950	M6	146.60	5.82	73.29%	1.10	67.66%	12.97
940	M7	153.77	5.95	74.94%	1.12	70.97%	13.60
930	M8	163.80	4.36	54.88%	0.82	75.60%	14.49

Table 2.4: Native Topography Model Characteristics Derived by the Proportional Method for the Cochiti Reach

River Station (ft)	USBR Cross-section Name	Top Width (ft)	Depth (ft)	Proportional % of Maximum Prototype Depth	Proportional Depth Allowed by Trapezoidal Model (ft)	Proportional % of Maximum Prototype Width	Proportional Width Allowed by Trapezoidal Model (ft)
990	M2	171.38	5.21	88.08%	1.32	73.87%	11.08
980	M3	159.84	4.05	68.58%	1.03	68.90%	10.33
970	M4	156.00	4.60	77.86%	1.17	67.24%	10.09
960	M5	147.79	5.37	90.83%	1.36	63.70%	9.56
950	M6	200.00	5.91	100.00%	1.50	86.21%	12.93
940	M7	218.00	5.07	85.75%	1.29	93.97%	14.10
930	M8	232.00	3.60	60.95%	0.91	100.00%	15.00

Additional cross sections were interpreted from the USBR survey data for accurate representations in the physical and computer models. Survey data from Cross Sections M7 and M8 of the Cochiti reach contained backwater areas, which were removed by limiting the extent of the cross section to the main channel. All secondary flow channels were removed from cross-section geometry to simplify the already dynamic flow conditions.

2.3 Model Calibration

The proposed physical model was calibrated with a Hydrologic Engineering Centers - River Analysis System (HEC-RAS) model using estimated roughness and downstream water surface control values. Estimated water surface elevations for discharges up to 16 cfs were created. The results indicated that overtopping would occur at flow rates above 8 cfs. In an effort to achieve a 16-cfs flow rate, flow area adjustments were completed to increase capacity. It was noted that the flow was being restricted by adverse slopes from the pool-riffle sequence. A 50% reduction of thalweg amplitude was applied to increase conveyance, while maintaining an average bed slope equal to that of the prototype, 0.000863 ft/ft (Walker 2009). Thalweg amplitude reductions for each bend are illustrated in Figure 2.5 and Figure 2.6.

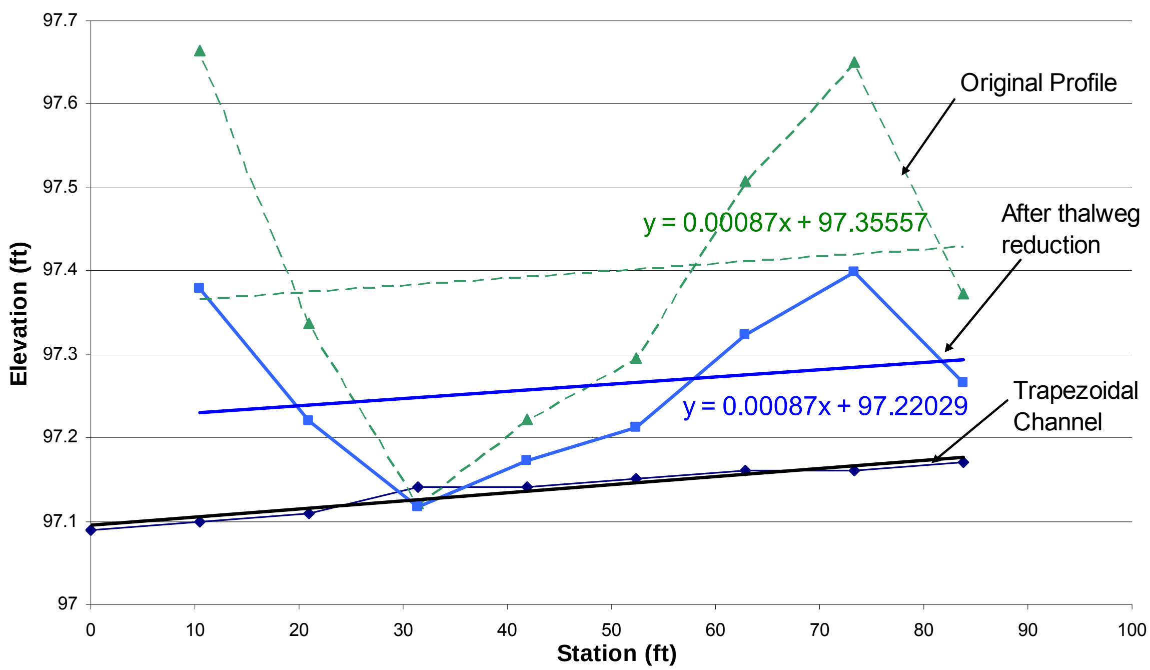

Figure 2.5: Illustration of the 50% Reduction of the Thalweg Amplitude for the Cochiti Reach (Walker 2009)

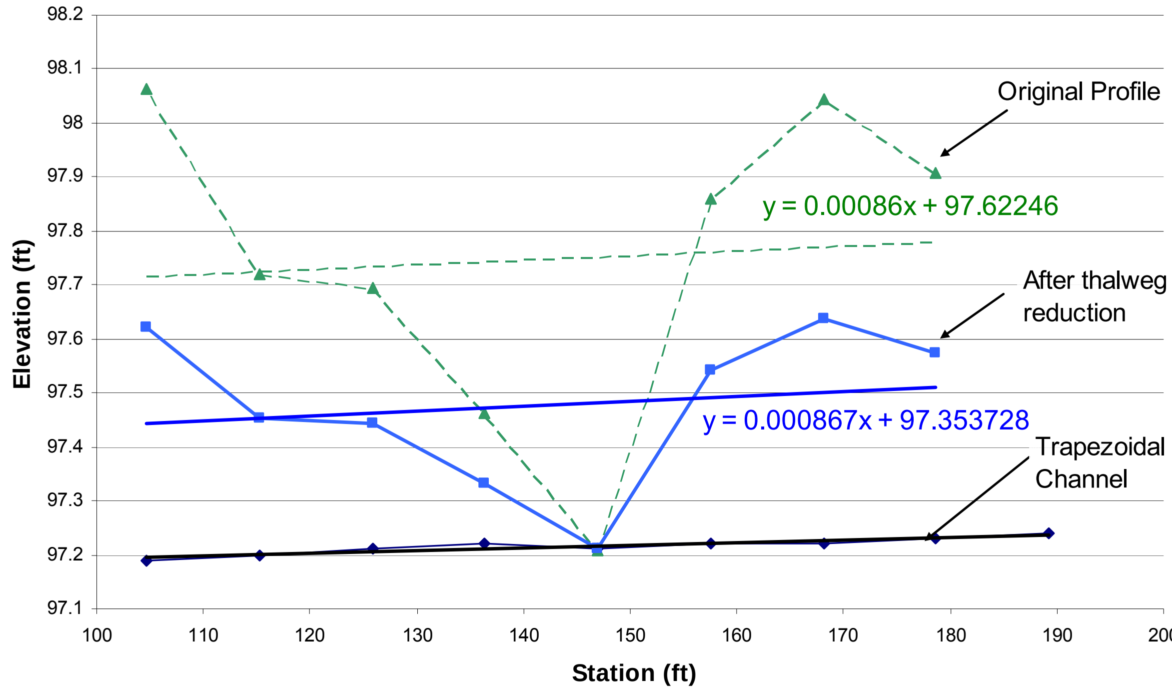

Figure 2.6: Illustration of the 50% Reduction of the Thalweg Amplitude for the San Felipe Reach (Walker 2009)

After reducing the thalweg amplitude, the 16-cfs flow rate was inhibited by a channel restriction located at the Cochiti M2 cross section. The cross section was modified as shown in Figure 2.7 and Figure 2.8. All cross sections developed by Walker (2009) are presented in Appendix A.

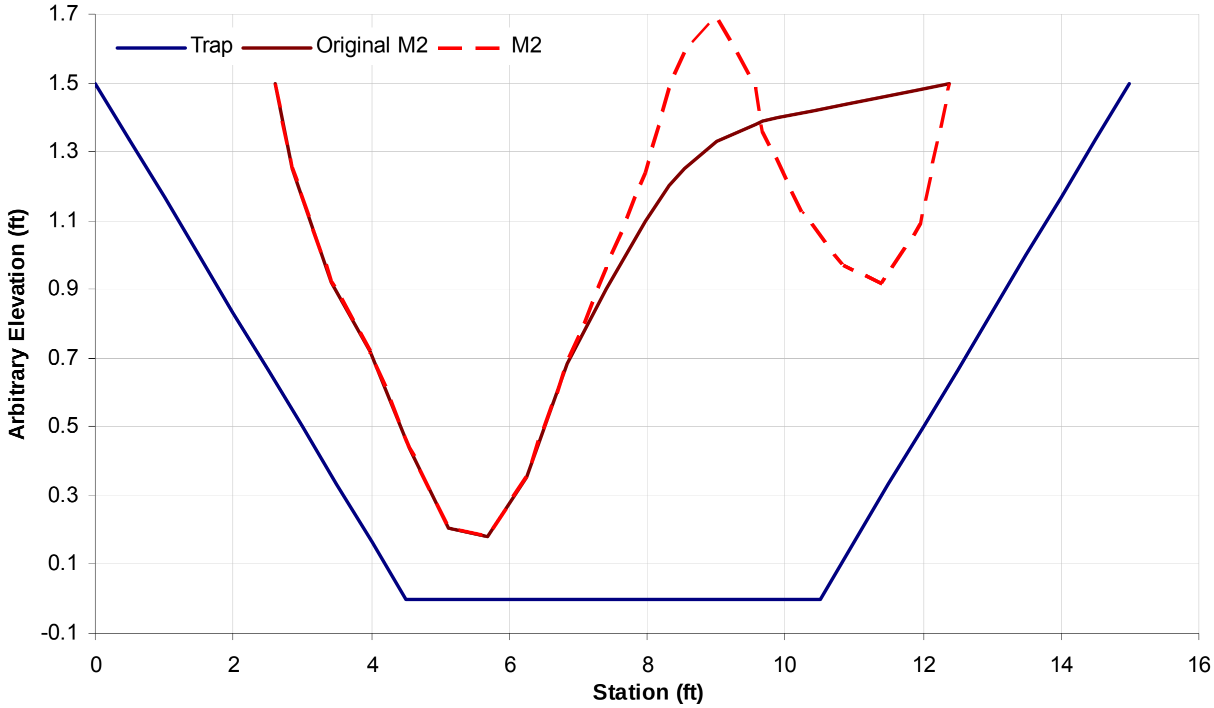

Figure 2.7: Original Design of Cochiti M2 Cross Section (Walker 2009)

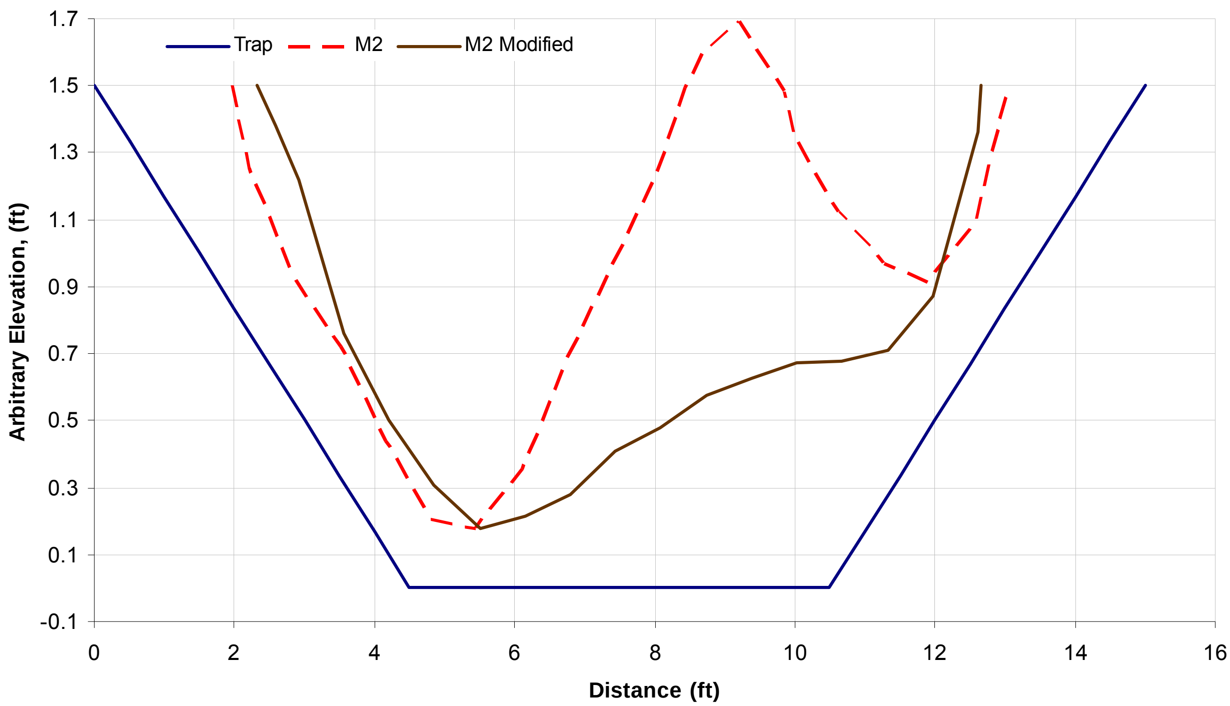

Figure 2.8: Modified M2 Cochiti Cross Section (Walker 2009)

2.4 Construction

The native topography model was designed and built to fit inside the trapezoidal model. Cross-section templates for the aforementioned proposed cross sections were fabricated with 1/2-in. plywood. Due to the 10.5-ft distance between templates, intermediate templates were designed and created by interpolating between cross sections. Figure 2.9 shows how the templates were held in place by cross members creating a skeleton to which the fill material could be applied. A geotextile fabric was placed between the skeleton and the prismatic configuration to ease removal when desired (Walker 2009).

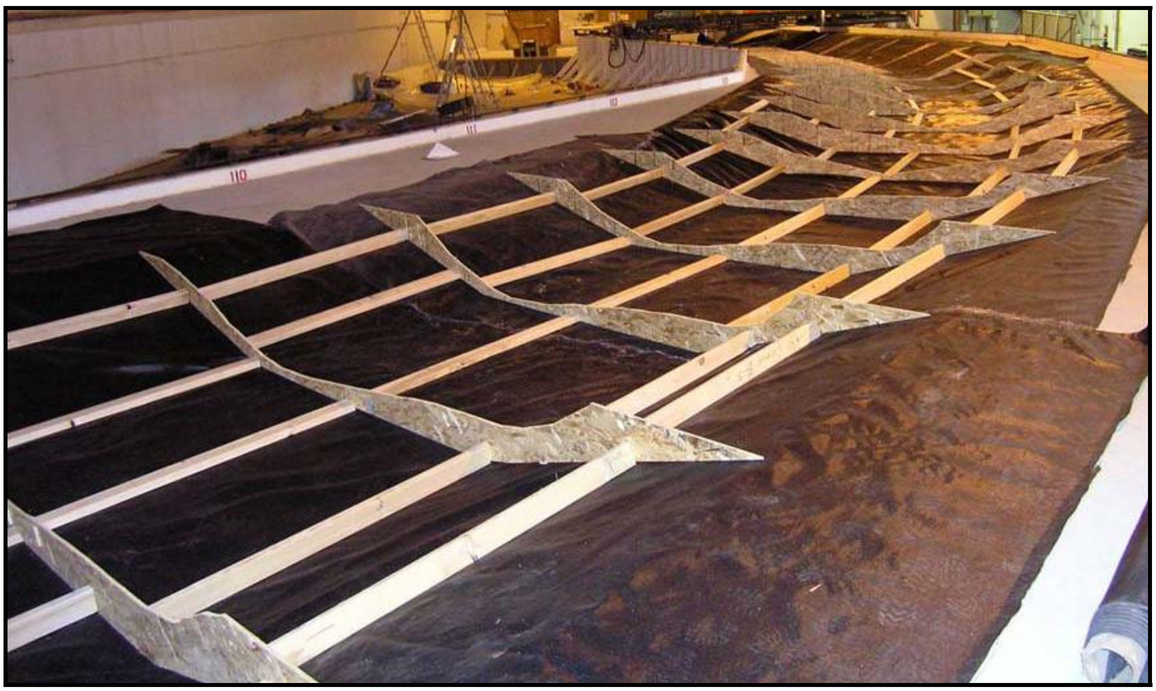

Figure 2.9: Skeleton to Facilitate Pouring of Fill Material (Walker 2009)

A fill material of 1/4-in. rock mixed with Portland cement was chosen to closely match the roughness of the trapezoidal model. Approximately 70 tons of fill material was used to fill the native topography skeleton. The fill material was then skreeted to conform to the template as depicted in Figure 2.10. Portland cement was applied generously to the 1/4-in. rock and cut-down or shifted into the rock with concrete trowels, as shown in Figure 2.11 (Walker 2009). Dowels were used to strengthen steep side slopes during the construction process.

Figure 2.10: Skreeting of Rock Fill (Walker 2009)

Figure 2.11: Shifting or Cutting-down Portland Cement into Gravel (Walker 2009)

After adding the Portland cement to the gravel and re-leveling the mixture to the skeleton, a top coat of cement was added and then sprinkled with water to harden the top layer. After 24 hours, a thorough soaking of water was used to activate the Portland cement in the deeper portions of the mix (Walker 2009).

2.5 Spur-dike Construction

To ensure the correct location of the spur dikes to be constructed, the beginning and end points of the spur dike were surveyed using an arbitrary coordinate system tailored to the Hydromachinery Laboratory and referenced in AutoCAD. The shape of the bed where the spur dike was to be placed was then determined using a bed mapper created with dowel rods that were able to slide to the shape of the bed and then tightened to maintain that position (see Figure 2.12). The dowel-mapped bed was then traced and cut from a piece of 3/4-in. plywood. The tops of the plywood templates were surveyed referencing the proper spur-dike elevation determined by the sum of the depth of flow and the bed elevation at the tip of the spur dike. The spur dikes were then cut to the proper elevation and checked for levelness. An illustration of spur-dike variables is given in Figure 2.13. Finally, the tip of the spur-dike crest was surveyed allowing for the spur-dike face to be drawn and cut out. The plywood template provides vertical reference for rock placement and ensures that the spur dikes are impermeable with respect to the flow, consistent with Heintz (2002).

Figure 2.12: Dowel Bed-mapping Procedure

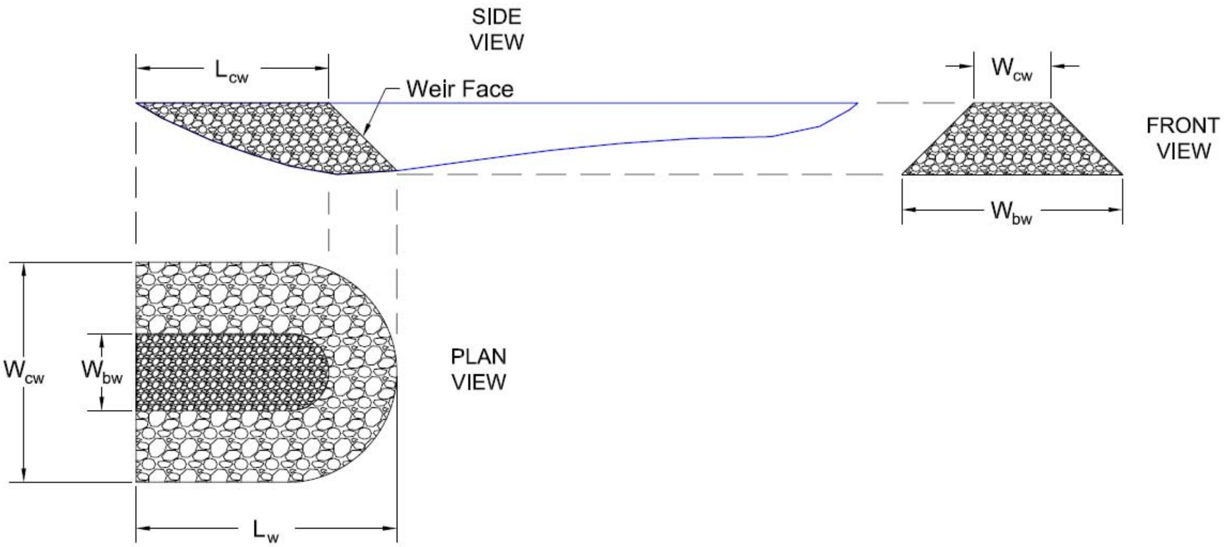

Figure 2.13: Illustration Defining Spur-dike Variables (modified from Heintz (2002))

A plan view or horizontal template was then cut from black plastic. The template consisted of a half circle with a 2-ft radius representing the tip of the spur dike and a 4-ft rectangular portion for the end of the spur dike, which is shown in Figure 2.14. The templates provided a horizontal reference for surveying and rock placement. Once the vertical and horizontal templates were cut to the proper lengths and elevations, 3- to 6-in. rock determined by the intermediate axis, was placed to conform to the templates. An example of rock placement during spur-dike construction is found in Figure 2.15. An estimated crest width of 1 ft was utilized, which was previously determined to provide a suitable prototype construction width, giving dump trucks and other equipment space to operate (Heintz 2002). An as-built survey was then conducted, finalizing the spur-dike construction process.

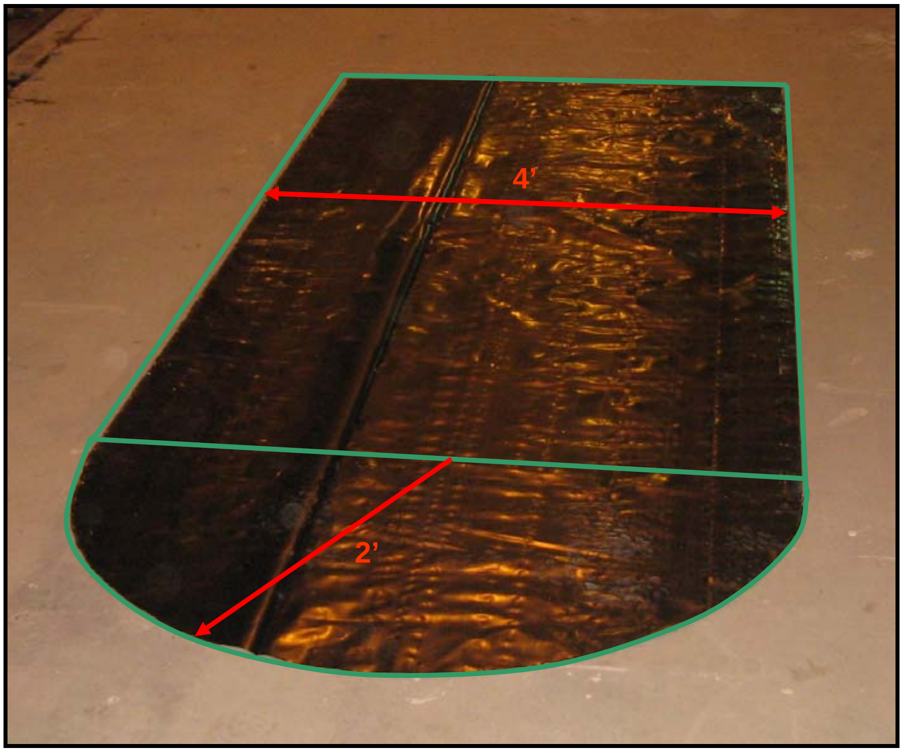

Figure 2.14: Bed Template Used to Determine Rock Placement

(a) plan view (b) profile view

Figure 2.15: Rock Placement

3 TEST PROGRAM

3.1 Test Matrix

For greater efficiency, it was decided to design spur dikes for the native topography model based on findings from the spur-dike tests completed in the prismatic model. The most and least effective designs at reducing outer bank velocities for prismatic configurations were chosen for implementation in the native topography channel. The design characteristics for the spur-dike configurations are presented in Table 3.1.

Table 3.1: Design Characteristics for the Native Topography Spur-dike Design Configurations

Spur-dike Design Configuration	Planform Angle, θ (°)	% XS Flow Area Blocked at 12 cfs	Crest Slope, Φ_w (°)	Flow Rate, Q (cfs)	Bend (Type I or Type III)	Bend (DS or US)	Spacing Ratio, SR
NW01*	90	10.75	0	12	Type III	DS	5.9
NW02**	60	19.40	0	12	Type I	US	3.4
NW03**	60	19.40	0	12	Type III	DS	3.4
NW04*	90	10.75	0	12	Type I	US	5.9

DS = downstream, US = upstream, XS = cross section
* same properties as TSW04 downstream bend (Type III) from trapezoidal testing configuration
** same properties as TSW10 upstream bend (Type I) from trapezoidal testing configuration

3.2 Spur-dike Design

The native topography spur-dike configurations were designed using procedures similar to those used for the prismatic model spur dikes. The native topography design procedures differed from the prismatic procedures because of the variations in cross-sectional geometry. The similarities and differences are described herein.

3.2.1 Prismatic Spur-dike Design

The prismatic design procedure is based on a literature review conducted by Heintz (2002). The premise of the procedure is that the spacing ratio and percent area blocked govern the spur-dike design. The spacing ratio is defined by the length of the arc between spur dikes divided by the length of the spur dikes, which is calculated in Equation 3.1:

$$SR = \frac{L_{arc}}{L_w} \qquad \textbf{Equation 3.1}$$

where

SR = spacing ratio;

L_{arc} = length of arc between spur dikes [L]; and

L_w = length of spur dike [L].

Figure 3.1 depicts the definitions of the variables in Equation 3.1. The length of the spur dikes is a result of percent flow area blocked calculations. Heintz notes that the spacing ratio is a useful tool for design because it can be related to the relative curvature of the bend, which is shown by the final derivation, Equation 3.2. This is important because the relative curvature of the bend is related to migration rates and planform geometry. The lengths of the spur dikes for prismatic spur-dike designs were constant for each design due to the uniform cross-section geometry.

$$SR = R_c \frac{\theta_w}{L_r} \qquad \textbf{Equation 3.2}$$

where

R_c = relative curvature;

θ_w = angle between spur dikes (º); and

L_r = structure length ratio.

Relative curvature may be determined using Equation 3.3:

$$R_c = \frac{r}{TW} \qquad \textbf{Equation 3.3}$$

where

r = radius of curvature [L]; and

TW = channel top width [L].

The structure length ratio is described by Equation 3.4:

$$L_r = \frac{L_w}{TW} \qquad \textbf{Equation 3.4}$$

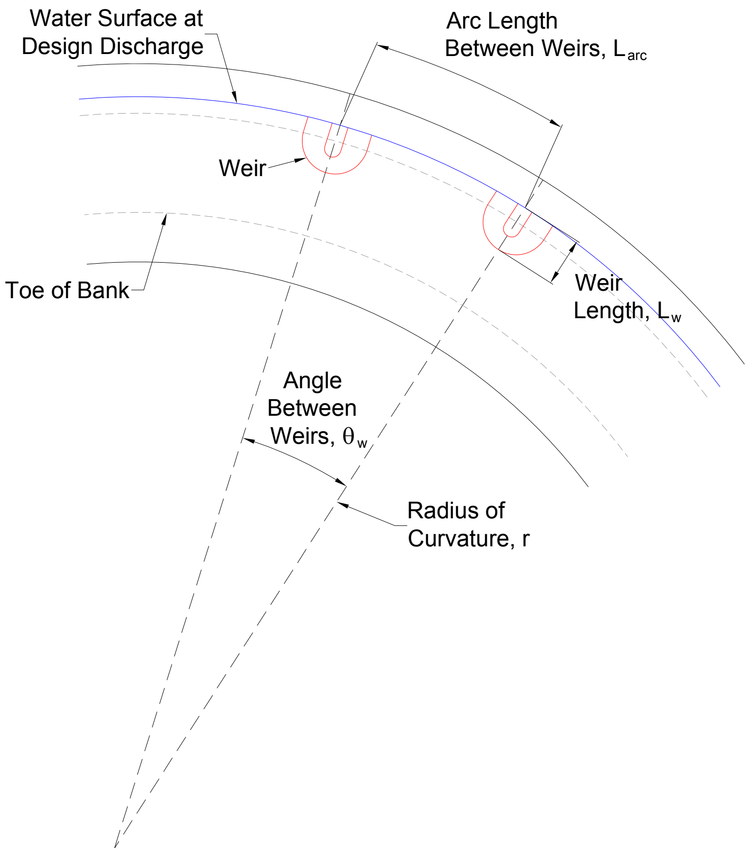

Figure 3.1: Spacing Ratio Variable Description (modified from Heintz (2002))

When designing spur dikes with planform angles other than 90°, perpendicular to the flow, the projected spur-dike length is used to define the spacing ratio, which is shown in Equation 3.5. A definition sketch of the projected spur-dike length is presented in Figure 3.2. Planform angles increase from upstream to downstream from a line drawn tangential to the bank as shown in Figure 3.3.

$$SR = \frac{L_{arc}}{L_{w,proj}}$$ **Equation 3.5**

where

$L_{w,proj}$ = length of the spur dike projected onto the cross section perpendicular to flow [L].

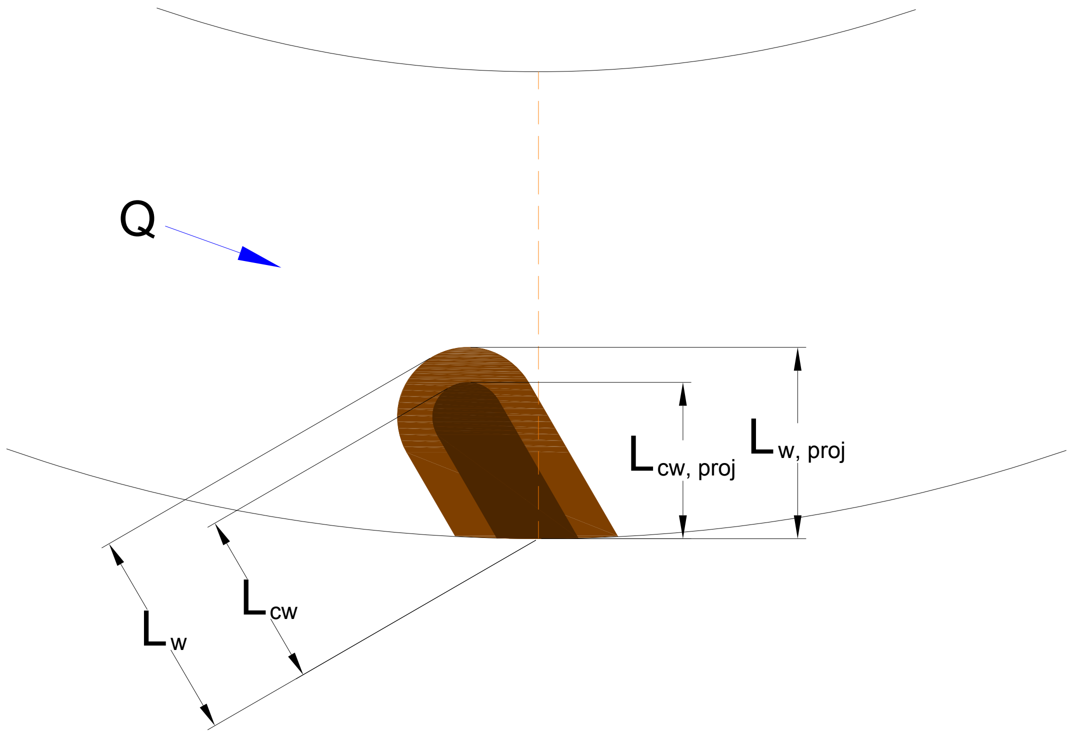

Figure 3.2: Plan View of Spur-dike Length and Projected Length Definitions (modified from Schmidt (2005))

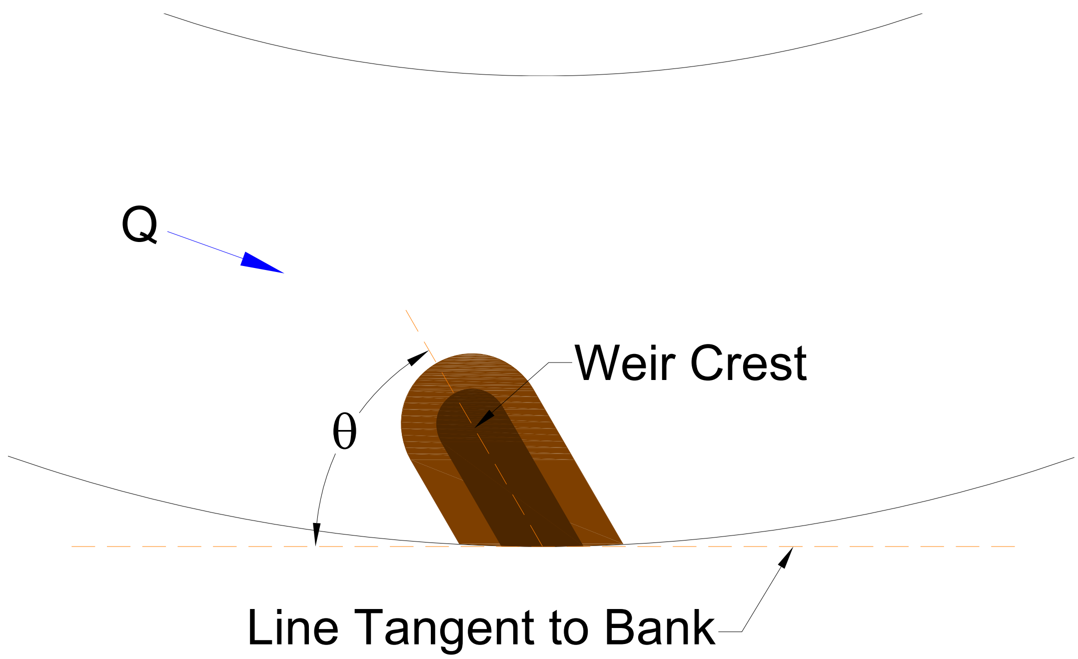

Figure 3.3: Illustration of Spur-dike Planform Angle as it Increases Upstream to Downstream (modified from Darrow (2004))

The number of spur dikes required to satisfy the spacing ratio criteria can be determined with Equation 3.6:

$$\text{Number of Spur Dikes} = \frac{L_B}{L_{arc}} \qquad \textbf{Equation 3.6}$$

where

L_B = length of the bend [L].

The integer of the resultant number of spur dikes is used. To determine the locations of the spur dikes in the bend, the length of the bend not attributed to the length of arc between spur dikes, or the length of the remainder, is needed so that the remainder is accounted for. The length of the remainder is determined using Equation 3.7. The length of the remainder is then distributed equally to the beginning and end of the bend.

$$L_{rem} = L_B - ((\text{Number of Spur Dikes} - 1)L_{arc}) \qquad \textbf{Equation 3.7}$$

where

L_{rem} = length of the remainder [L].

To determine the points of intersection of the spur dikes with the design discharge waterline, a fundamental relationship between the length of an arc and the radius creating the arc can be used to determine the offset angle in radians from the start of the bend. This relationship is shown as Equation 3.8:

$$d\theta = \frac{S}{R} \qquad \textbf{Equation 3.8}$$

where

$d\theta$ = offset angle (radians);

S = arc length [L]; and

R = arc radius [L].

The reader is referred to Schmidt (2005) for information regarding spur-dike designs with variable crest slopes.

3.2.2 NATIVE TOPOGRAPHY SPUR-DIKE DESIGN

Spur-dike variables and definitions for the native topography configurations remain consistent with those of the prismatic configurations. An exception was made to the design procedure to accommodate for variations in spur-dike lengths. Due to the geometric variability throughout natural bends, individual spur-dike lengths differ to retain a specified percent flow area blocked for a given cross section. In order to determine the length of arc between spur dikes (L_{arc}) as defined by Heintz (2002), a single value for the length of spur dikes is required. The result is an average spur-dike length taken as a cross-sectional spur-dike average ($\overline{L}_{xsweiravg}$), which is determined by taking the average of the lengths of spur dikes projected perpendicular to the flow for representative cross sections throughout the bend as a result of fulfilling percent flow area blocked criterion. The $\overline{L}_{xsweiravg}$ is then used in conjunction with a given spacing ratio (SR) to determine the length of arc between spur dikes as shown in Equation 3.9:

$$L_{arc} = SR \cdot \overline{L}_{xsweiravg}$$ **Equation 3.9**

where

$\overline{L}_{xsweiravg}$ = average spur-dike length taken as a cross-sectional spur-dike average [L].

The number of spur dikes required to satisfy the spacing ratio criterion can be determined with Equation 3.10, where L_B is the length of the bend:

$$\text{Number of Spur Dikes} = \frac{L_B}{L_{arc}}$$ **Equation 3.10**

The integer of the resultant number of spur dikes is used. To determine the locations of the spur dikes in the bend, the length of the bend not attributed to the length of arc between spur dikes is needed so that the remainder is accounted for. The length of the remainder (L_{rem}) is determined using Equation 3.11. The length of the remainder is then distributed equally to the beginning and end of the bend.

$$L_{rem} = L_B - \left(\left(\text{Number of Spur Dikes} - 1\right) L_{arc}\right)$$ **Equation 3.11**

To determine the points of intersection of the spur dikes with the design discharge waterline, the fundamental relationship given by Equation 3.12 is used to determine the offset angle in radians from the start of the bend:

$$d\theta = \frac{L}{R}$$ **Equation 3.12**

Converting these values to degrees, the designer is able to successively determine the locations of each spur dike throughout the bend as shown in Figure 3.4. The cross sections perpendicular to the flow with end points at the spur-dike locations and the design discharge waterline on the opposite bank are then used to determine the final design spur-dike lengths based on the percent flow area blocked criteria.

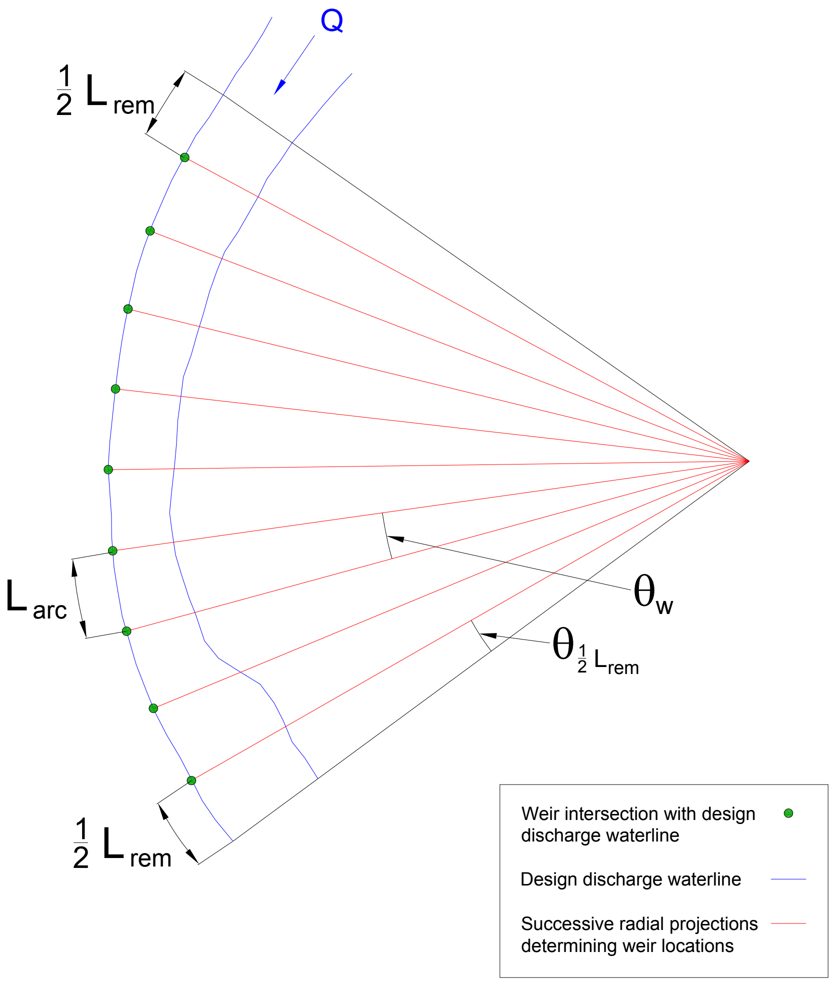

Figure 3.4: Illustration of Spur-dike Locations as a Result of Design Procedure

When a spur-dike planform angle is chosen that is not perpendicular to the flow, 90°, the percent flow area blocked is based on the flow depths and cross-section variations of the perpendicular cross section, or projected length as defined in Figure 3.2. This decision was made because of the difficulty for designers to obtain cross-section information at variable planform angles and to remain consistent with the prismatic design procedure.

4 DATA COLLECTION

4.1 Data-collection Locations

To determine differences created by spur-dike fields and the effects of individual spur dikes, two types of data-collection locations were created: cross-section and spur-dike locations. The cross-section locations allow for an analysis of differential conveyances as a result of spur-dike placement to baseline conditions. The spur-dike locations allow for a more in depth understanding of flow around individual spur dikes.

4.1.1 Cross-section Data-collection Locations

Data-collection locations (DCLs) at individual cross sections were determined by the use of the equal top width method for the eighteen cross sections along the model reach. This method subdivides the design discharge channel width into equal segments where the midpoint of each segment is taken as the testing location. This method allows for estimates of flow conveyance under natural circumstances (Walker 2009). To remain consistent with the testing procedures used to collect data in the prismatic model, the cross sections were divided into seven segments. Figure 4.1 shows the model cross-section data-collection locations. Each of the seven segments contains a data-collection location for the cross-section at which it is located. Each cross-section data-collection location is denoted by the cross-section number and a letter. The letter designation ranges from a to g depending upon its proximity to the left channel bank. The designations are discussed further in Chapter 5.

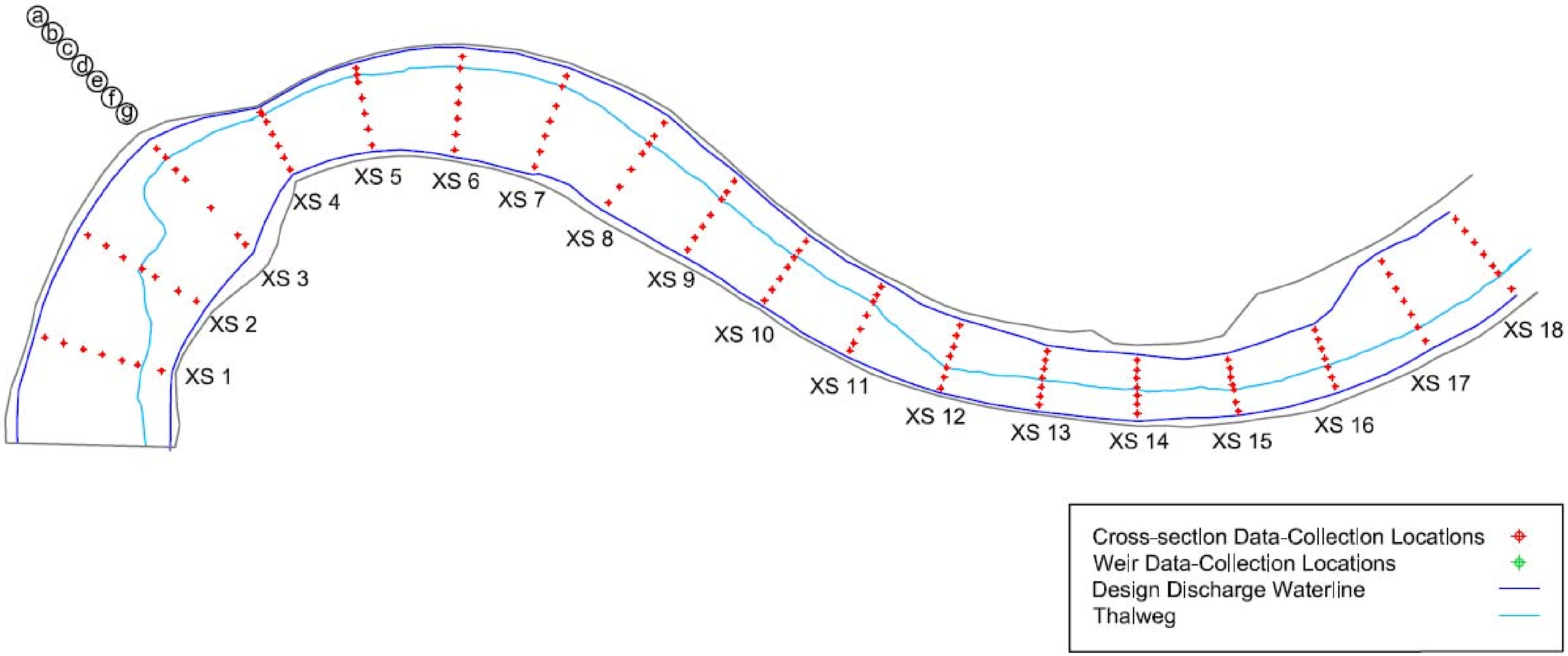

Figure 4.1: Model Cross-section Locations and DCLs (modified from Walker (2009))

Some exceptions to the equal top width method were made to gather data at areas of interest, or where testing locations were not feasible. An exception made was to use the thalweg as the testing location as opposed to the midpoint of the segment encompassing the thalweg. When this occurred, data-collection location points were recalculated and spaced evenly based on the remainder of the width from the thalweg to the far bank. Cross Sections 5, 8, 10, and 11 were affected by thalweg proximity (Walker 2009). At data-collection locations on steep banks, testing was found to be too difficult. When steep banks were present after the equal top width determination, the water surface station adjacent to the steep bank and adjacent thalweg station were averaged together to determine a comparable data-collection location. This occurred at Cross Sections 3 and 4 (Walker 2009). The reader is referred to Walker (2009) for further information regarding the decision to use the equal top width method.

4.1.2 SPUR-DIKE DATA-COLLECTION LOCATIONS

Spur-dike data-collection locations for the native topography configurations were determined in such a manner to remain as consistent as possible with prismatic spur-dike data-collection locations. Due to the inability to define the bank toe, which was referenced by prismatic data-collection locations, an estimated comparable length of 2 ft from the waterline was used as the distance projected perpendicular to the flow for the inner and outer bank positions. The upstream (US), downstream (DS), and center spur-dike locations are located 1 ft from the edge of the corresponding spur dike. Figure 4.2 depicts the various spur-dike data-collection locations and corresponding names. Nomenclature used for database development refers to either the bank or spur-dike position and the corresponding descriptive location. An example of this would be “spur-dike position – upstream and bank position – outer” which would refer to the testing location 2 ft from the waterline as projected perpendicular to the flow on the outer bank and 1 ft from the spur-dikes edge on the upstream spur-dike face. The center spur-dike locations were determined by use of AutoCAD and a line projected from the center of the radius of curvature to the perpendicular face of the spur dike for planform angles other than 90°. Spur-dike positions referred to as “between” were determined by dividing the L_{arc} in half or by radial projection from the center of an adjacent spur dike ($\theta_w/2$). Each spur dike has a total of seven testing locations.

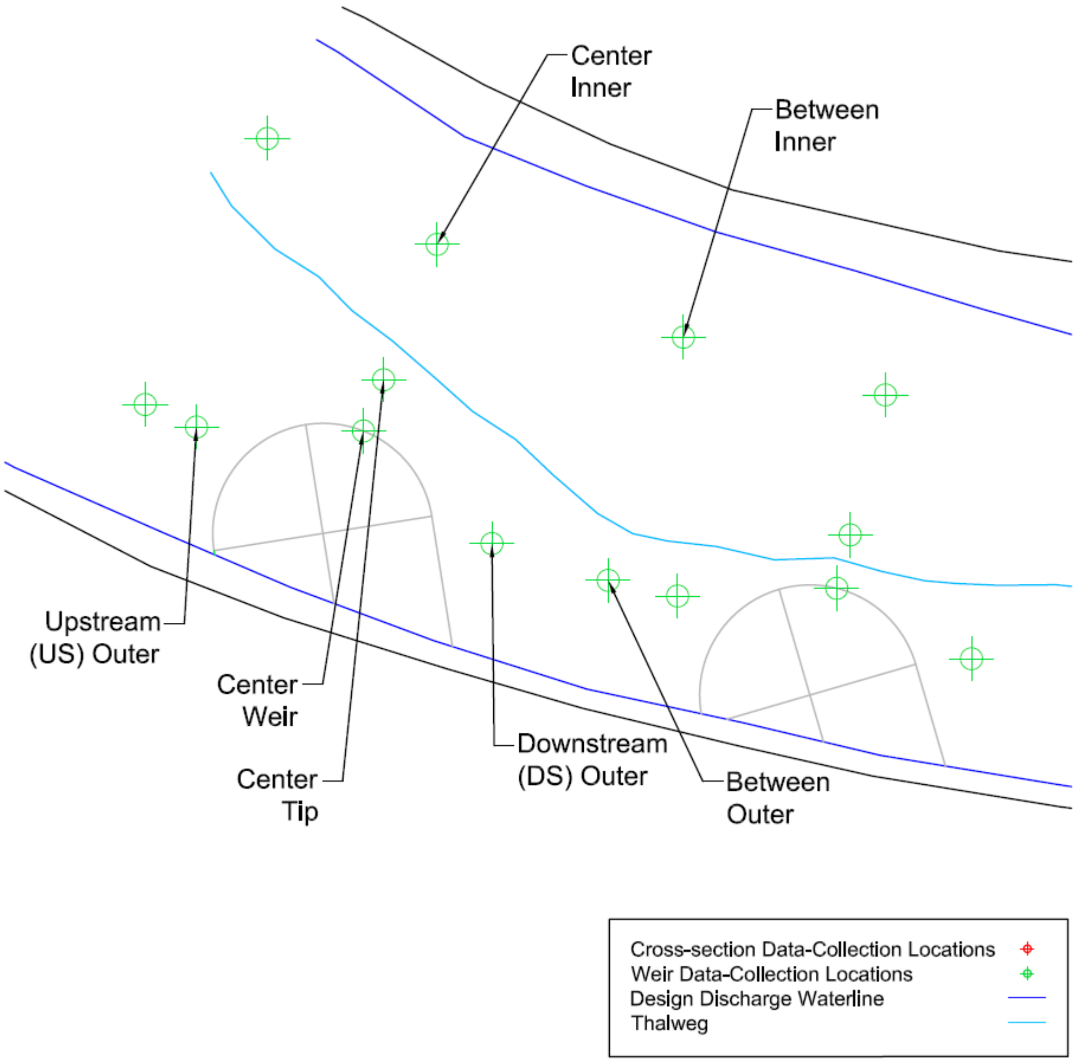

Figure 4.2: Example of Spur-dike DCLs (not to scale)

4.2 INSTRUMENTATION

Data acquisition included flow velocity, shear stress, and depth measurements at the various data-collection locations throughout the model. A mobile data-acquisition cart, shown in Figure 4.3, is equipped with the instrumentation used to collect the aforementioned parameters. The instrumentation is described in further detail in the following sections.

Figure 4.3: Data-acquisition Cart

4.2.1 FLOW RATE MEASUREMENT

The laboratory is equipped with two 85-horsepower pumps that recirculate flow to the headbox through two 12-in. polyvinyl chloride (PVC) pipes from a sump located at the downstream end of the model. The flow is controlled by butterfly valves mounted on a bypass that diverts flow back to the sump. The flow rate is maintained by additional butterfly valves that create back pressure to the pumps. The flow is measured by a Georg Fischer® SIGNET 2550 Insertion Magmeter installed in each pipe as shown in Figure 4.4. The SIGNET 2550 is accurate within ±2%. The magmeters are supplemented with digital readouts both at the valves and the data-acquisition cart.

(a) SIGNET 2550 Insertion Magmeters (b) digital display boxes

Figure 4.4: Flow Measurement Instrumentation (Kinzli 2005)

4.2.2 FLOW DEPTH MEASUREMENTS

The flow depth was measured at each testing location with the use of a standard point gage capable of measuring ±0.001 ft. The point gage is mounted on the cart and leveled to ensure accurate results. The flow depth is calculated as the difference between bed and water surface elevations.

4.2.3 FLOW VELOCITY MEASUREMENTS

Three-dimensional flow velocity measurements were taken with a SonTek® Acoustic Doppler Velocimeter (ADV). The probe has three arms corresponding to the x, y, and z axes which relate to the downstream, lateral, and vertical flow directions, respectively. Flow velocity measurements were recorded by a personal computer at a rate of 25 Hz for 60 sec. It is important to note that the sampling rate for the prismatic configurations was 10 Hz for 30 sec. The ADV probe was mounted on a standard point gage, shown in Figure 4.5, to ensure accuracy of the testing locations throughout the water column. The sampling volume is located 0.164 ft (5 cm) below the acoustic transmitter. The offset hinders measurements in the upper portion of the water column at low flow depths. For example, a flow depth less than 1.64 ft would limit data collection at the 10% depth location. The ADV probe was mounted such that the downstream direction was perpendicular to the cart, which in turn was oriented perpendicular to the flow.

The data were later processed with WinADV software where summaries of the data collected are calculated.

Figure 4.5: ADV Mounted on Point Gage and Data-acquisition Cart (Darrow 2004)

4.2.4 SHEAR STRESS MEASUREMENTS

Shear stress was measured by utilizing a Preston Tube, which is capable of taking direct measurements on the bed and banks from the data-acquisition cart. The Preston Tube has two tubes: a 1/4-in. bottom tube with an 11/64-in. port open to the current that collects the dynamic pressure, and 1/8-in. upper tube that receives the hydrostatic pressure through two small 1/32-in. ports on each side of the tube that are directed perpendicular to the flow. Figure 4.6 shows the two tubes of the Preston Tube. The differential pressure between the two tubes is the flow velocity head which is read by a Rosemount, low-range (maximum: 5 in.), pressure transducer. The signal is then relayed to the computer where LABView, data-acquisition software by National Instruments, Inc., records and processes the data over 30-sec intervals. The data are initially processed by converting the receiving amps to a voltage based on a scale of 4 to 20 mA corresponding to 1 to 5 Volts (V) by Ohm's Law. The recorded voltage is converted to differential pressure in inches by Equation 4.1. Finally, the shear stress is calculated based on a calibration conducted by Sclafani (2009). The calibration equation for the native topography bed is given in Equation 4.2:

$$dH = 0.75dV - 0.75$$ **Equation 4.1**

where

dH = differential head in inches [L]; and

dV = differential voltage recorded [$L^2MT^{-2}Q^{-1}$].

$$\tau_0 = 0.2986 \cdot dH$$ **Equation 4.2**

where

τ_o = boundary shear stress in pounds per square foot (psf) [$ML^{-1}T^{-2}$].

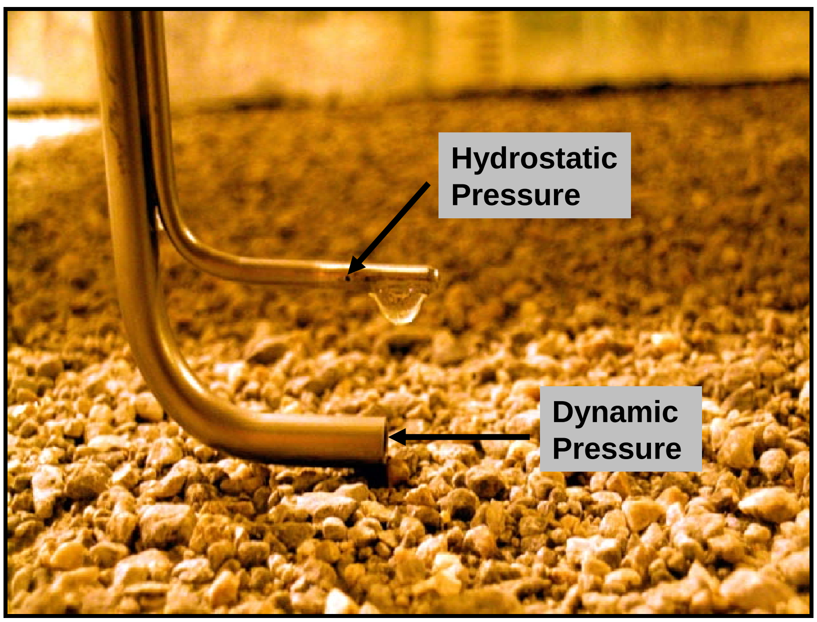

Figure 4.6: Preston Tube Illustration (modified from Sclafani (2009))

4.3 TEST PROCEDURE

The testing sequence begins by stabilizing the flow at the design discharge of 12 cfs, after filling the sump with water supplied by a 36-in. line connected directly to Horsetooth Reservoir. Cart locations are predetermined by cross referencing tape measurements along the channel with AutoCAD. These reference locations are checked by surveying with a total station using an arbitrary coordinate system tailored to the Hydromachinery Laboratory. Percent depths for cross-section and spur-dike data-collection locations for the ADV data collection were predefined by the USBR. The percent depths for spur-dike locations were originally specified as 5%-depth increments but changed by the USBR for the NW03 and NW04 tests. The percent depths at which ADV data were collected and the corresponding total number of test points are given in Table 4.1. Figure 4.7 and Figure 4.8 show the cross-section data-collection locations and the number of ADV data test points for both bends. The percent depths are based on the total flow depth at each location.

Table 4.1: Percent Depths per DCL Determination

	Number of Test Points						
Percent Depth of Tests	**25**	**23**	**21**	**19**	**15**	**13**	**9**
	97.5%	97.5%	97.5%	97.5%	95.0%	95.0%	95.0%
	95.0%	95.0%	95.0%	95.0%	92.5%	92.5%	92.5%
	92.5%	92.5%	92.5%	92.5%	90.0%	90.0%	90.0%
	90.0%	90.0%	90.0%	90.0%	87.5%	87.5%	85.0%
	87.5%	87.5%	87.5%	87.5%	85.0%	85.0%	80.0%
	85.0%	85.0%	85.0%	85.0%	82.5%	80.0%	70.0%
	80.0%	80.0%	80.0%	80.0%	80.0%	75.0%	50.0%
	77.5%	77.5%	75.0%	75.0%	75.0%	70.0%	30.0%
	75.0%	75.0%	70.0%	70.0%	70.0%	65.0%	10.0%
	72.5%	70.0%	65.0%	65.0%	65.0%	60.0%	
	70.0%	65.0%	60.0%	60.0%	60.0%	50.0%	
	67.5%	60.0%	55.0%	55.0%	55.0%	30.0%	
	65.0%	55.0%	50.0%	50.0%	50.0%	10.0%	
	60.0%	50.0%	45.0%	45.0%	30.0%		
	55.0%	45.0%	40.0%	40.0%	10.0%		
	50.0%	40.0%	35.0%	35.0%			
	45.0%	35.0%	30.0%	30.0%			
	40.0%	30.0%	25.0%	20.0%			
	35.0%	25.0%	20.0%	10.0%			
	30.0%	20.0%	15.0%				
	25.0%	15.0%	10.0%				
	20.0%	10.0%					
	15.0%	5.0%					
	10.0%						
	5.0%						

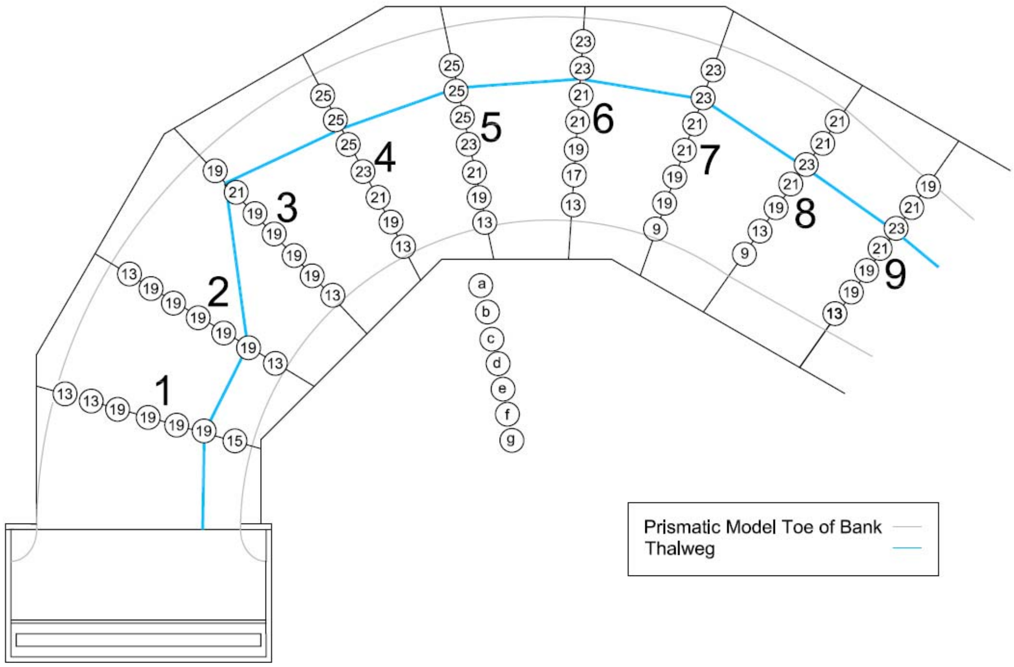

Figure 4.7: Upstream or Cochiti Bend Cross-section DCLs with Reference to Number of Test Points

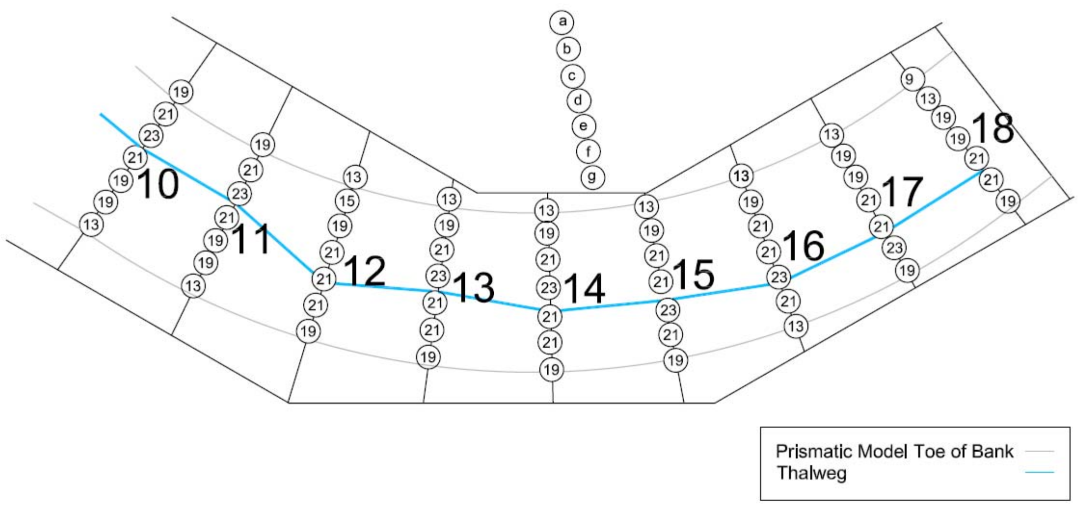

Figure 4.8: Downstream or San Filipe Bend Cross-section DCLs with Reference to Number of Test Points

Shear stress measurements were taken at each testing location after ensuring the validity of the zero-differential pressure at each cross section. The zero-differential pressure was validated by placing the Preston Tube in a bucket filled with still water. The data were later processed and stored in a database.

5 COMPLETED NATIVE TOPOGRAPHY SPUR-DIKE CONFIGURATIONS

The designated testing configurations include four spur-dike designs:

1. Native Topography Spur-dike Design 1 (NW01),
2. Native Topography Spur-dike Design 2 (NW02),
3. Native Topography Spur-dike Design 3 (NW03), and
4. Native Topography Spur-dike Design 4 (NW04).

Each of these spur-dike designs was developed based on the geometric parameters outlined in the testing matrix presented in Table 3.1. The geometric parameters presented in Table 3.1 were determined based on the prismatic model test configurations TSW04 and TSW10, which are presented in

Table 5.1. The data collected from each configuration include flow depths, velocities, and boundary shear stress, which are reported in the accompanying Electronic Appendix. Appendices B, C, and D provide plots of the water surface profiles, flow velocity vectors, and shear stresses from the Preston tube measurements, respectively. The flow velocity vector plots presented in Appendix C utilize the U flow velocity vector and V flow velocity vector as presented with the accompanying flow velocity data. The U vector is the flow velocity vector in the x-direction corrected so as to account for the data-collection cart position. The V vector is the flow velocity vector in the y-direction, accounting for the data-collection cart position. The shear stress plots in Appendix D were developed by creating rasters for the collected shear stress data in ArcMAP. The rasters were created using the minimum curvature Spline interpolation. The parameters for this interpolation were a tension spline, a weighting factor of 0.05, 6 points, and an output cell size of 0.18588.

Table 5.1: Prismatic Model Test Configurations (modified from Schmidt (2005))

Prismatic Model Configuration	Planform Angle, θ (°)	% XS Flow Area Blocked at 12 cfs	Crest Slope, Φ_w (°)	Flow Rate, Q (cfs)	Bend (Type I or Type III)	Bend (DS or US)	Spacing Ratio, SR
TSW04	90	10.75	0	12	Type III	DS	5.9
TSW10	60	19.40	0	12	Type I	US	3.4

DS = downstream, US = upstream, XS = cross section

5.1 NATIVE TOPOGRAPHY SPUR-DIKE DESIGN 1 (NW01)

NW01 spur dikes were designed based on the geometric parameters used for the design of prismatic test Configuration TSW04, described in Table 5.1, located in the downstream bend. The TSW04 spur-dike design was the least effective of the prismatic spur-dike designs. The NW01 design parameters and spur-dike dimensions are presented in Table 5.2. The NW01 design using these parameters resulted in a total of eight spur dikes, which were distributed evenly throughout the Cochiti (or downstream) bend. Figure 5.1 shows the NW01 spur dikes at the design discharge. The NW01 spur dikes and data-collection locations are plotted in Figure 5.2.

Table 5.2: NW01 Spur-dike Design Parameters and Results

Spur-dike Number	Planform Angle, θ (°)	% XS Flow Area Blocked	Spacing Ratio, SR	Bend (DS or US)	L_B (ft)	L_w (ft)	L_{cw} (ft)	XS Flow Area Blocked (ft^2)	Calculated % XS Flow Area Blocked
1	90	10.75	5.9	DS	90.61	2.23	1.71	0.64	10.81%
2	90	10.75	5.9	DS	90.61	2.00	1.34	0.54	10.79%
3	90	10.75	5.9	DS	90.61	1.78	0.94	0.62	10.75%
4	90	10.75	5.9	DS	90.61	1.52	0.83	0.52	10.82%
5	90	10.75	5.9	DS	90.61	1.47	0.79	0.45	10.85%
6	90	10.75	5.9	DS	90.61	1.71	1.01	0.52	10.93%
7	90	10.75	5.9	DS	90.61	1.83	1.08	0.65	10.76%
8	90	10.75	5.9	DS	90.61	2.00	1.34	0.58	10.90%

DS = downstream, US = upstream, XS = cross section

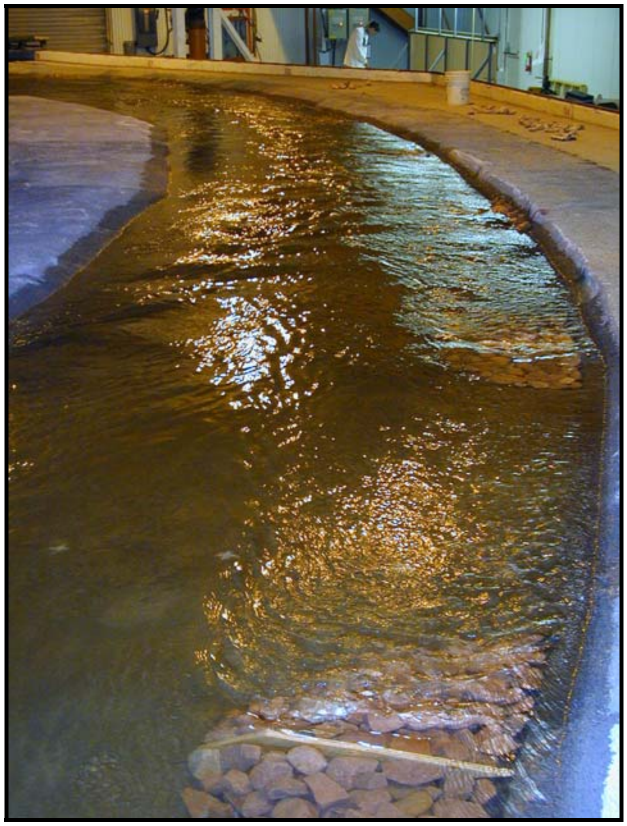

Figure 5.1: NW01 Spur Dikes at Design Discharge Looking Downstream

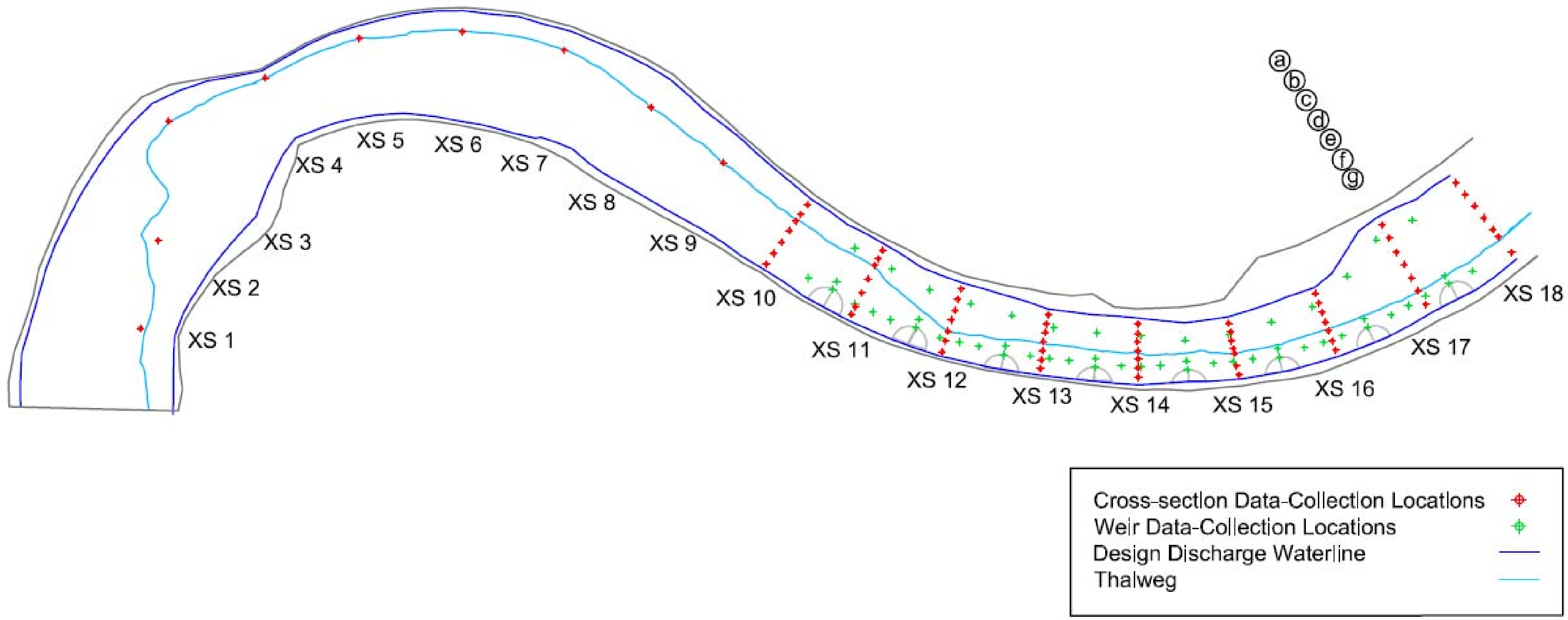

Figure 5.2: NW01 Configuration with Data-collection Locations

5.2 NATIVE TOPOGRAPHY SPUR-DIKE DESIGN 2 (NW02)

The NW02 configuration was designed based on the geometric parameters used for the design of prismatic test configuration TSW10, described in Table 5.1, located in the San Felipe, or upstream, bend. The TSW10 spur-dike design was the most effective of the prismatic spur-dike designs. Table 5.3 provides the spur-dike design parameters as well as the spur-dike dimensions from the native topography spur-dike design. The NW02 spur dikes are presented as installed and during testing at the design discharge in Figure 5.3. The NW02 spur dikes and data-collection locations are plotted in Figure 5.4.

Table 5.3: NW02 Spur-dike Design Parameters and Results

Spur-dike Number	Planform Angle, θ (º)	% XS Flow Area Blocked	Spacing Ratio, *SR*	Bend (DS or US)	L_B (ft)	L_w (ft)	L_{cw} (ft)	XS Flow Area Blocked (ft^2)	Calculated % XS Flow Area Blocked
1	60	19.40	3.4	US	99.40	5.88	5.12	2.49	19.42%
2	60	19.40	3.4	US	99.40	4.91	4.13	2.43	19.40%
3	60	19.40	3.4	US	99.40	5.05	4.28	2.28	19.37%
4	60	19.40	3.4	US	99.40	3.74	2.76	1.78	19.36%
5	60	19.40	3.4	US	99.40	2.45	1.32	1.36	19.43%
6	60	19.40	3.4	US	99.40	2.39	1.29	1.43	19.39%
7	60	19.40	3.4	US	99.40	3.25	2.15	1.58	19.40%
8	60	19.40	3.4	US	99.40	3.28	2.32	1.49	19.41%
9	60	19.40	3.4	US	99.40	2.88	2.00	1.11	19.45%

DS = downstream, US = upstream, XS = cross section

(a) installed spur dikes (b) spur dikes during testing

Figure 5.3: NW02 Spur-dike Configuration

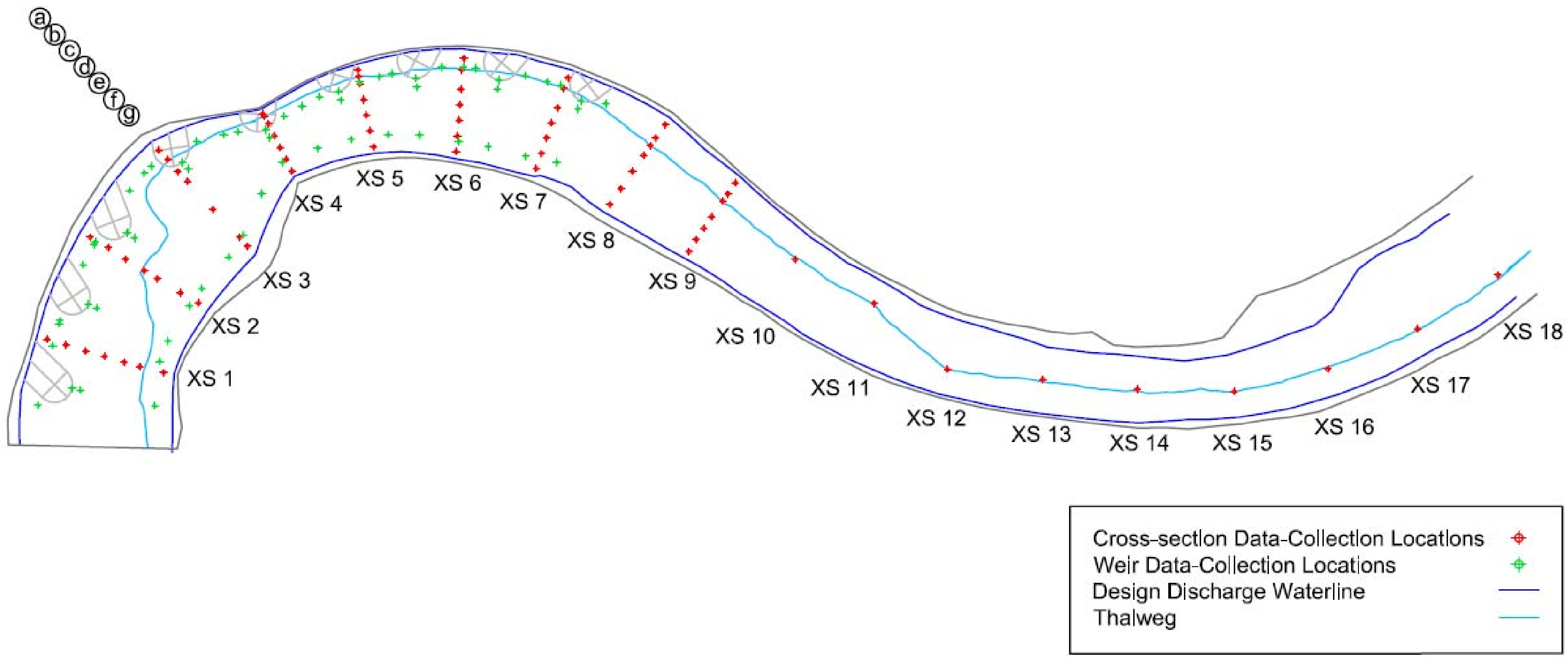

Figure 5.4: NW02 Configuration with Data-collection Locations

5.3 NATIVE TOPOGRAPHY SPUR-DIKE DESIGN 3 (NW03)

The NW03 Configuration was designed based on the same geometric parameters as NW02, prismatic test configuration TSW10, except it was designed to be installed in the downstream bend. Table 5.4 provides the spur-dike design parameters as well as the spur-dike dimensions from the native topography spur-dike design. The NW03 spur dikes are shown as installed and during testing at the design discharge in Figure 5.5. The NW03 spur dikes and data-collection locations are plotted in Figure 5.6.

Table 5.4: NW03 Spur-dike Design Parameters and Results

Spur-dike Number	Planform Angle, θ (º)	% XS Flow Area Blocked	Spacing Ratio, *SR*	Bend (DS or US)	L_B (ft)	L_w (ft)	L_{cw} (ft)	XS Flow Area Blocked (ft^2)	Calculated % XS Flow Area Blocked
1	60	19.40	3.4	DS	90.61	3.51	2.92	1.20	19.45%
2	60	19.40	3.4	DS	90.61	3.29	2.59	0.92	19.41%
3	60	19.40	3.4	DS	90.61	2.89	1.93	1.04	19.45%
4	60	19.40	3.4	DS	90.61	2.70	1.76	0.95	19.43%
5	60	19.40	3.4	DS	90.61	2.68	1.66	0.97	19.42%
6	60	19.40	3.4	DS	90.61	2.76	1.72	0.88	19.41%
7	60	19.40	3.4	DS	90.61	3.08	2.07	0.96	19.43%
8	60	19.40	3.4	DS	90.61	3.45	2.48	1.13	19.45%
9	60	19.40	3.4	DS	90.61	3.31	2.54	1.02	19.46%

DS = downstream, US = upstream, XS = cross section

(a) installed spur dikes (b) spur dikes during testing

Figure 5.5: NW03 Spur-dike Configuration

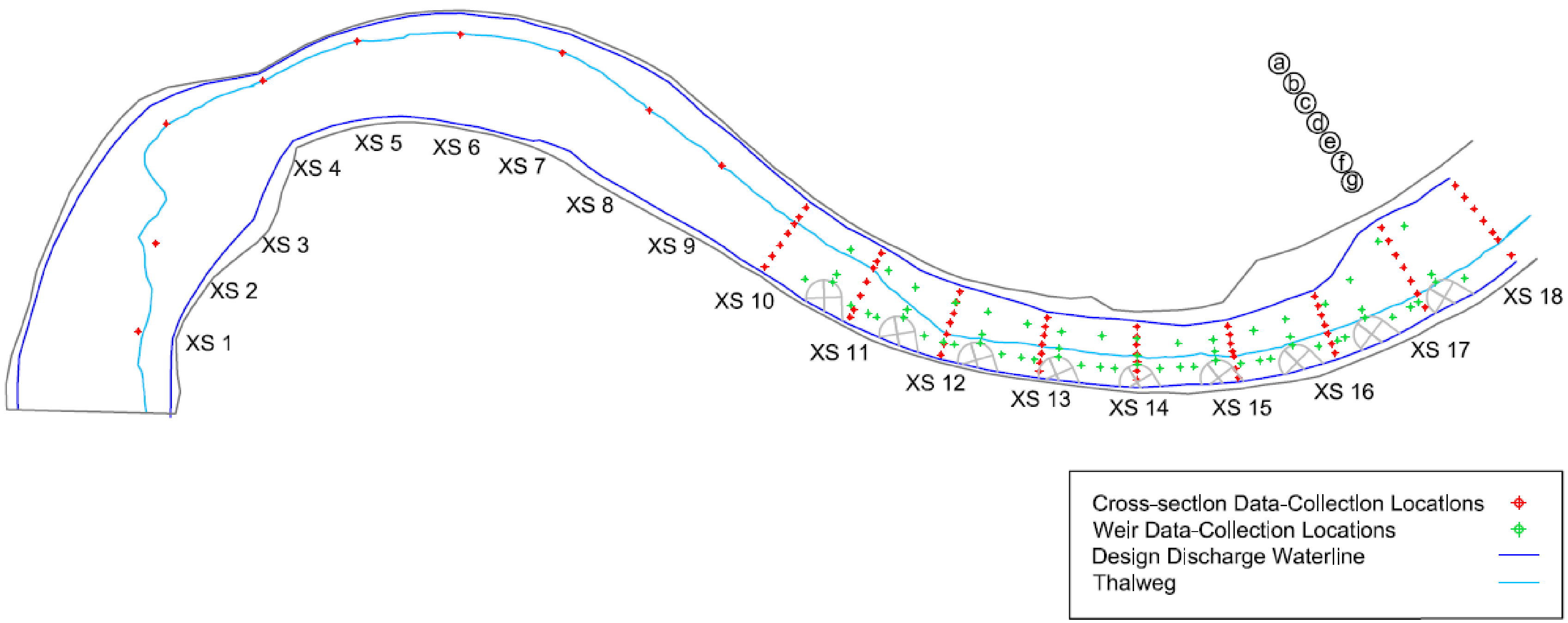

Figure 5.6: NW03 Configuration with Data-collection Locations

5.4 NATIVE TOPOGRAPHY SPUR-DIKE DESIGN 4 (NW04)

NW04 spur-dikes were designed with the same geometric parameters as the NW01 spur-dikes installed in the upstream bend. The NW04 spur-dike design parameters as well as the spur-dike dimensions are found in Table 5.5. Figure 5.7 shows NW04 spur dikes as installed and during testing at the design discharge. The NW04 spur dikes and data-collection locations are plotted in Figure 5.8.

Table 5.5: NW04 Spur-dike Design Parameters and Results

Spur-dike Number	Planform Angle, θ (°)	% XS Flow Area Blocked	Spacing Ratio, *SR*	Bend (DS or US)	L_B (ft)	L_w (ft)	L_{cw} (ft)	XS Flow Area Blocked (ft^2)	Calculated % XS Flow Area Blocked
1	90	10.75	5.9	US	99.40	3.15	2.61	1.16	10.76%
2	90	10.75	5.9	US	99.40	2.93	2.16	1.34	10.75%
3	90	10.75	5.9	US	99.40	2.57	1.66	0.92	10.77%
4	90	10.75	5.9	US	99.40	1.42	0.35	0.67	10.83%
5	90	10.75	5.9	US	99.40	1.71	0.59	0.70	10.73%
6	90	10.75	5.9	US	99.40	1.89	0.86	0.72	10.74%
7	90	10.75	5.9	US	99.40	1.90	0.94	0.62	10.82%

DS = downstream, US = upstream, XS = cross section

(a) installed spur dikes

(b) spur dikes during testing

Figure 5.7: NW04 Spur-dike Configuration

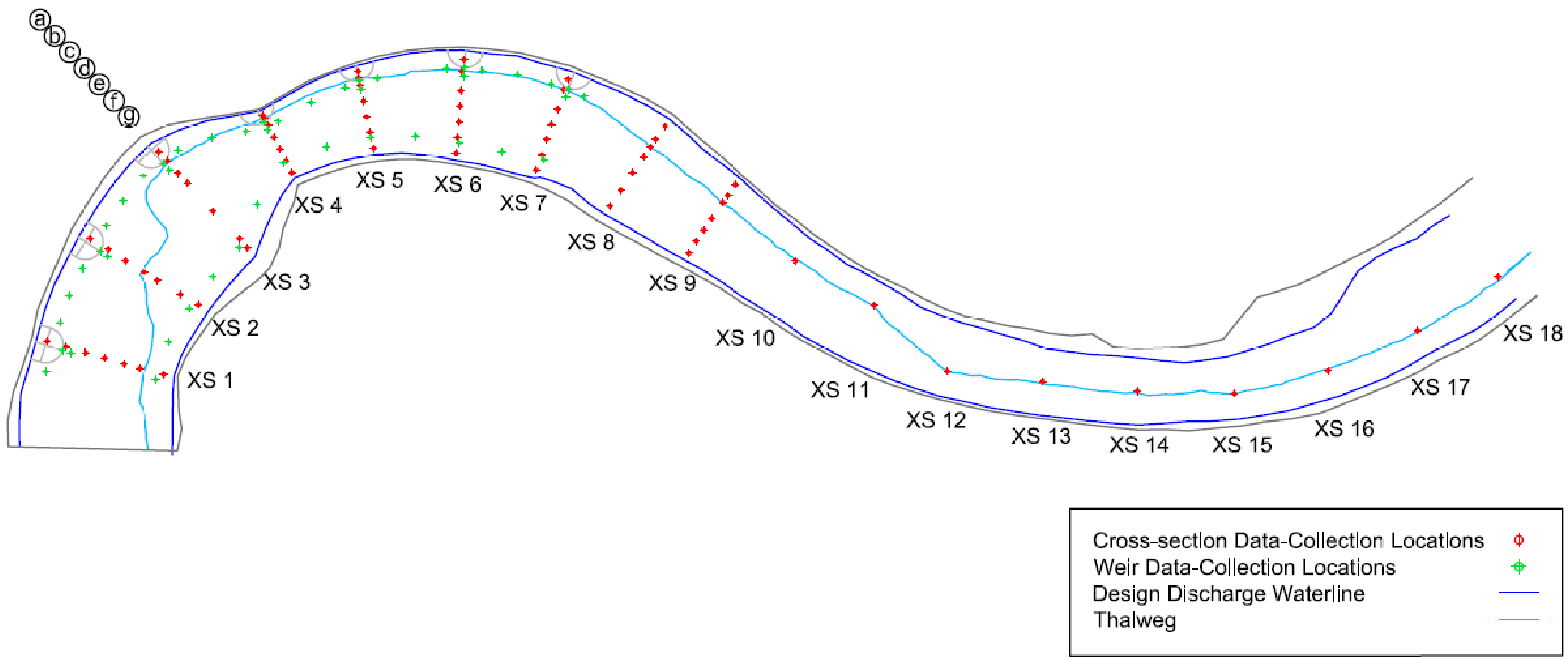

Figure 5.8: NW04 Configuration with Data-collection Locations

5.5 COMBINED SPUR-DIKE TEST CONFIGURATIONS

In addition to testing the four spur-dike design configurations, two of the test configurations included multiple sets of spur dikes:

1. FY 2007 Configuration 2 and
2. FY 2008 Configuration 5.

FY 2007 Configuration 2 included NW01 spur dikes in the downstream bend and NW02 spur dikes in the upstream bend. FY 2008 Configuration 5 included NW03 spur dikes in the downstream bend, and NW04 spur dikes in the upstream end. For these configurations, data were collected only along the thalweg of the downstream bend, as shown in Figure 5.9 and Figure 5.10. The data collected at these points should indicate the influence that a set of spur dikes has on a downstream set of spur dikes. Flow velocity profiles were developed for these data and are plotted in Figure 5.11 and Figure 5.12.

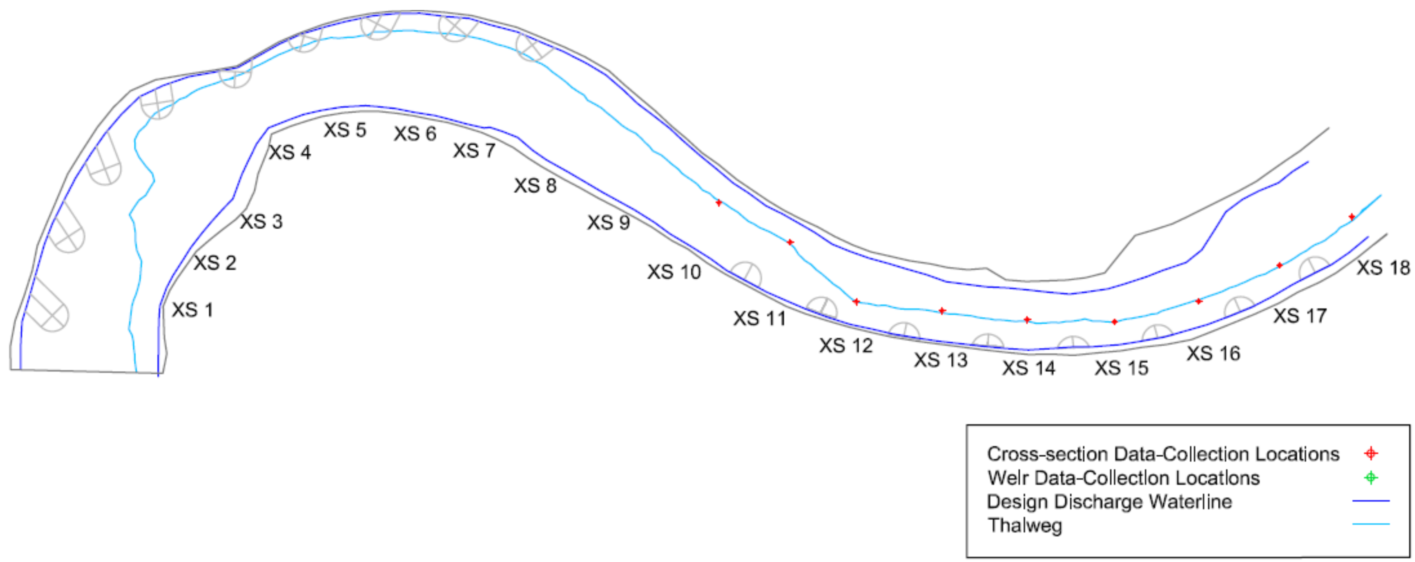

Figure 5.9: FY 2007 Configuration 2 (NW01 Spur Dikes (DS) with NW02 Spur Dikes (US))

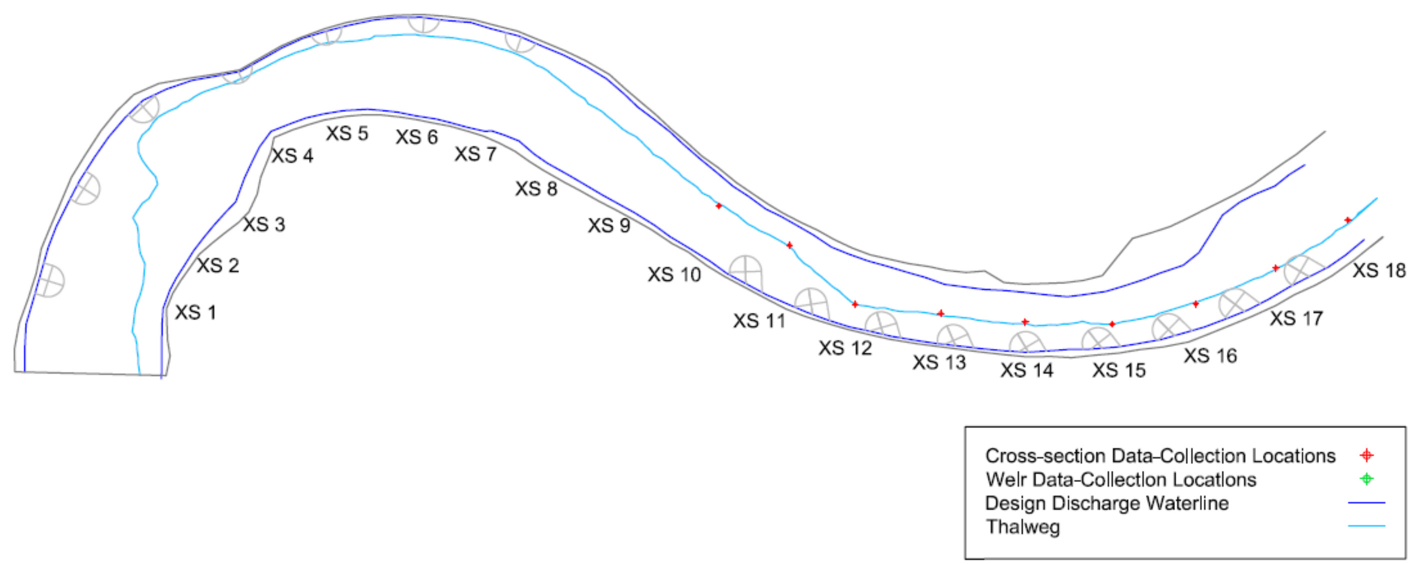

Figure 5.10: FY 2008 Configuration 5 (NW03 Spur Dikes (DS) with NW04 Spur Dikes (US))

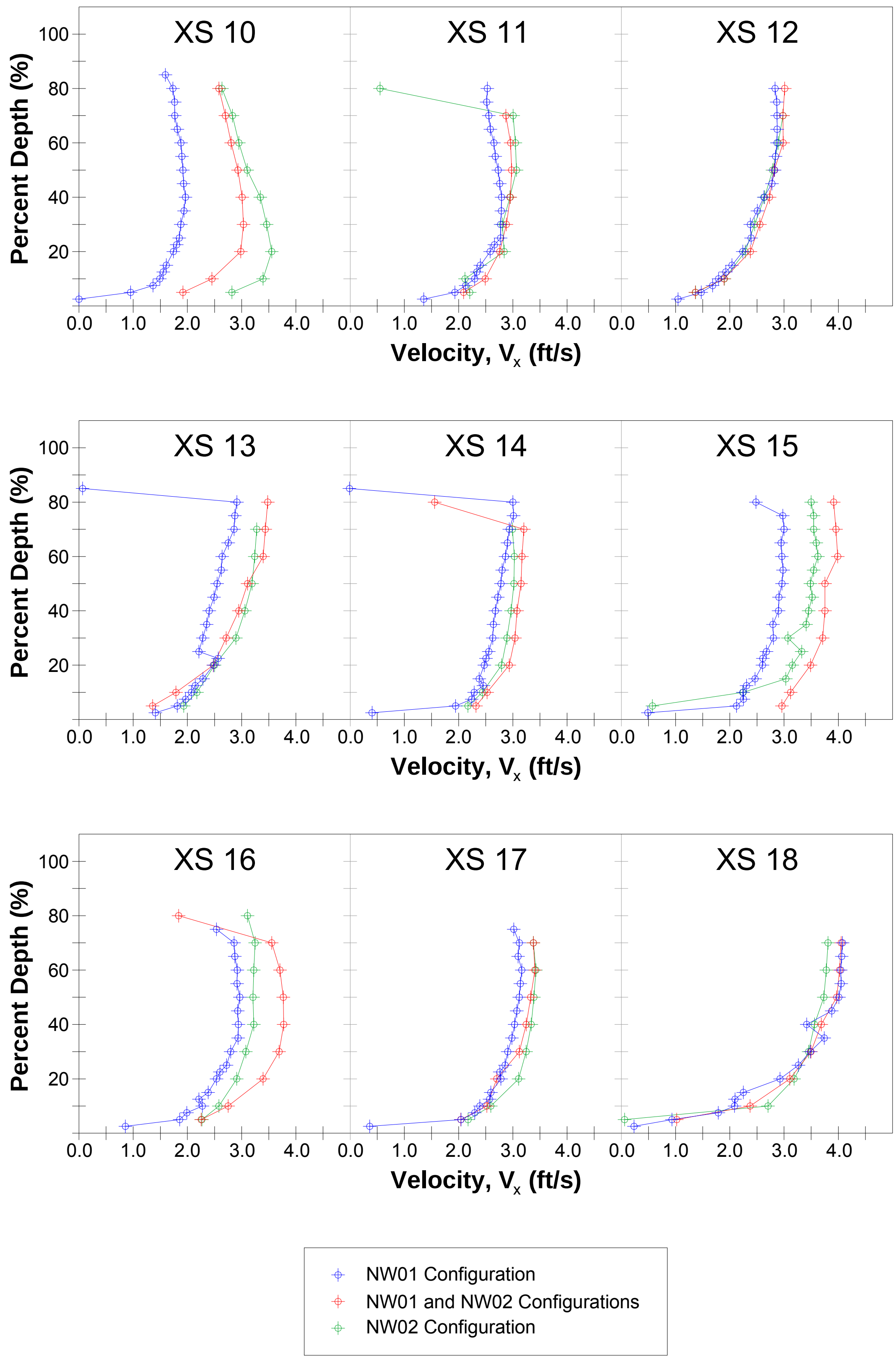

Figure 5.11: Flow Velocity Profiles for the Downstream Bend with NW01 and NW02 Configurations

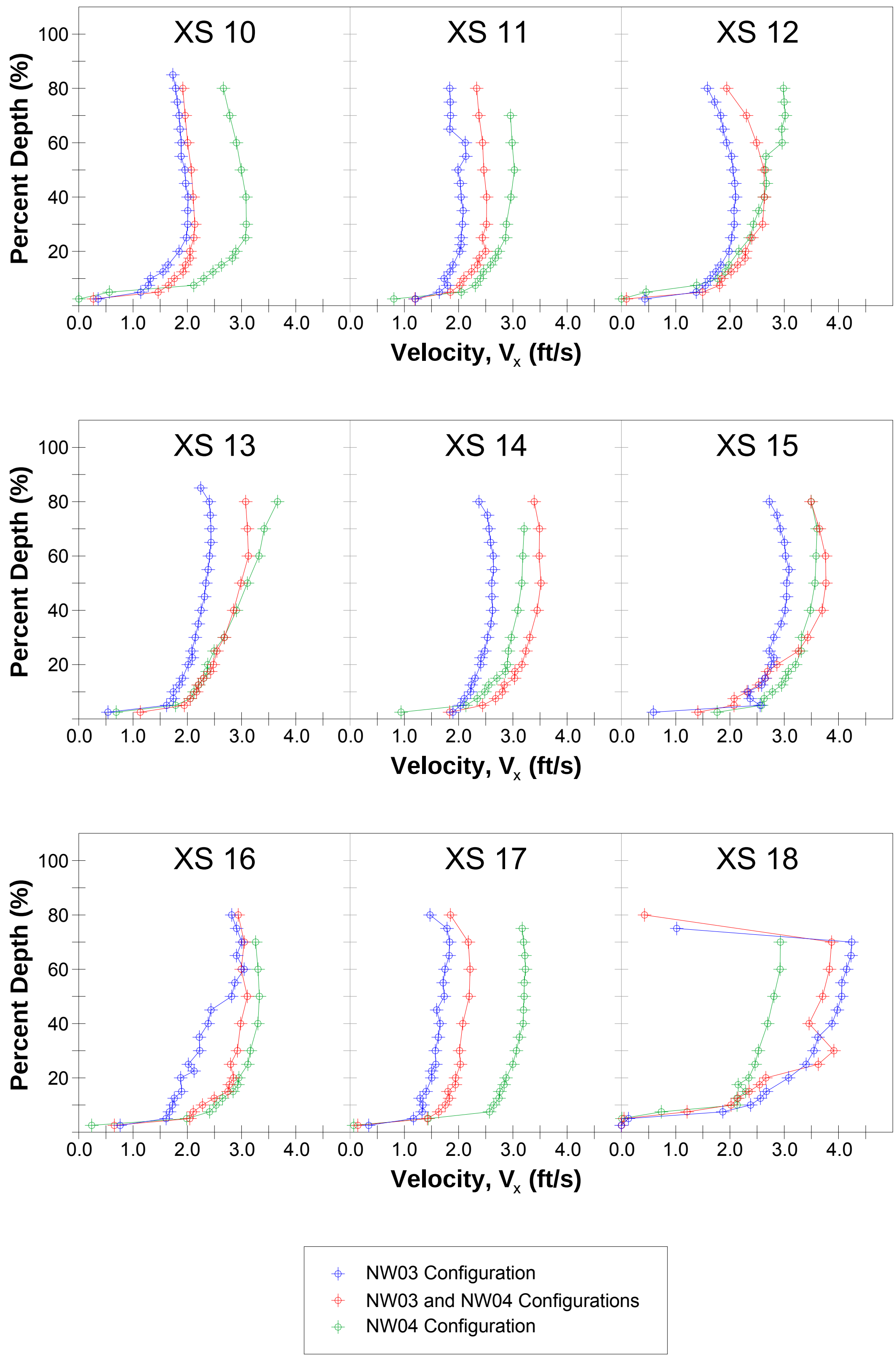

Figure 5.12: Flow Velocity Profiles for the Downstream Bend with NW03 and NW04 Configurations

6 SUMMARY

To aid in the development of design guidelines for spur dikes, testing was performed from 2007 to 2009 on a physical model at Colorado State University at the request of the U. S. Bureau of Reclamation. The undistorted physical model was designed to simulate geometric characteristics of bends found along the Middle Rio Grande study reach at a 1:12 Froude scale. The model was constructed and tested in the Hydromachinery Laboratory at the Engineering Research Center. Four different spur-dike designs were generated for the native topography model. The spur-dike designs were tested with six different test configurations. This report is accompanied by the data from the testing of each spur-dike configuration. Descriptions of the model development, model construction, spur-dike design, test program, and test matrix are presented in this report. In addition, graphical representations of the resulting data are provided for reference.

7 REFERENCES

Cox, A. L. (2005). A Study of In-stream Rehabilitation Structures in Sand-bed Channels. M.S. Thesis, Colorado State University, Department of Civil Engineering, Fort Collins, CO.

Darrow, J. D. (2004). Effects of Bendway Weir Characteristics on Resulting Flow Conditions. M.S. Thesis, Colorado State University, Department of Civil Engineering, Fort Collins, CO.

Davinroy, R. D., Rapp, R. J., and Myhre R. E. (1998). Hydroacoustic Study of Fishes in Bendway Weir Fields of the Middle Mississippi River. In: Proceedings of the ASCE 1998 Wetlands Engineering and River Restoration Conference.

Derrick, D. L. (1998). Four Years Later, Harland Creek Bendway Weir/Willow Post Bank Stabilization Demonstration Project. In: Proceedings of the 1998 International Water Resources Engineering Conference, Part 1 (of 2), August 3-7, Memphis, TN.

Heintz, M. L. (2002). Investigation of Bendway Weir Spacing. M.S. Thesis, Colorado State University, Department of Civil Engineering, Fort Collins, CO.

Kasper, K. E. (2005). Accuracy of HEC-RAS to Calculated Flow Depths and Total Energy Loss With and Without Bendway Weirs in a Meander Bend. M.S. Thesis, Colorado State University, Department of Civil Engineering, Fort Collins, CO.

Kinzli, K. (2005). Effects of Bendway Weir Characteristics on Resulting Eddy and Channel Flow Conditions. M.S. Thesis, Colorado State University, Department of Civil Engineering, Fort Collins, CO.

Richard, G. A. (2001). Quantification and Prediction of Lateral Channel Adjustments Downstream from Cochiti Dam, Rio Grande, NM. Ph.D. Dissertation, Colorado State University, Department of Civil Engineering, Fort Collins, CO.

Schmidt, P. G. (2005). Effects of Bendway Weir Field Geometric Characteristics on Channel Flow Conditions. M.S. Thesis, Colorado State University, Department of Civil Engineering, Fort Collins, CO.

Sclafani, P. (2009). Methodology for Predicting Maximum Velocity and Shear Stress in a Sinuous Channel with Bendway Weirs Using 1-D HEC-RAS Modeling Results. M.S. Thesis, Colorado State University, Department of Civil and Environmental Engineering, Fort Collins, CO.

Shields Jr., F. D., Knight, S. S., and Cooper, C. M. (1998). Addition of Spurs to Stone Toe Protection for Warmwater Fish Habitat. *Journal of American Water Resources Association,* 34(6):1427-1436.

Walker, K. G. (2009). Comparison of a Generalized Trapezoidal Hydraulic Model to a Native Topography Patterned Bed Surface Model of the Rio Grande. M.S. Thesis, Colorado State University, Department of Civil and Environmental Engineering, Fort Collins, CO.

U. S. Bureau of Reclamation (USBR) (2000). Meander Bend Surveys, Geomorphic Data Analysis & Field Data Collection Report July 1999 through January 2000. Report submitted to the U.S. Department of the Interior, Bureau of Reclamation, Albuquerque, NM, March.

APPENDIX A

NATIVE TOPOGRAPHY MODEL CROSS-SECTION PLOTS WITH DATA-COLLECTION LOCATIONS AND BED-SURVEY ELEVATIONS (MODIFIED FROM WALKER (2009))

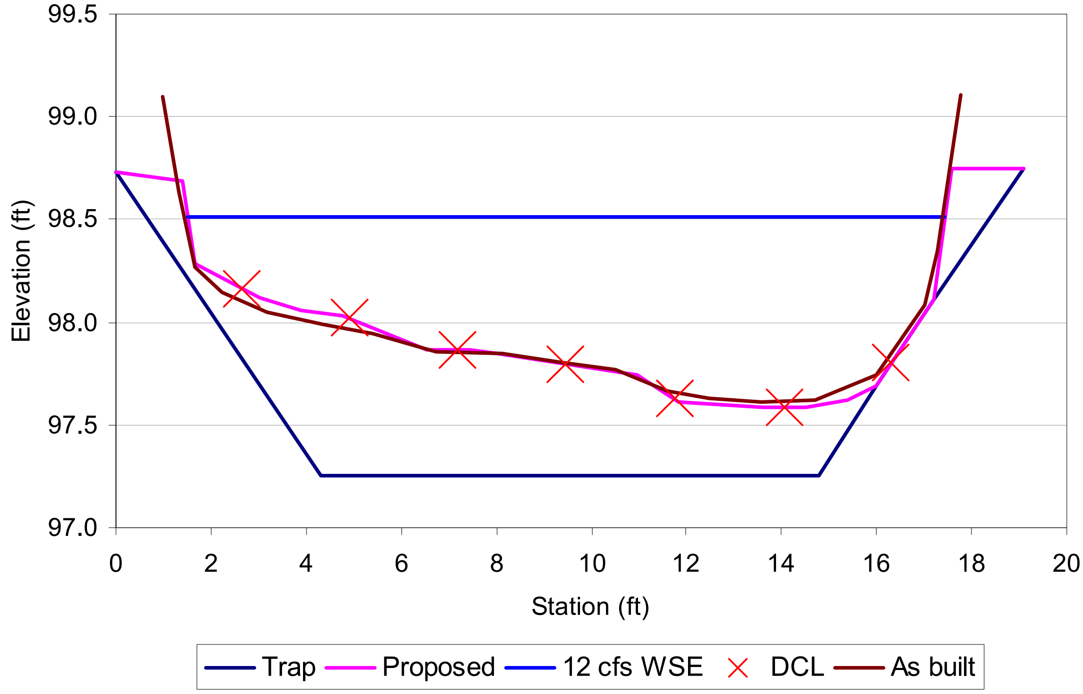

Figure A.1: Cross Section 1 DCLs and Bed-survey Elevations, Equal Top Width Method

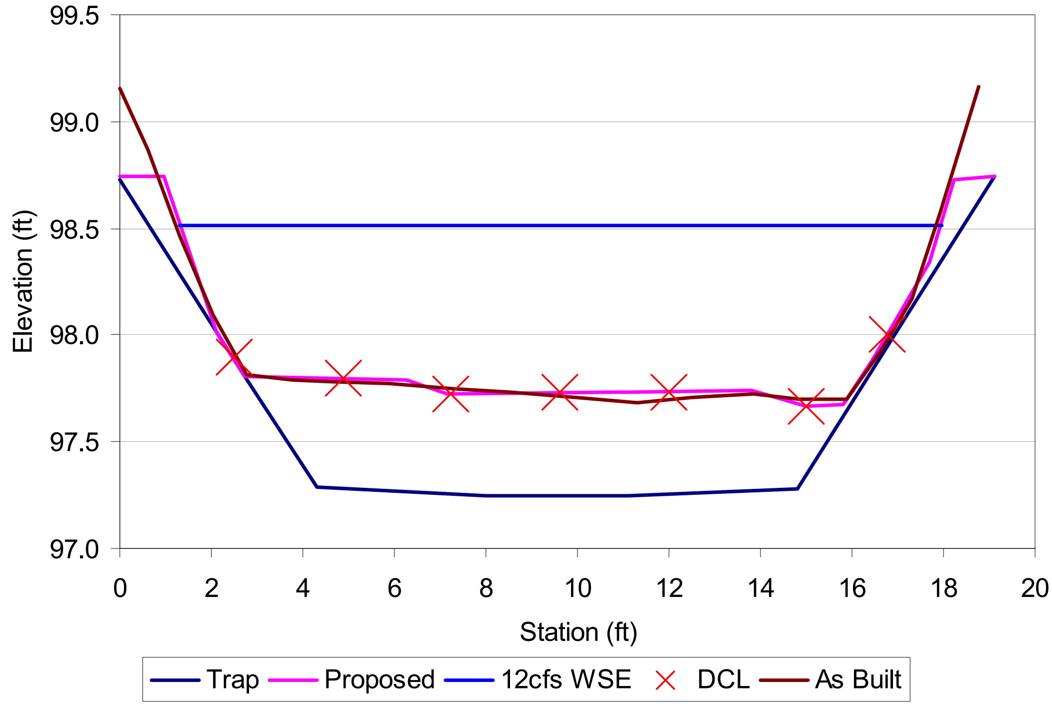

Figure A.2: Cross Section 2 DCLs and Bed-survey Elevations, Equal Top Width Method

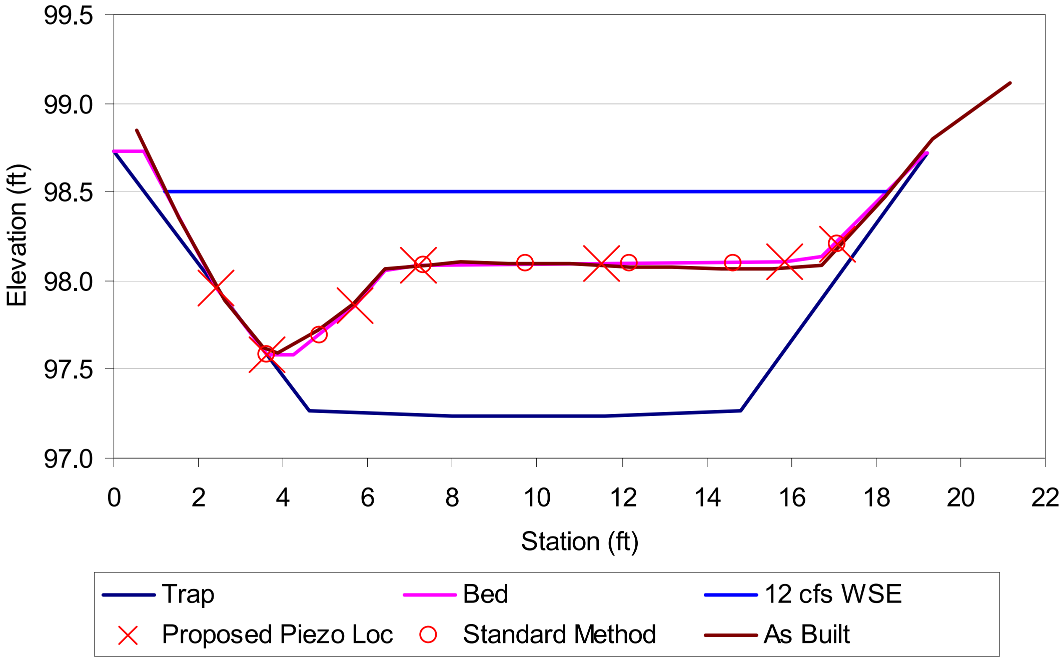

Figure A.3: Altered (impacted by a steep left bank) Cross Section 3 DCLs and Bed-survey Elevations, Equal Top Width Method

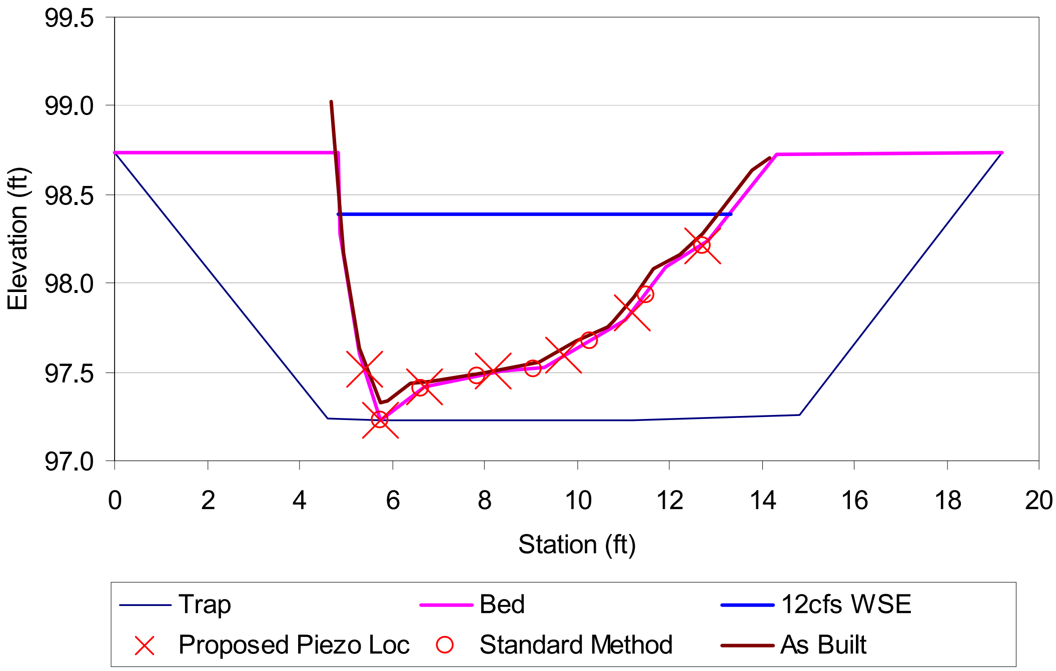

Figure A.4: Altered (impacted by a steep left bank) Cross Section 4 DCLs and Bed-survey Elevations, Equal Top Width Method

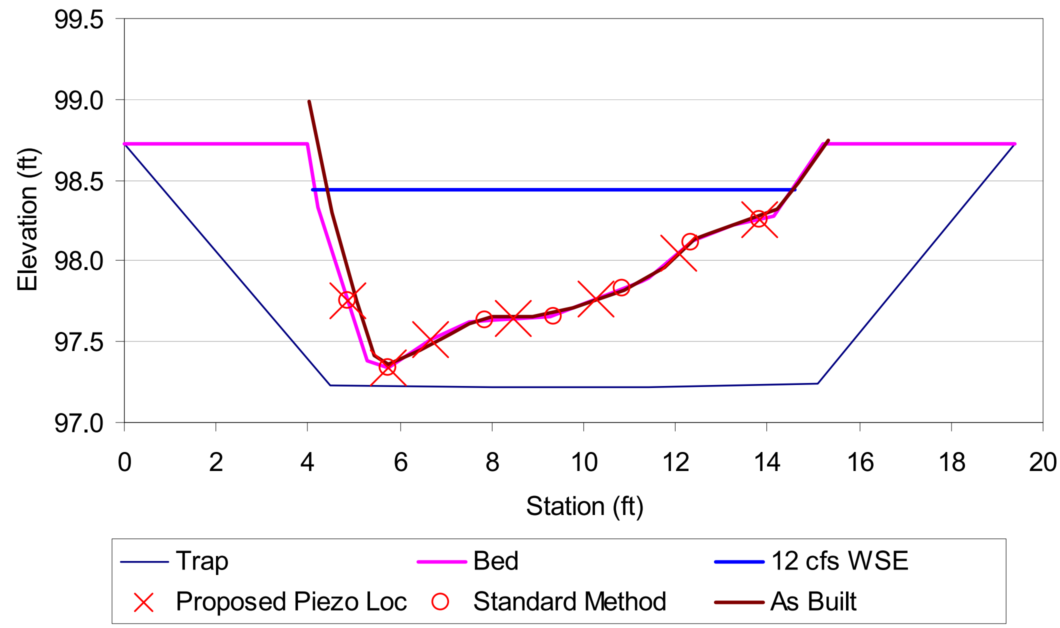

Figure A.5: Altered (affected by thalweg proximity) Cross Section 5 DCLs and Bed-survey Elevations, Equal Top Width Method

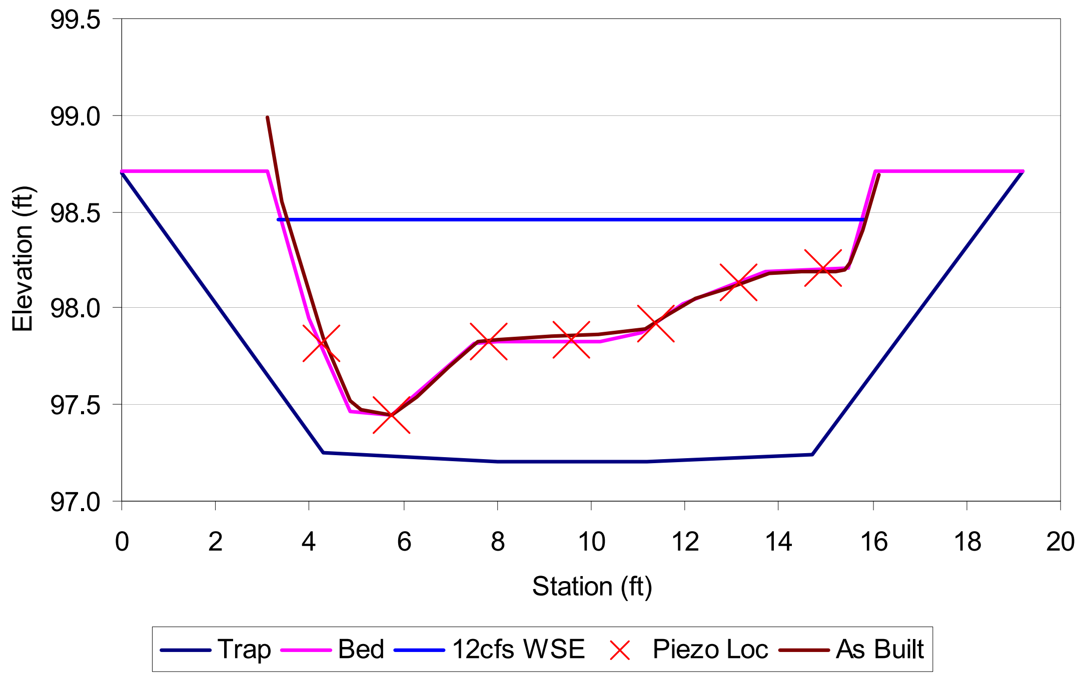

Figure A.6: Cross Section 6 DCLs and Bed-survey Elevations, Equal Top Width Method

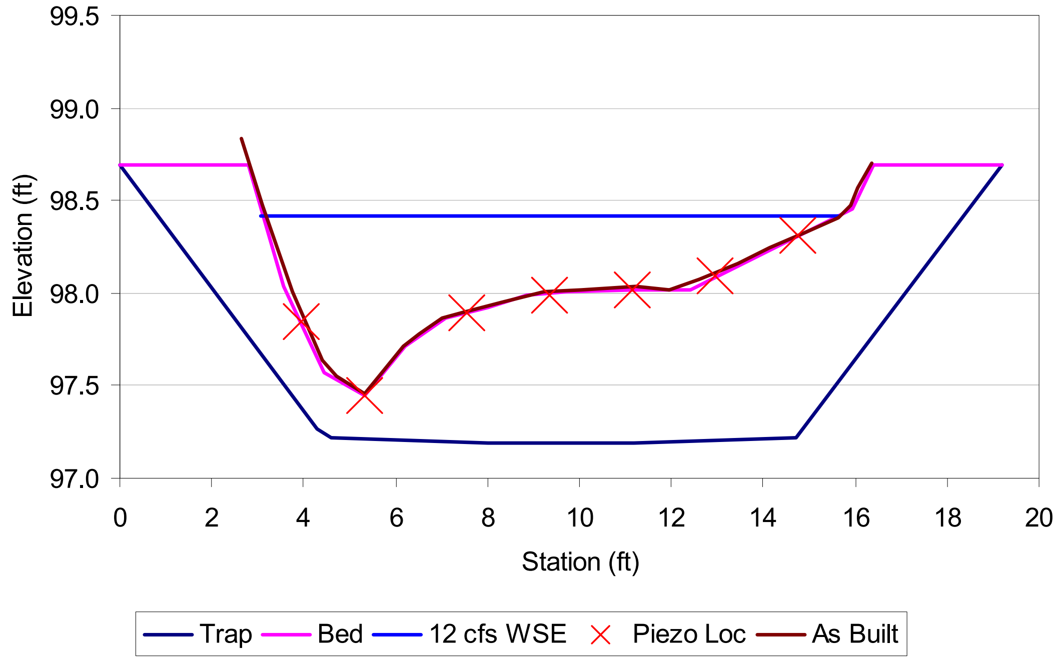

Figure A.7: Cross Section 7 DCLs and Bed-survey Elevations, Equal Top Width Method

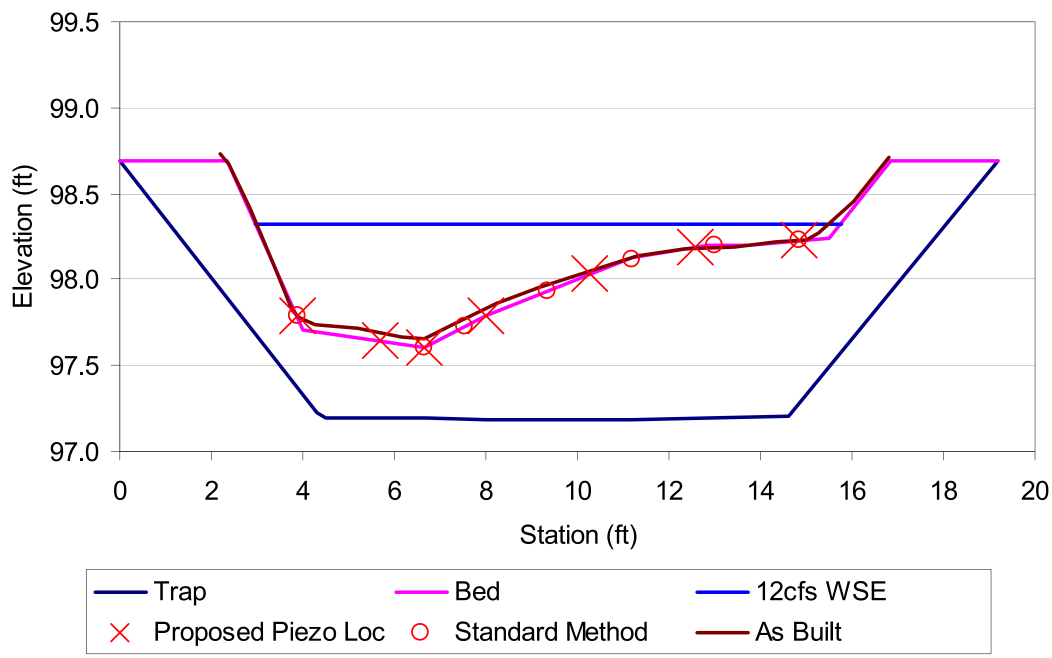

Figure A.8: Altered (affected by thalweg proximity) Cross Section 8 DCLs and Bed-survey Elevations, Equal Top Width Method

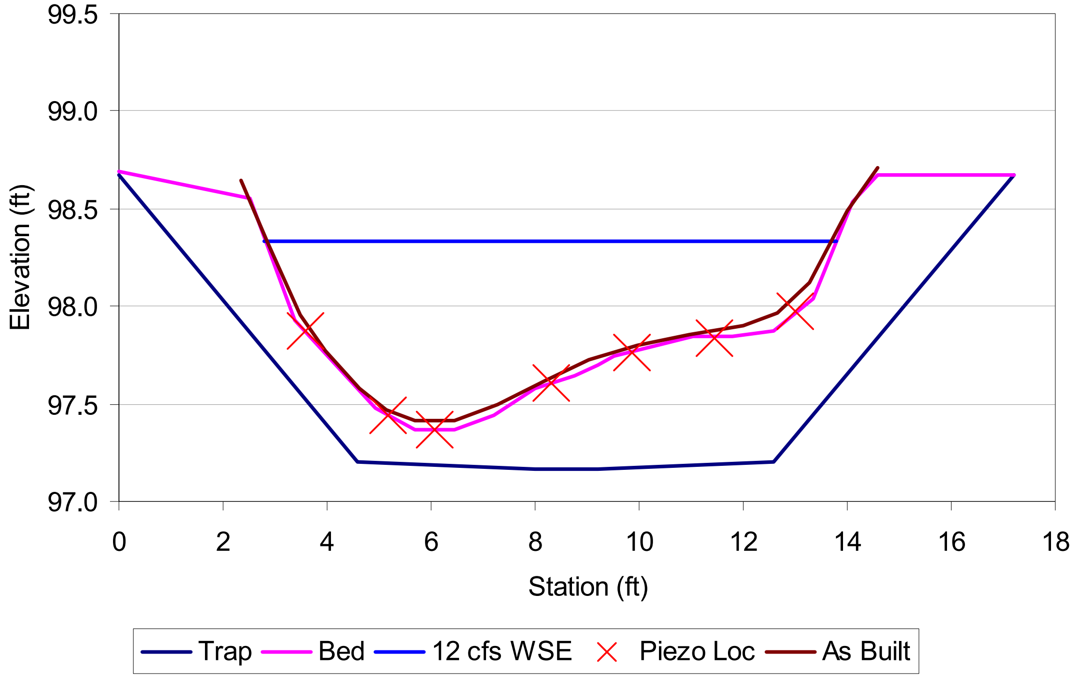

Figure A.9: Cross Section 9 DCLs and Bed-survey Elevations, Equal Top Width Method

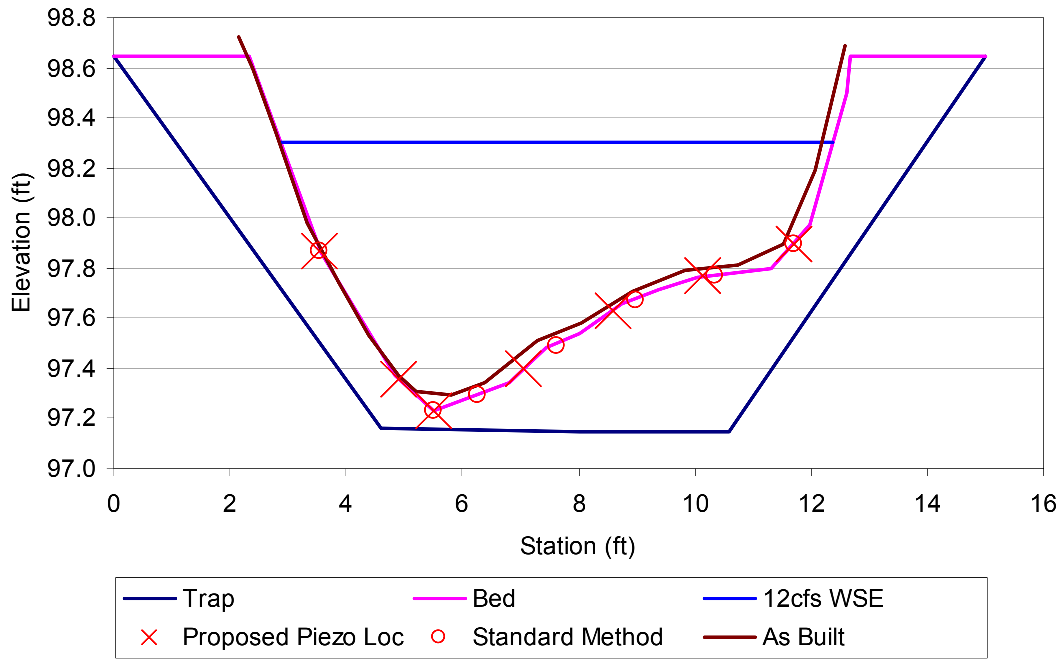

Figure A.10: Altered (affected by thalweg proximity) Cross Section 10 DCLs and Bed-survey Elevations, Equal Top Width Method

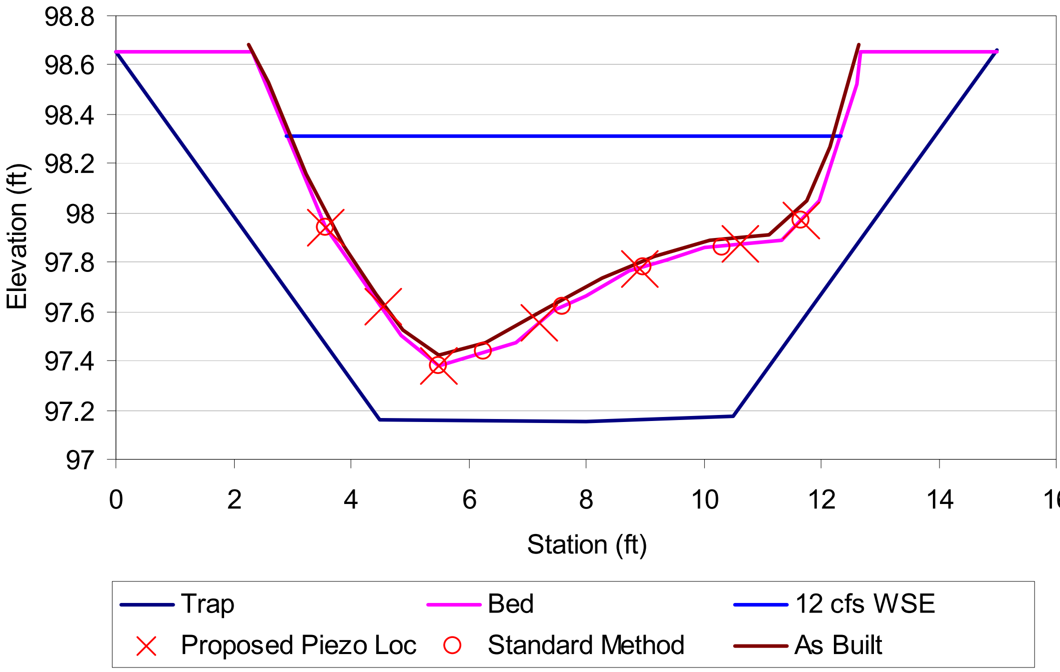

Figure A.11: Altered (affected by thalweg proximity) Cross Section 11 DCLs and Bed-survey Elevations, Equal Top Width Method

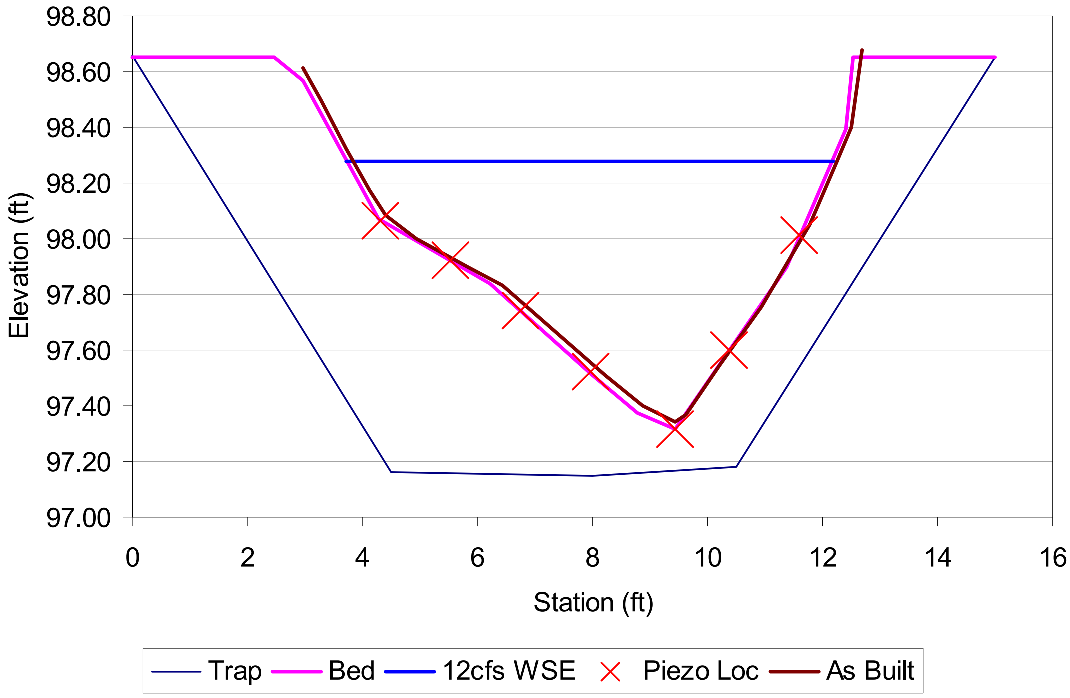

Figure A.12: Cross Section 12 DCLs and Bed-survey Elevations, Equal Top Width Method

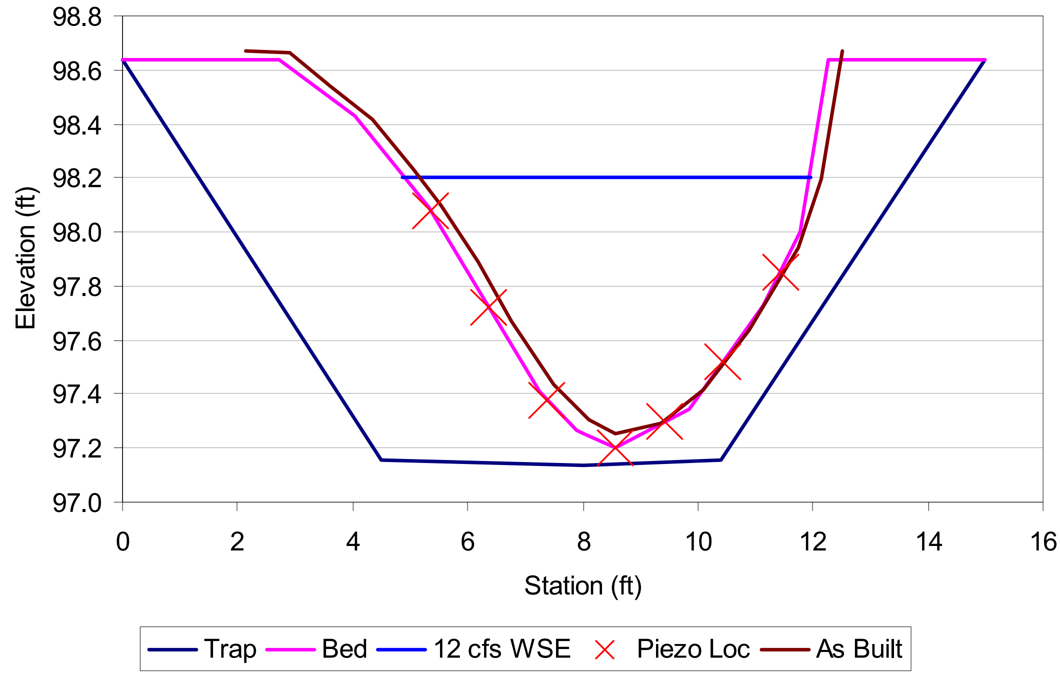

Figure A.13: Cross Section 13 DCLs and Bed-survey Elevations, Equal Top Width Method

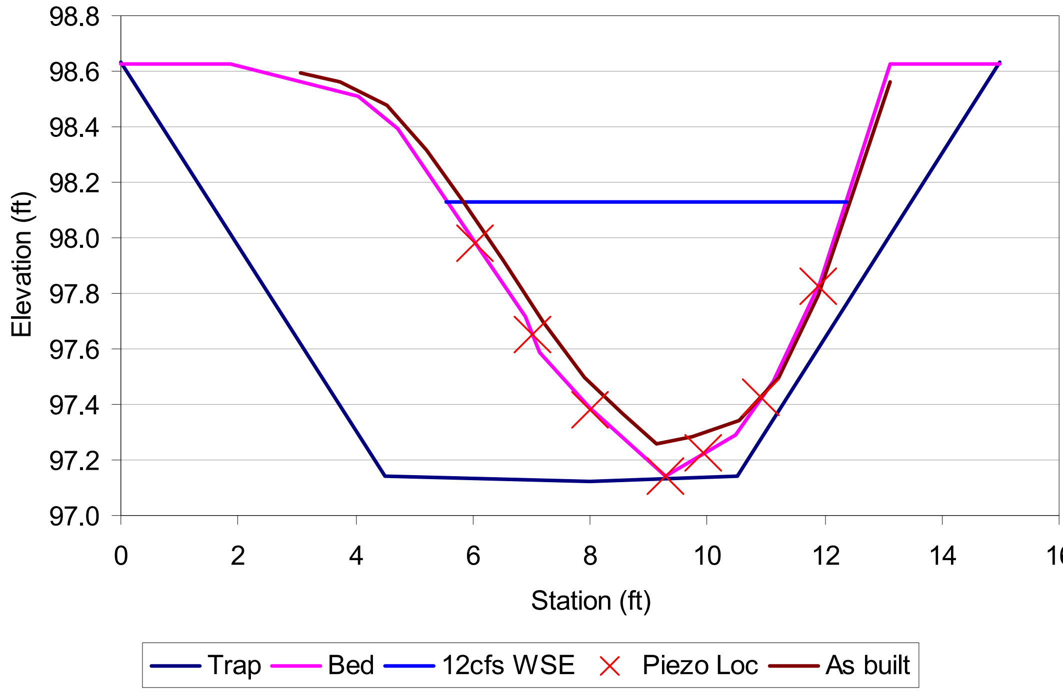

Figure A.14: Cross Section 14 DCLs and Bed-survey Elevations, Equal Top Width Method

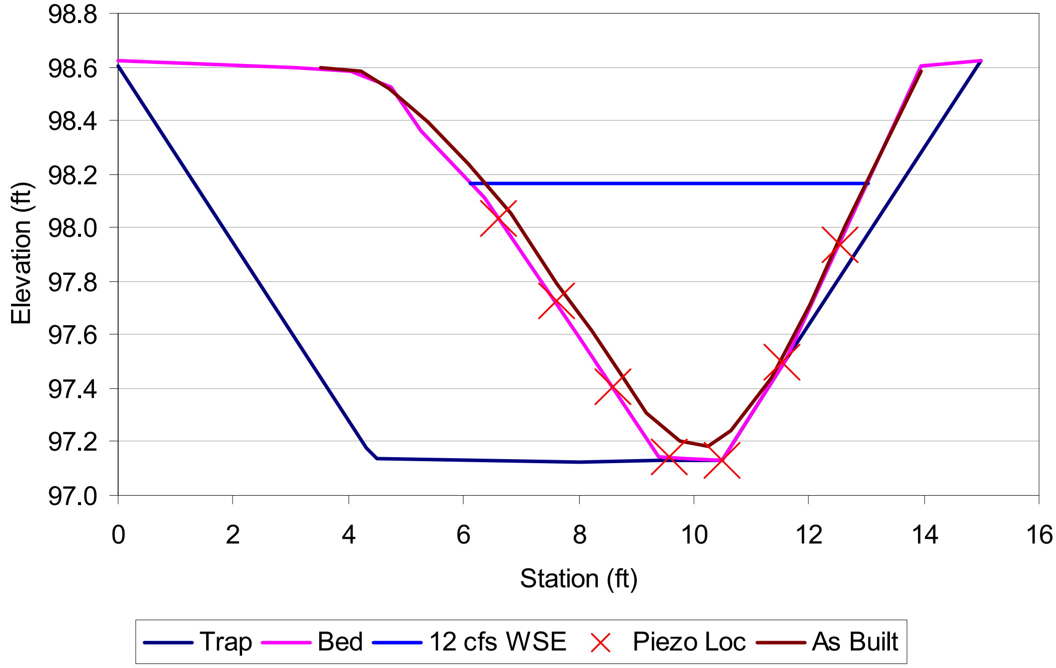

Figure A.15: Cross Section 15 DCLs and Bed-survey Elevations, Equal Top Width Method

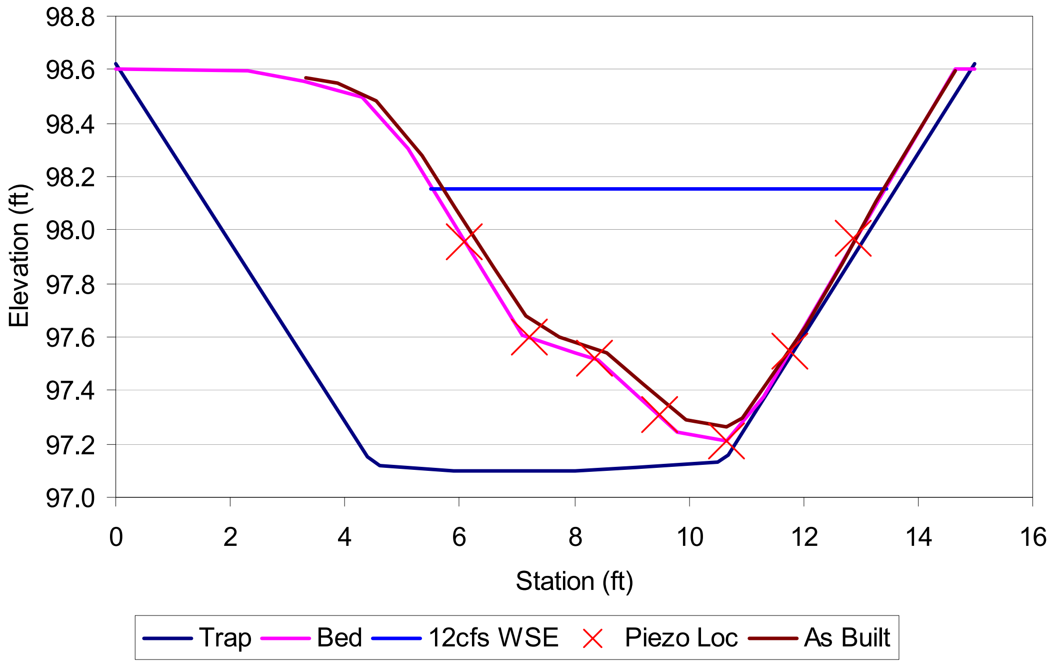

Figure A.16: Cross Section 16 DCLs and Bed-survey Elevations, Equal Top Width Method

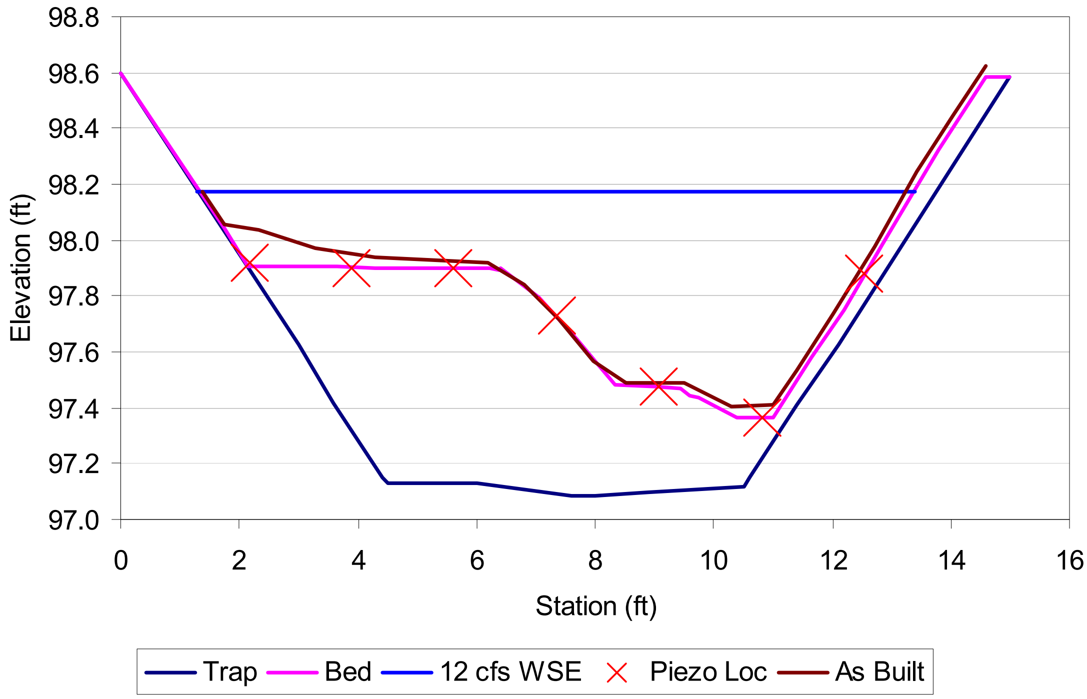

Figure A.17: Cross Section 17 DCLs and Bed-survey Elevations, Equal Top Width Method

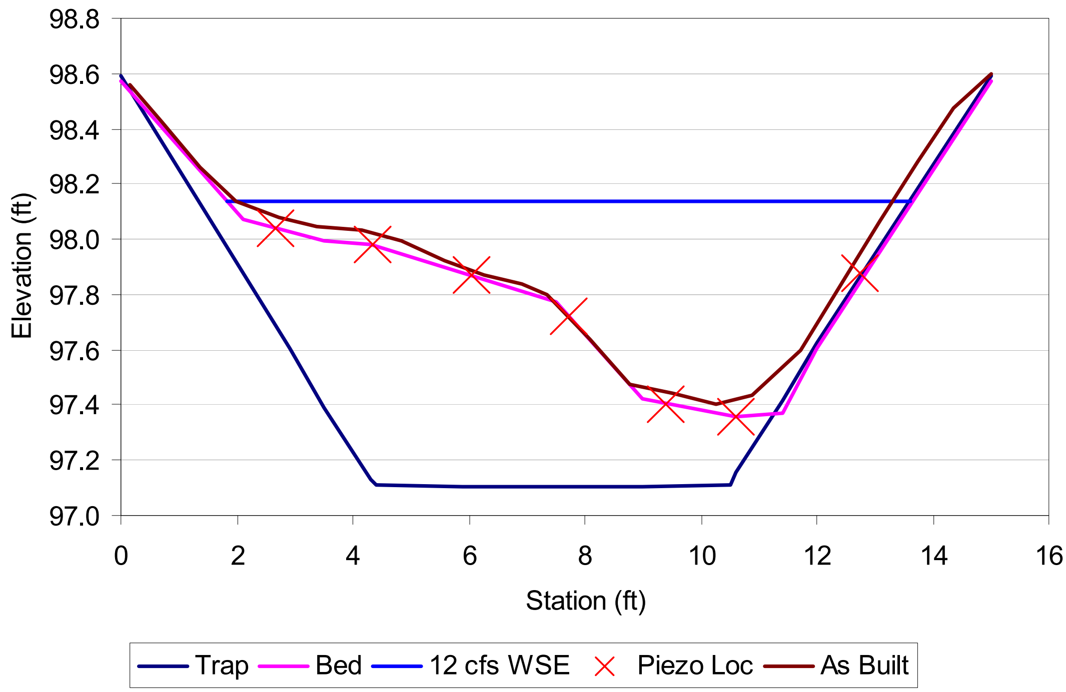

Figure A.18: Cross Section Eighteen DCLs and Bed-survey Elevations, Equal Top Width Method

APPENDIX B

NATIVE TOPOGRAPHY SPUR-DIKE CONFIGURATION WATER SURFACE PROFILES

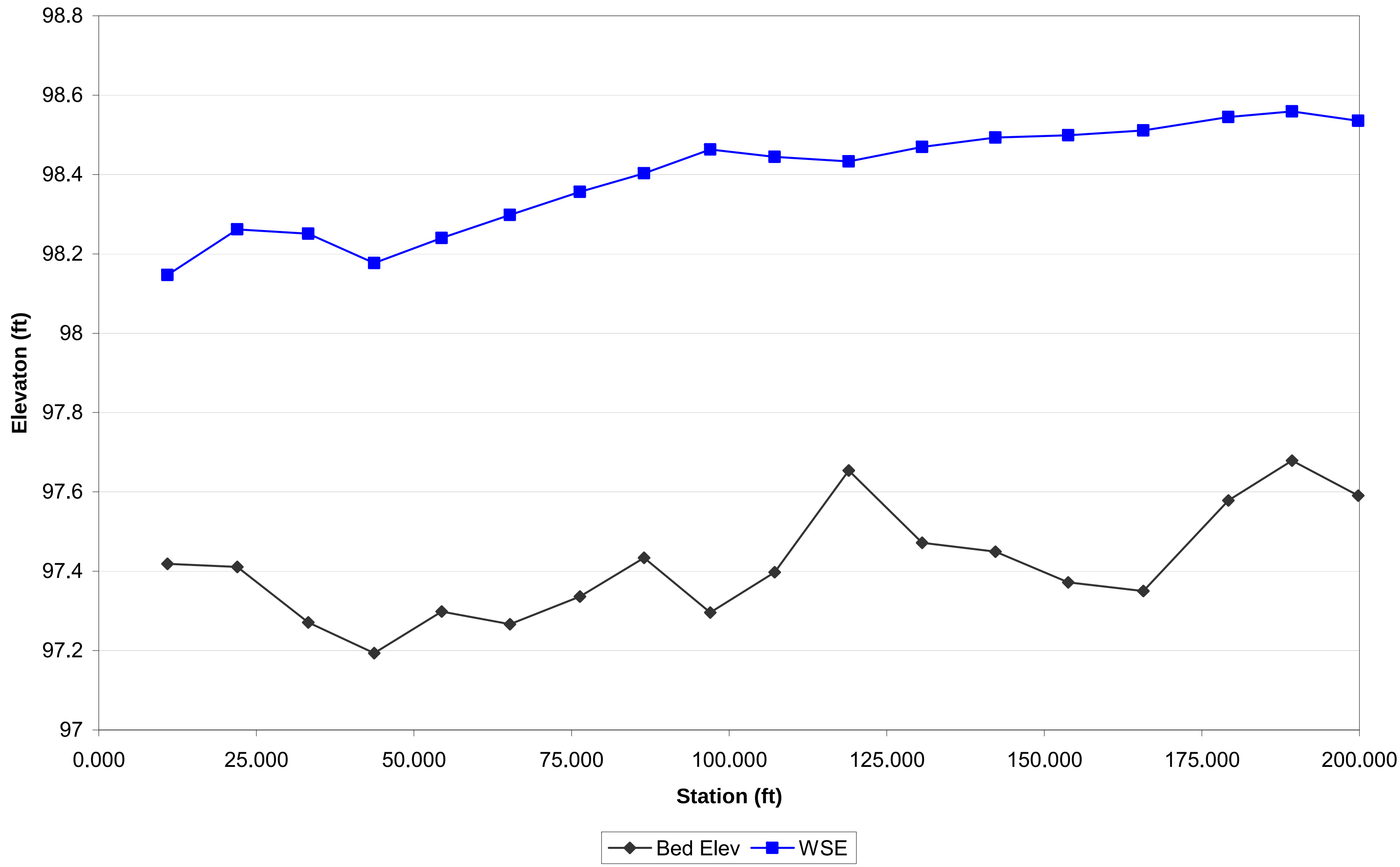

Figure B.1: NW01 Water-surface Profile

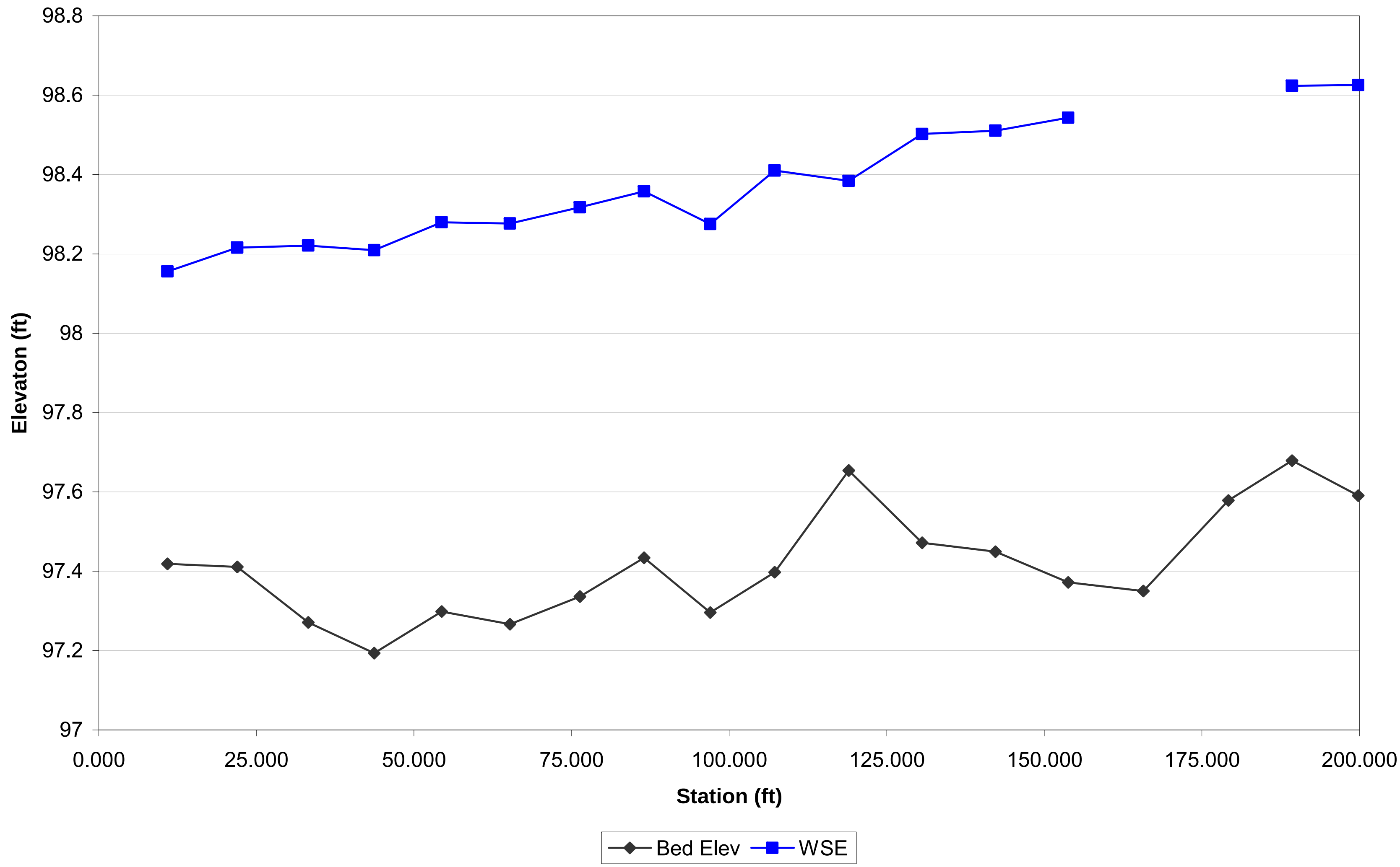

Figure B.2: NW02 Water-surface Profile

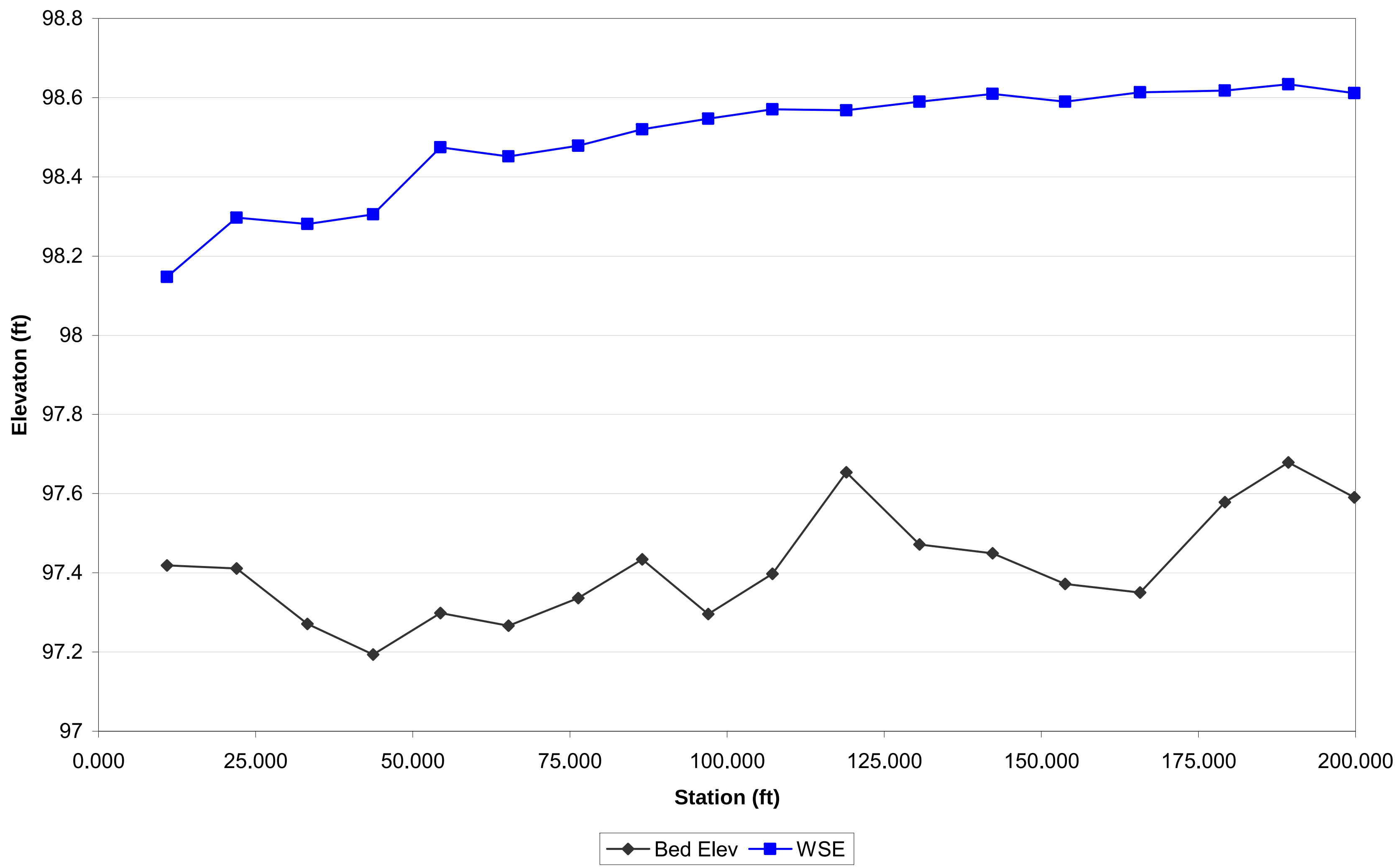

Figure B.3: NW03 Water-surface Profile

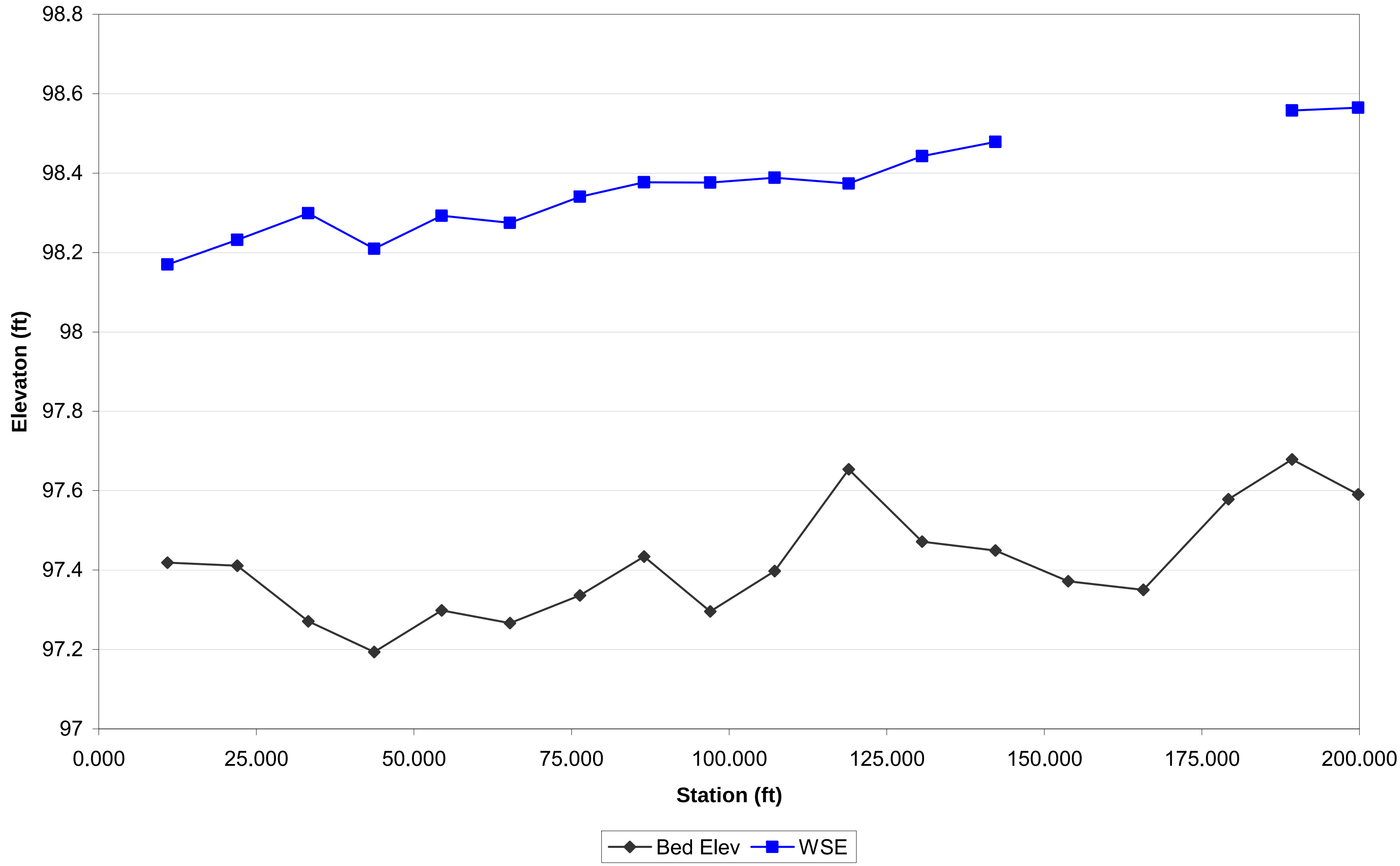

Figure B.4: NW04 Water-surface Profile

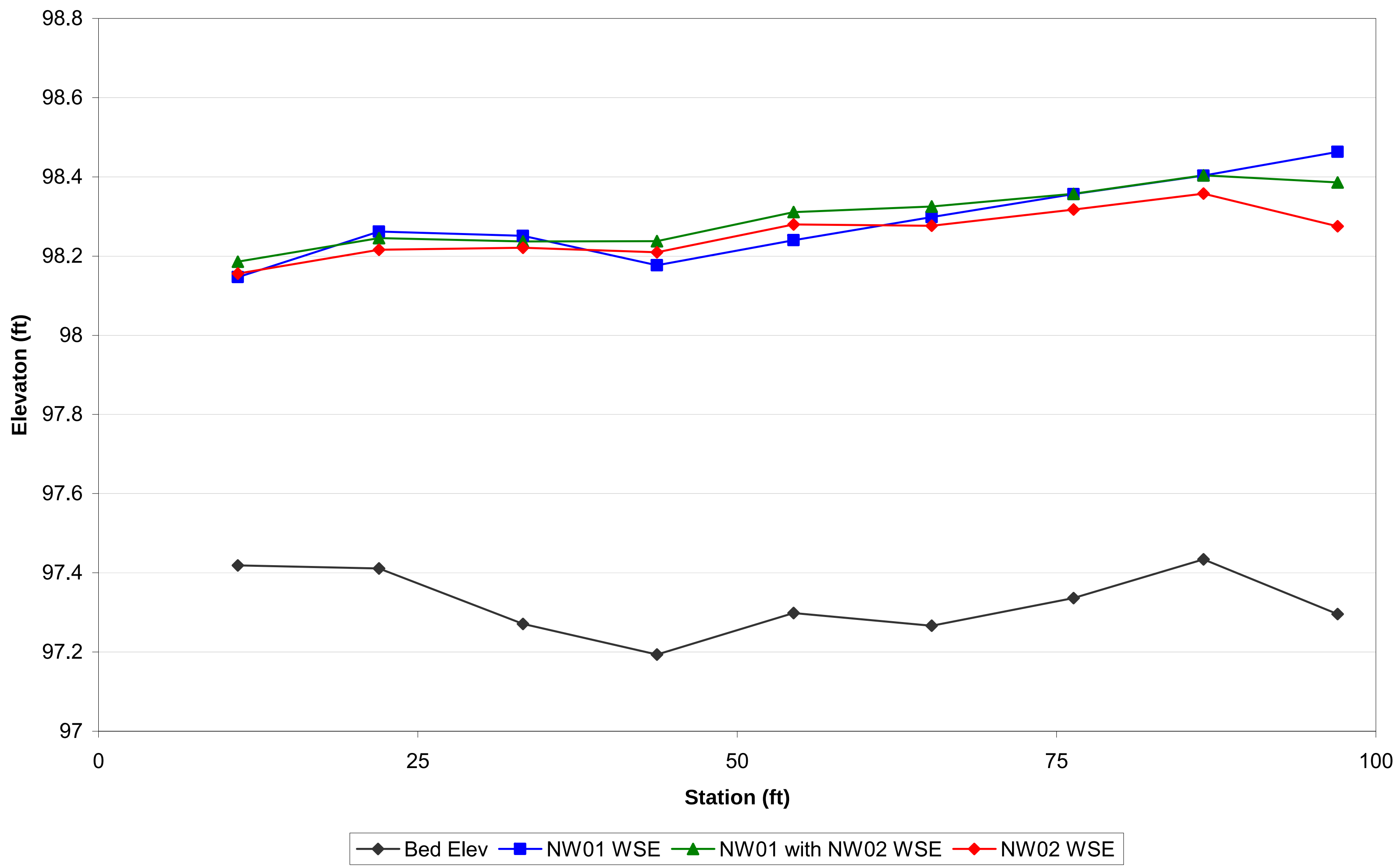

Figure B.5: FY 2007 Configuration 2 Water-surface Profile

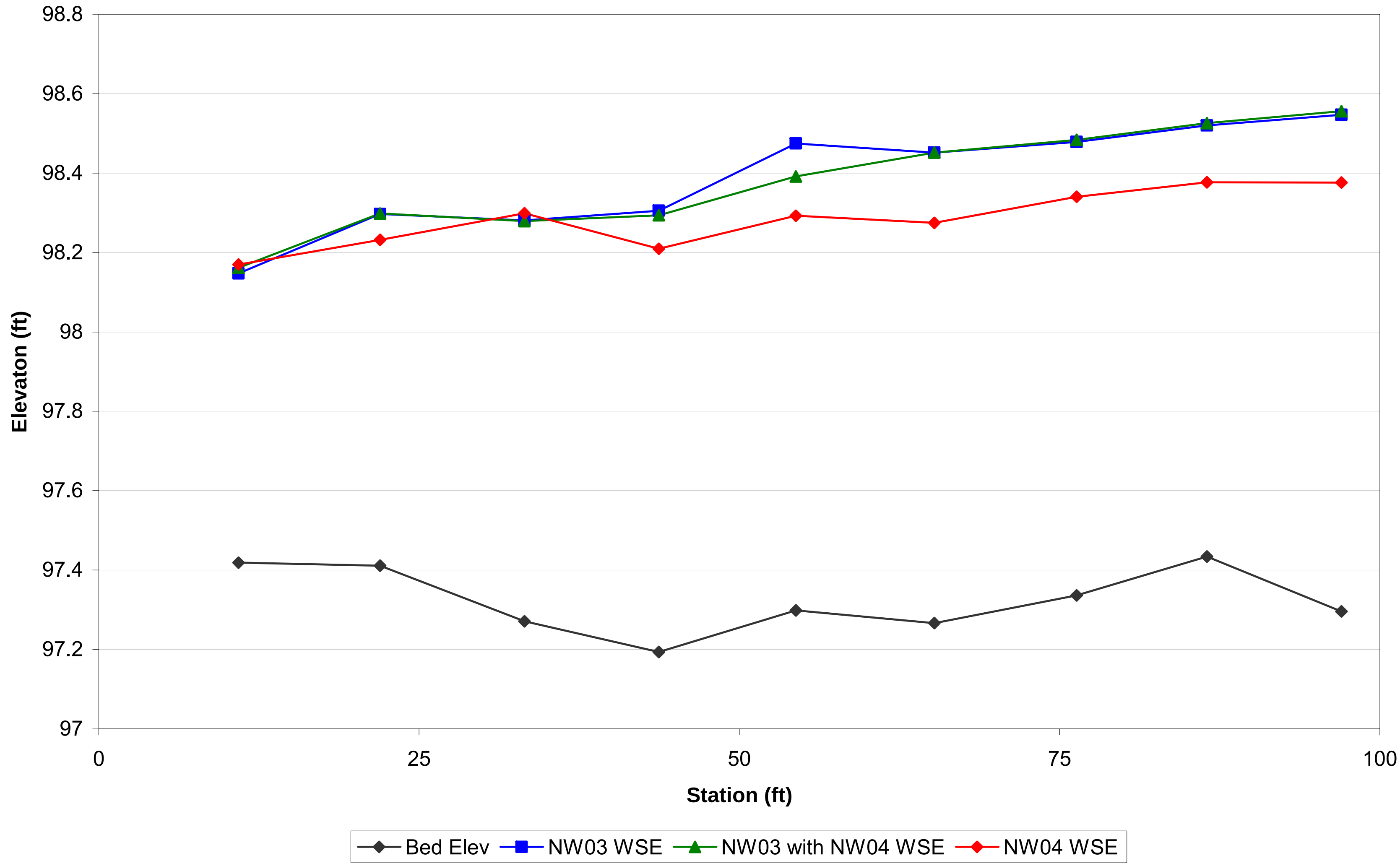

Figure B.6: FY 2008 Configuration 5 Water-surface Profile

APPENDIX C

NATIVE TOPOGRAPHY SPUR-DIKE CONFIGURATION 60%-DEPTH AVERAGE FLOW VELOCITY PLOTS

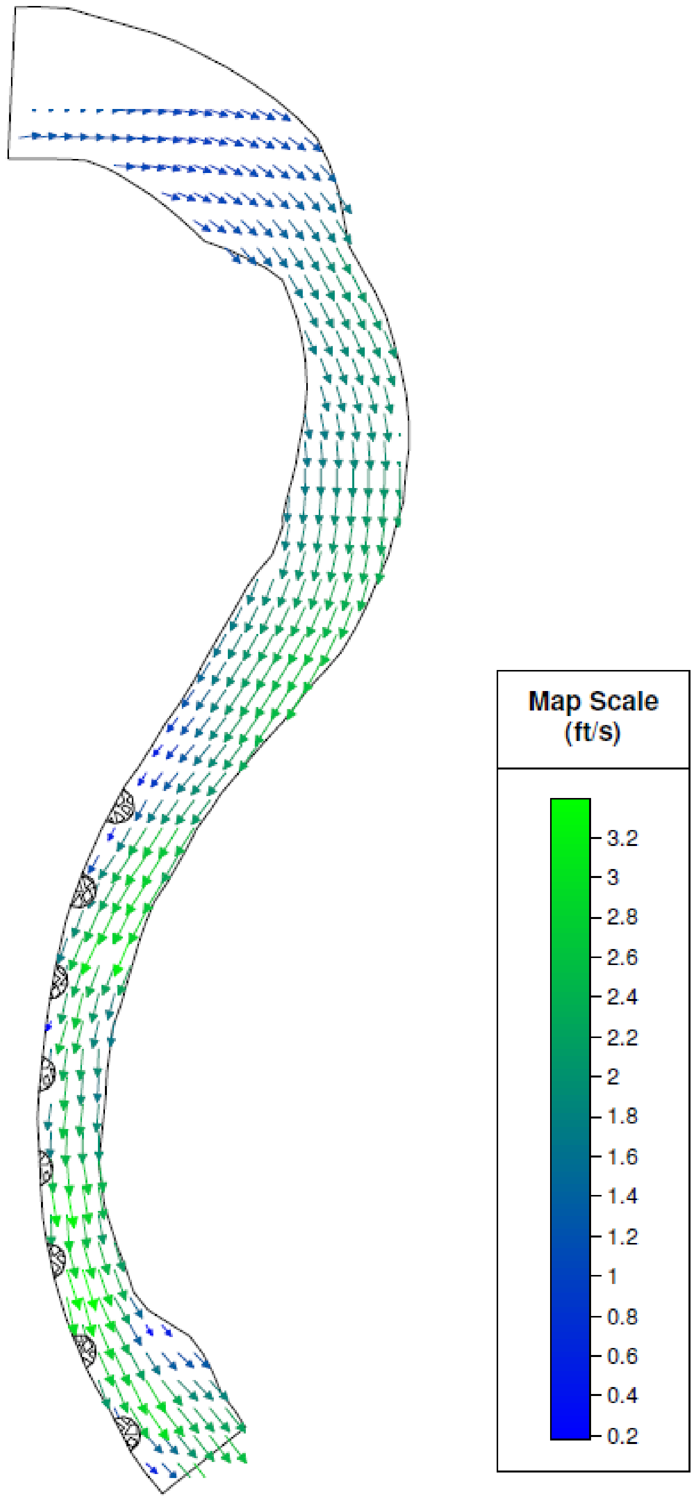

Figure C.1: NW01 Flow Velocity-vector Plot

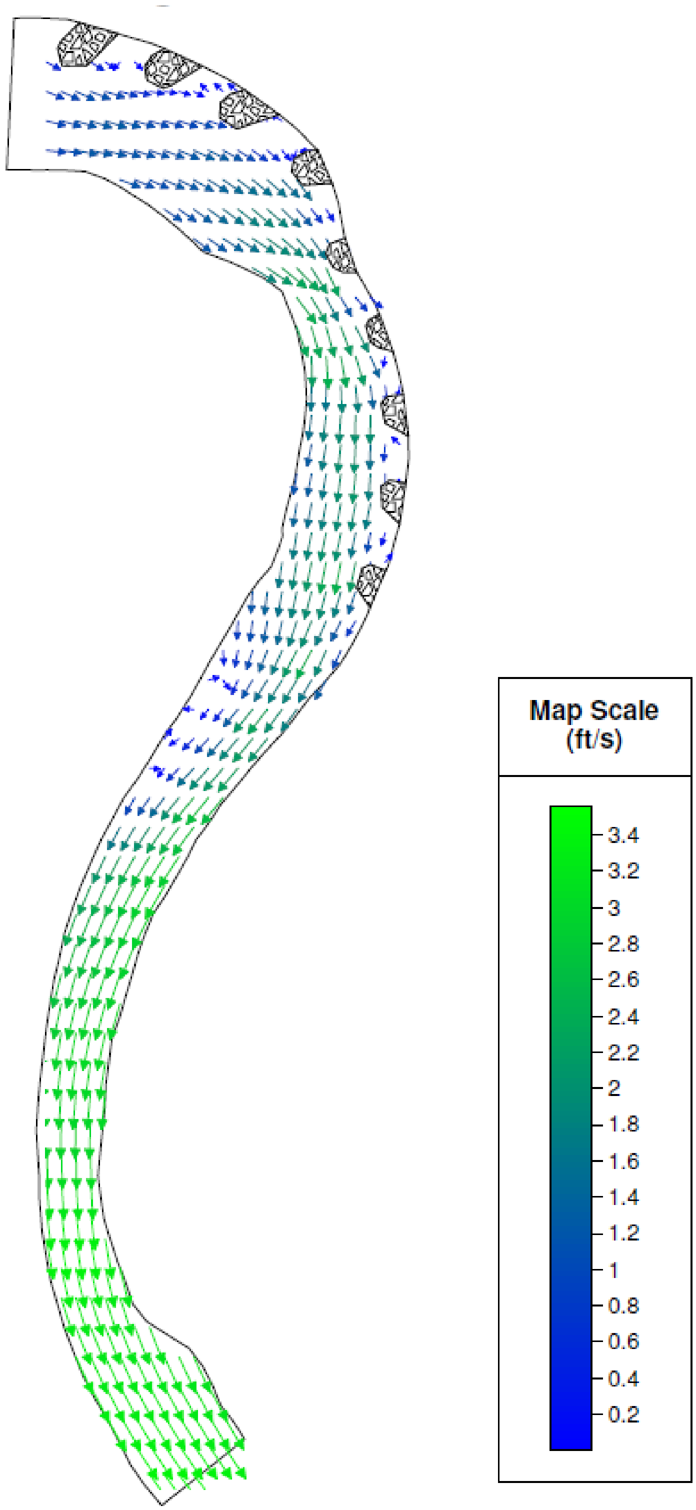

Figure C.2: NW02 Flow Velocity-vector Plot

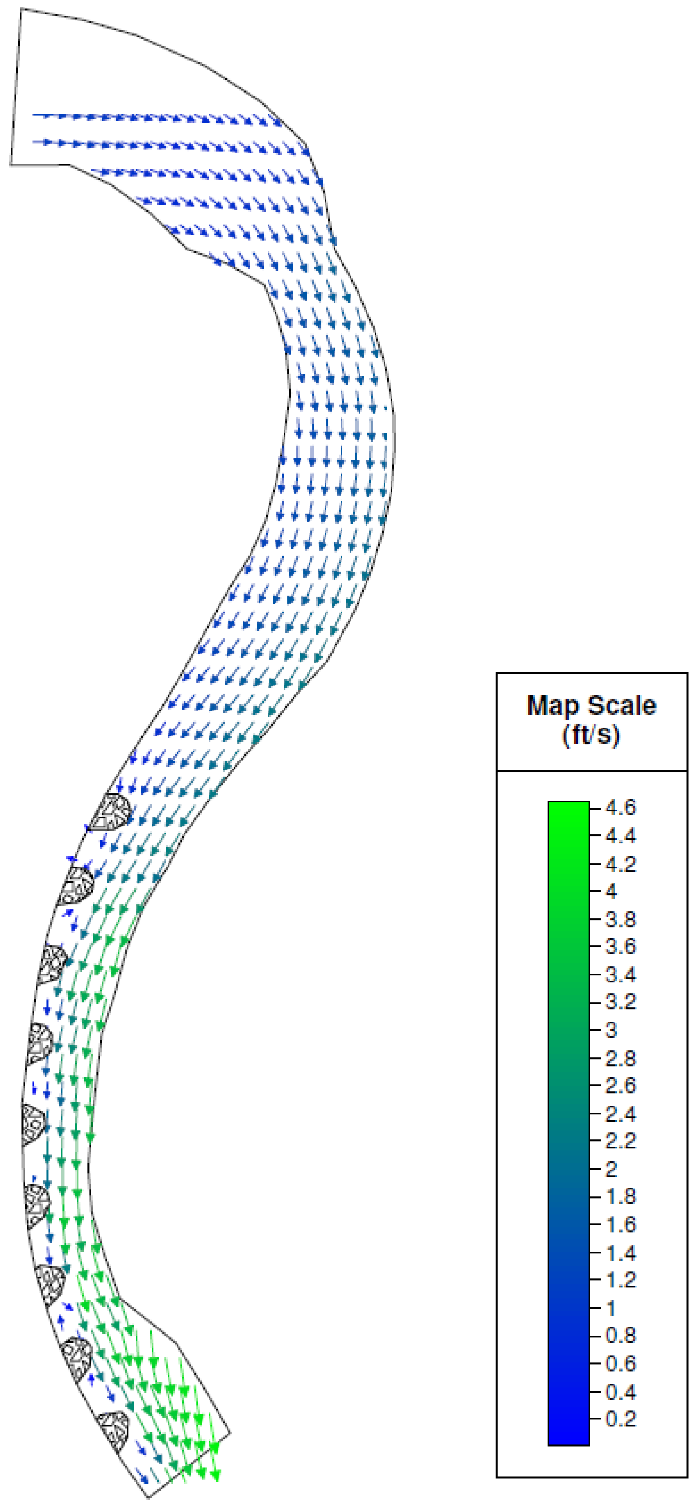

Figure C.3: NW03 Flow Velocity-vector Plot

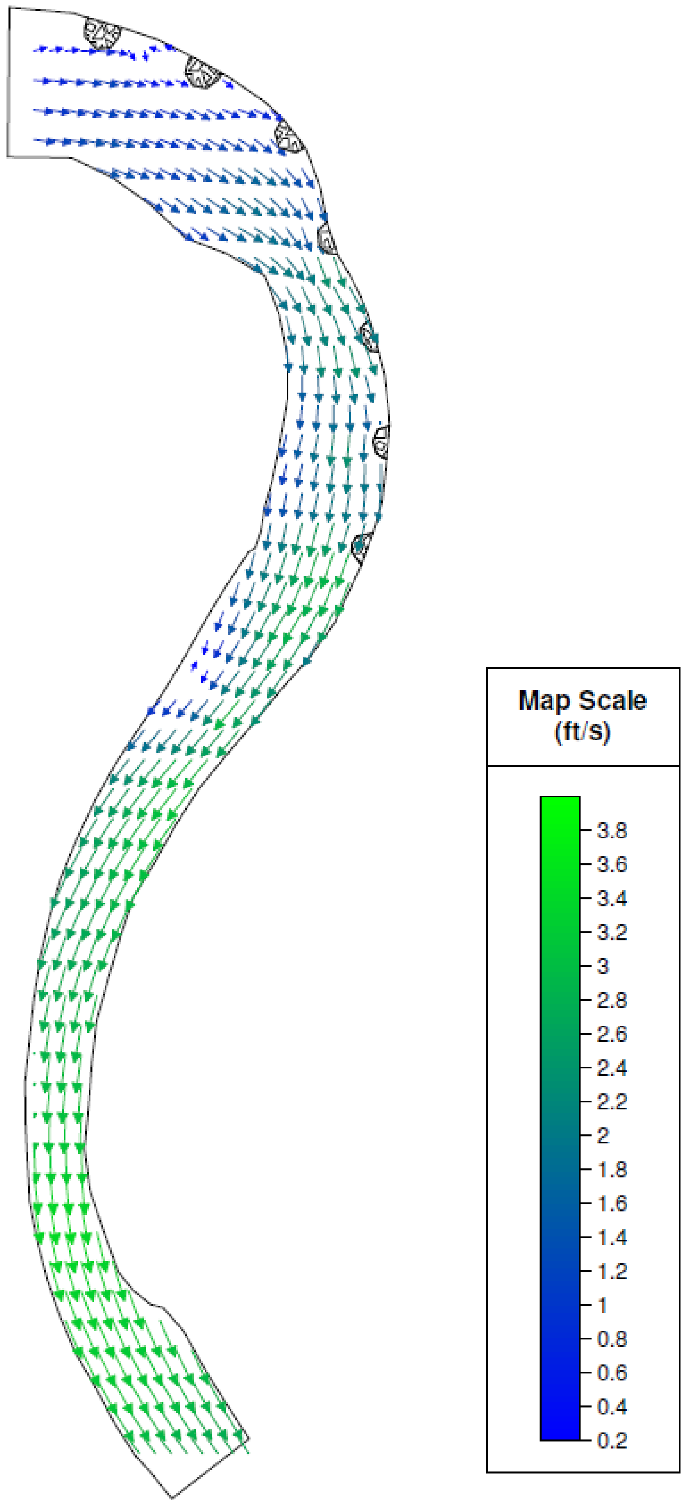

Figure C.4: NW04 Flow Velocity-vector Plot

APPENDIX D

NATIVE TOPOGRAPHY SPUR-DIKE CONFIGURATION SHEAR STRESS PLOTS

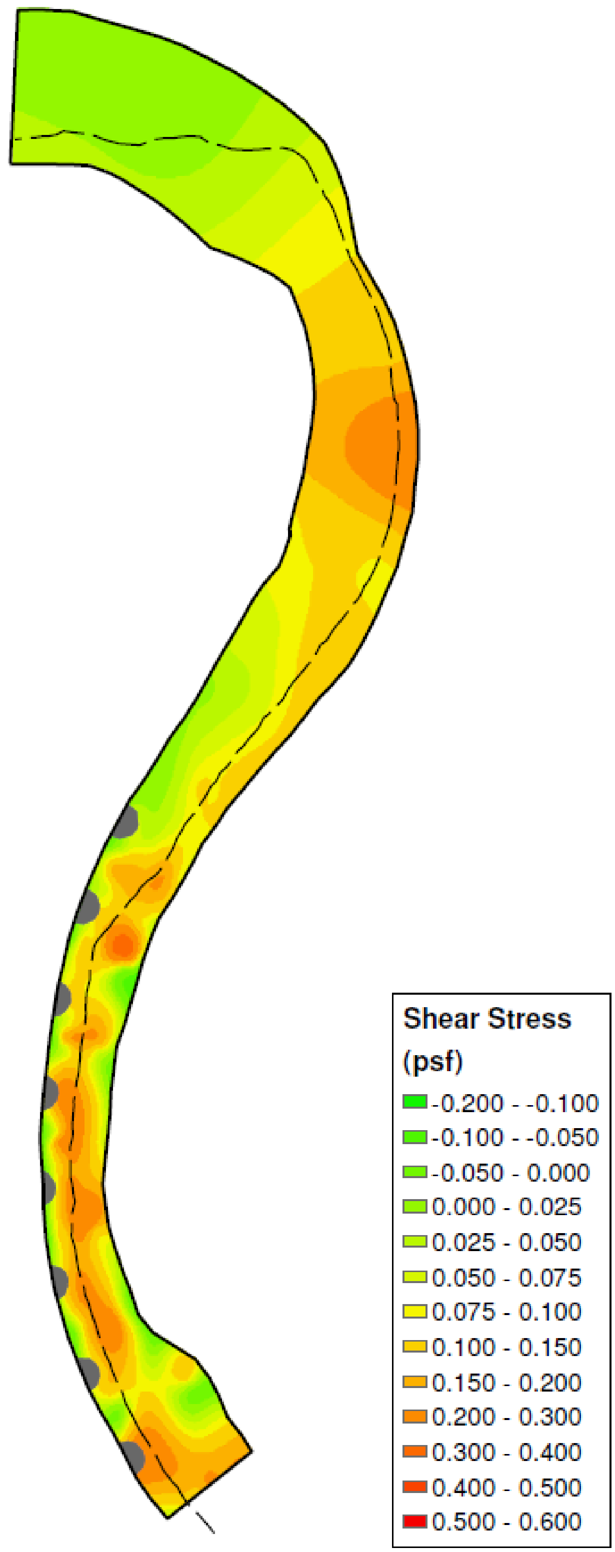

Figure D.1: NW01 Boundary Shear Stress Plot

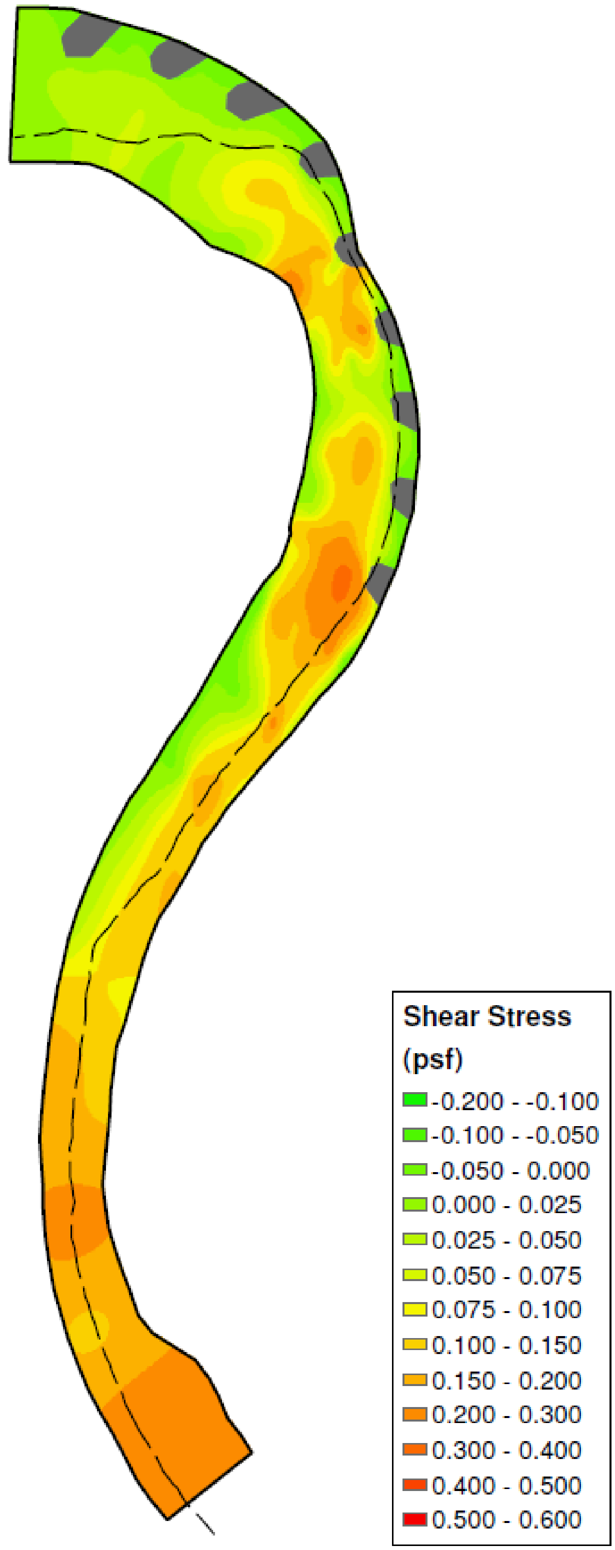

Figure D.2: NW02 Boundary Shear Stress Plot

Figure D.3: NW03 Boundary Shear Stress Plot

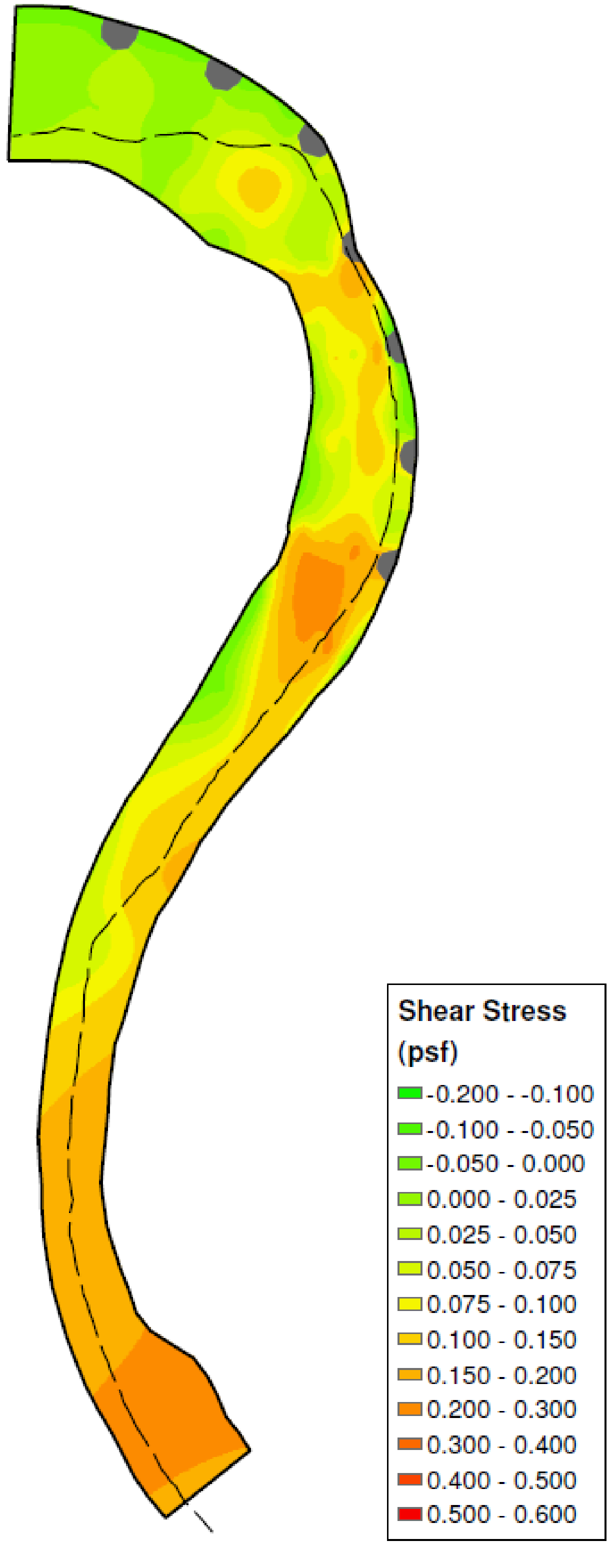

Figure D.4: NW04 Boundary Shear Stress Plot

APPENDIX E

ELECTRONIC APPENDIX

The Electronic Appendix includes the following Excel® files:

- *Velocity Summary NW01-NW04.xls*: All flow velocity and water-surface elevation data
- *Shear Stress Summary NW01-NW04.xls*: All shear stress data from Preston tube measurements